FRA 80-5, III

REPORT NO. FRA/ORD-80/5, III

SLEEVE EXPANSION OF BOLT HOLES IN RAILROAD RAIL

Volume III - Field Experiment Results

D.V. Lindh
R.Q. Taylor
D.M. Rose

BOEING COMMERCIAL AIRPLANE COMPANY
P.O. Box 3707
Seattle WA 98124

FEBRUARY 1980

FINAL REPORT

Prepared for

U.S. DEPARTMENT OF TRANSPORTATION
FEDERAL RAILROAD ADMINISTRATION
Office of Research and Development
Washington DC 20590

Technical Report Documentation Page

1. Report No.	2. Government Accession No.	3. Recipient's Catalog No.
FRA/ORD-80/5,III		

4. Title and Subtitle
SLEVE EXPANSION OF BOLT HOLES IN RAILROAD RAIL
Volume III, Field Experiment Results

5. Report Date
Feb. 1980

6. Performing Organization Code

7. Author(s)
D.V. Lindh, R.Q. Taylor, and D.M. Rose

8. Performing Organization Report No.
DOT-TSC-FRA-80-5, III

9. Performing Organization Name and Address
Boeing Commercial Airplane Company*
P.O. Box 3707
Seattle WA 98124

10. Work Unit No. (TRAIS)
RR019/R0323

11. Contract or Grant No.
DOT-TSC-1048-3

12. Sponsoring Agency Name and Address
U.S. Department of Transportation
Federal Railroad Administration
Office of Research and Development
Washington DC 20590

13. Type of Report and Period Covered
Final Report
July 1975-July 1979

14. Sponsoring Agency Code

15. Supplementary Notes
*Under contract to: U.S. Department of Transportation
Research and Special Programs Administration
Transportation Systems Center
Cambridge MA 02142

16. Abstract

The bolt-hole cold-expansion process has been demonstrated by laboratory tests to significantly affect the initiation and propagation of fatigue cracks from rail bolt holes such that a reduction of the incidence of rail-bolt-hole failure in cold-expanded rail would be expected. A field-verification experiment was implemented in 1977 and reported in Volume I of this report.

This volume contains the results of the field experiment, an examination of the effect of fatigue ratio (R) on the observed laboratory fatigue-life improvement of cold-expanded bolt holes, an investigation of crack growth of rails in a vacuum environment, and a comparison of the fatigue performance of cold-expanded bolt holes with rail flashwelds.

17. Key Words
Cold expansion
Crack
Fatigue
Mandrel
Rail bolt hole
Sleeve
Flashwelds
Vacuum
Crack growth rate

18. Distribution Statement
DOCUMENT IS AVAILABLE TO THE PUBLIC THROUGH THE NATIONAL TECHNICAL INFORMATION SERVICE, SPRINGFIELD, VIRGINIA 22161

19. Security Classif. (of this report)	20. Security Classif. (of this page)	21. No. of Pages	22. Price
Unclassified	Unclassified	112	

Form DOT F 1700.7 (8-72) Reproduction of completed page authorized

PREFACE

This document is Volume III of a three-volume series. Volume I reports the results of an investigation of several processes that introduce compressive residual stresses into the rail joint to improve fatigue resistance and describes the planning and implementation of a field experiment to verify the fatigue improvement anticipated for the sleeve-expansion process. Volume II defines process parameters and outlines procedures for process control of the sleeve-expansion process.

METRIC CONVERSION FACTORS

Approximate Conversions to Metric Measures

Symbol	When You Know	Multiply by	To Find	Symbol
		LENGTH		
in	inches	*2.5	centimeters	cm
ft	feet	30	centimeters	cm
yd	yards	0.9	meters	m
mi	miles	1.6	kilometers	km
		AREA		
in^2	square inches	6.5	square centimeters	cm^2
ft^2	square feet	0.09	square meters	m^2
yd^2	square yards	0.8	square meters	m^2
mi^2	square miles	2.6	square kilometers	km^2
	acres	0.4	hectares	ha
		MASS (weight)		
oz	ounces	28	grams	g
lb	pounds	0.45	kilograms	kg
	short tons (2000 lb)	0.9	tonnes	t
		VOLUME		
tsp	teaspoons	5	milliliters	ml
Tbsp	tablespoons	15	milliliters	ml
fl oz	fluid ounces	30	milliliters	ml
c	cups	0.24	liters	l
pt	pints	0.47	liters	l
qt	quarts	0.95	liters	l
gal	gallons	3.8	liters	l
ft^3	cubic feet	0.03	cubic meters	m^3
yd^3	cubic yards	0.76	cubic meters	m^3
		TEMPERATURE (exact)		
°F	Fahrenheit temperature	5/9 (after subtracting 32)	Celsius temperature	°C

*1 in = 2.54 (exactly). For other exact conversions and more detailed tables, see NBS Misc. Publ. 286, Units of Weights and Measures, Price $2.25, SD Catalog No. C13.10:286.

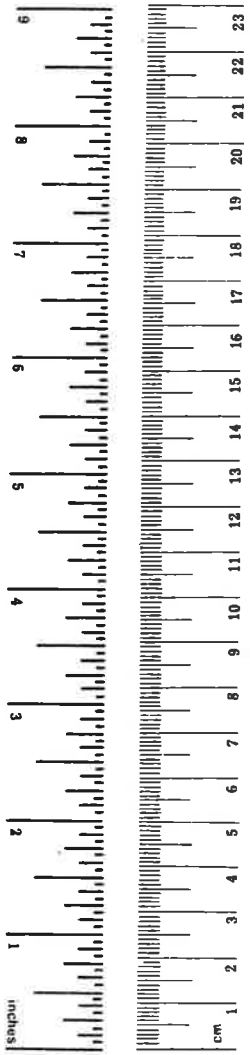

Approximate Conversions from Metric Measures

Symbol	When You Know	Multiply by	To Find	Symbol
		LENGTH		
mm	millimeters	0.04	inches	in
cm	centimeters	0.4	inches	in
m	meters	3.3	feet	ft
m	meters	1.1	yards	yd
km	kilometers	0.6	miles	mi
		AREA		
cm^2	square centimeters	0.16	square inches	in^2
m^2	square meters	1.2	square yards	yd^2
km^2	square kilometers	0.4	square miles	mi^2
ha	hectares (10,000 m^2)	2.5	acres	
		MASS (weight)		
g	grams	0.035	ounces	oz
kg	kilograms	2.2	pounds	lb
t	tonnes (1000 kg)	1.1	short tons	
		VOLUME		
ml	milliliters	0.03	fluid ounces	fl oz
l	liters	2.1	pints	pt
l	liters	1.06	quarts	qt
l	liters	0.26	gallons	gal
m^3	cubic meters	35	cubic feet	ft^3
m^3	cubic meters	1.3	cubic yards	yd^3
		TEMPERATURE (exact)		
°C	Celsius temperature	9/5 (then add 32)	Fahrenheit temperature	°F

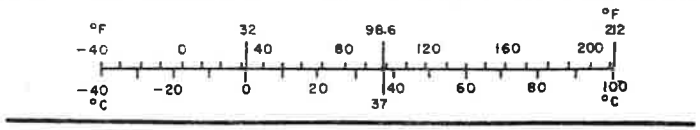

CONTENTS

FIGURES

TABLES

ABBREVIATIONS AND SYMBOLS

AAR	Association of American Railroads
$\mathbb{C}_L$	centerline
K_{max}	maximum value stress-intensity parameter
ΔK	stress-intensity parameter range
kip	1000 pounds
lb	pound
m	meter
MN	meganewton
p	probability
P_B	probability (bolt-hole failure occurs in the BROACHED area, given it occurs in one of the three treatment areas B, C, CE)
P_C	probability (bolt-hole failure occurs in the CLEANED area, given it occurs in one of the three treatment areas B, C, CE)
P_{CE}	probability (bolt-hole failure occurs in the COLD-EXPANDED area, given it occurs in one of the three treatment areas C, B, CE)
P_N	probability (bolt-hole failure occurs in the NOTHING area, given it occurs in the 16-mile section of track)
P_{max}	maximum load, lb
P_{min}	minimum load, lb
R	minimum stress/maximum stress (fatigue ratio)
torr	1 millimeter of Hg vacuum
yd	yard

1. INTRODUCTION

This document reports the results of a field experiment and the performance and results of three associated experiments:

- Studies on the effect of negative fatigue ratio (reverse bending) on rail sections with cold-expanded (sleeve-expanded) bolt holes
- Investigation of flaw growth in vacuum
- Life of flash-weld rail joints fabricated from uncropped rails with cold-expanded and non-cold-expanded holes .

2. ANALYSIS OF FIELD-EXPERIMENT RESULTS

2.1 FIELD-EXPERIMENT PLAN

The design of the field test was discussed in detail in Volume I, sections 4.1 through 4.4. It should be reemphasized that problems encountered in implementing the original balanced design forced modifications to the design. The resultant experiment, covering 16 miles of westbound track near Silvercreek, Nebraska, is summarized in figure 1.

The field test was composed of four treatments:

1. NOTHING–joints untreated
2. CLEANED–joints cleaned and greased and bolts tightened
3. BROACHED–joints cleaned and greased, bolt holes broached, and bolts tightened
4. COLD-EXPANDED–joints cleaned and greased, bolt holes broached and cold expanded, and bolts tightened

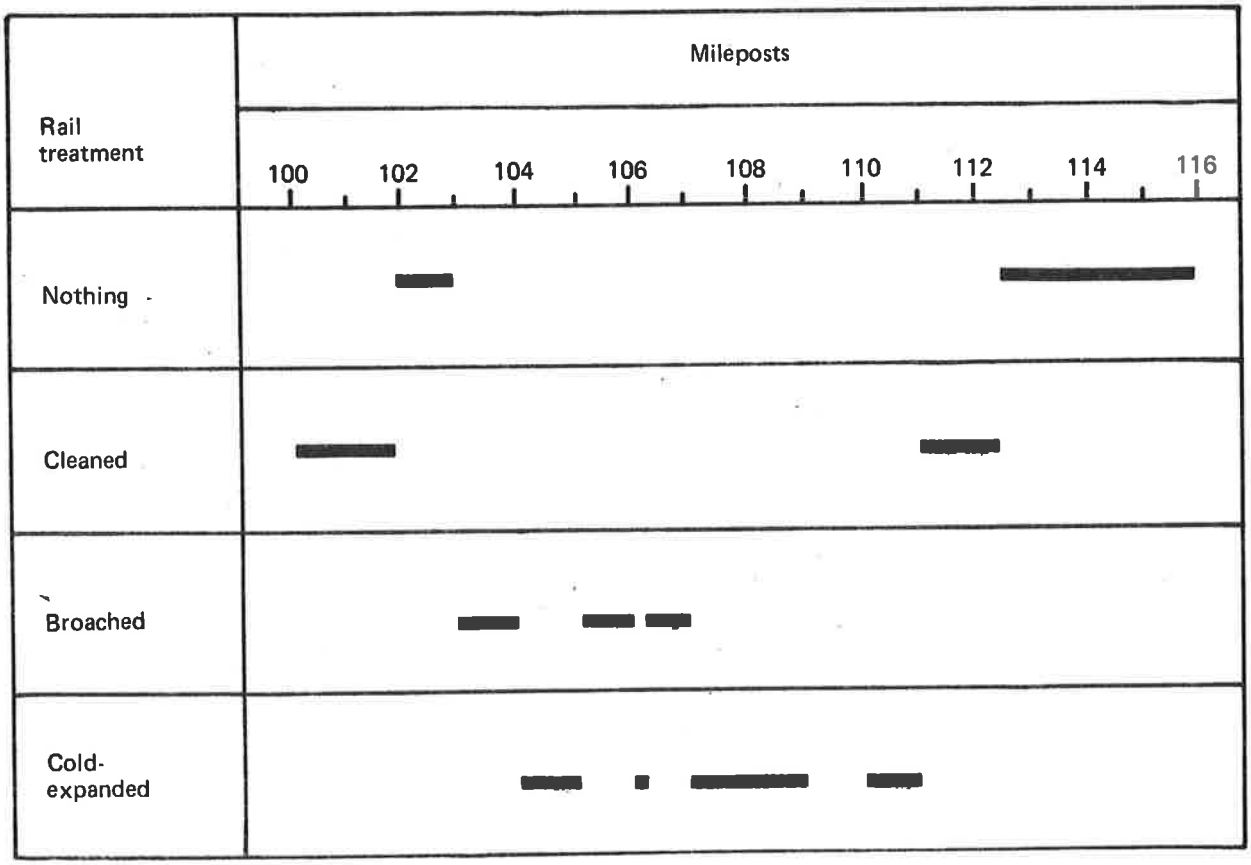

Figure 1.–Test Plan Implemented at Silvercreek, Nebraska Site

The NOTHING and CLEANED treatments differed primarily in that the CLEANED rails had tightened joint bars, helping to distribute the load over the rail.

Table 1 shows the bolt-hole experience of this area prior to implementation of the field test (November 1976). All four treatment areas had roughly comparable failure rates for the 5 years prior to test. The test for equal failure rates for the four treatments (table 2), showed that there was no statistically significant difference among the treatment groups (observed significance level greater than 0.5). This test was based upon approximating the failure distribution by the exponential. Hence, constant failure rates would imply that the number failures per area would be directly proportional to the number of miles of track in that area.

There appeared to be a somewhat elevated failure rate in 1974 and 1976, possibly indicative of aging or accumulated damage. Thus, with this area originally not scheduled for relay in the next few years, the potential for observing a sufficient number of failures to delineate the effectiveness of the four treatments seemed highly probable. The increased number of failures in 1976 might not be attributed to aging, but instead to the use of an improved rail-flaw-detection car by Union Pacific in the latter part of that year.

Holes sufficiently out of round did not clean up with the broaching. If the rail was in the broached section, no anomaly was recorded. If the rail was in the cold-expanded section, the hole was not cold expanded and the hole was painted yellow. These nonexpanded holes thus were "removed" from the cold-expanded area, but not from the broached area.

Three rails with 1/4 -inch bolt-hole cracks were broached, cold expanded, and left in service. These rails were visually examined every 30 days to measure the effectiveness of the cold-expansion process on small undetected cracks in rail with accumulated damage or wear.

All pretreatment bolt-hole cracks greater than 1/2 inch were presumed removed from the cold-expanded area (the pattern of residual stress imposed by the treatment extends about 1/2 inch from the edge of the bolt hole).

Table 1.—Bolt-Hole Failures for 5 Years prior to Field Test

	Treatment				
	Nothing	Cleaned	Broached	Cold expanded	Total
No. of miles	4.95	3.05	3.89	4.11	16.0
Bolt-hole failures					
1972	2	4	3	4	13
1973	11	0	0	0	11
1974	14	7	5	8	34
1975	6	3	6	4	19
1976	9	4	18	15	46
Total	42	18	32	31	123
Bolt-hole failures per mile	8.48	5.90	8.23	7.54	7.69
Bolt-hole failure rate per mile per year	1.70	1.18	1.65	1.51	1.54

Table 2.—Test for Homogeneous Failure Rate—Original Test Site

Treatment	Failures		
	Observed	Expected	(Observed - expected)^2/expected
Nothing	42	38.1	0.41
Cleaned	18	23.4	1.27
Broached	32	29.9	0.15
Cold expanded	31	31.6	0.01
			1.84 = chi-squared statistic

Notes:

If the four areas are homogeneous, then the 123 observed failures should be distributed over these areas proportional to the size of the areas.

Under the hypothesis of homogeneity,

$P_N = 4.95/16.0 = 0.31$, $P_C = 3.05/16.0 = 0.19$
$P_B = 3.89/16.0 = 0.24$, $P_{CE} = 4.11/16.0 = 0.26$

Where:

P_N = probability (bolt-hole failure occurs in the NOTHING area, given it occurs in this 16-mile section of track)

P_C = probability (bolt-hole failure occurs in the CLEANED area, given it occurs in this 16-mile section of track)

P_B = probability (bolt-hole failure occurs in the BROACHED area given it occurs in this 16-mile section track)

P_{CE} = probability (bolt-hole failure occurs in the COLD-EXPANDED area, given it occurs in this 16-mile section of track)

The expected number per treatment then was computed by multiplying the probability times 123 (e.g., 123 x 0.31 = 38.1).

To be statistically significant, and reject the homogeneity hypothesis, the chi-squared statistic would have to exceed 6.25 (at the 0.10 level).

2.2 RAIL-FAILURE INSPECTION DATA

During the field test, Union Pacific inspected the field-test area four times using an ultrasonic/magnetic detector of their design for crack detection. The field experiment originally was scheduled to last at least 2 years, but due to the increase in bolt-hole failures, Union Pacific relaid the track in April 1978 before another detector car run could be made. The length of the study was 1.17 years (November 1976 through January 1978, when the last test car was run). The bolt-hole rail-failure data as reported to Boeing by Union Pacific are summarized in table 3.

Project personnel made an effort to examine all bolt-hole failures from the cold-expanded region. Union Pacific cropped 2-foot lengths from failed rails in the cold-expanded region and six were examined in a Boeing laboratory by fractography experts.

*Table 3.—Bolt-Hole Failures during Field Test (Unamended)**

Mileposts	Treatment	Bolt-hole failure reported				
		1/77	4/77	9/77	1/78	Total
100.0–101.8	Cleaned	1	1	1	–	3
101.8–103.0	Nothing	–	1	4	–	5
103.0–104.0	Broached	5	–	2	–	7
104.0–105.0	Cold expanded	2	–	–	–	2
105.0–106.0	Broached	–	–	1	–	1
106.0–106.11	Cold expanded	–	–	–	–	–
106.11–107.0	Broached	–	1	2	1	4
107.0–109.0	Cold expanded	4	–	2	1	7
109.0–110.0	Broached	2	1	–	–	3
110.0–111.0	Cold expanded	1	2	1	–	4
111.0–112.25	Cleaned	2	3	5	1	11
112.25–116.0	Nothing	24	11	4	2	41
Total		41	20	22	5	88

Treatment	Miles	Failures	Failures/mile	Failures/mile/year
Nothing	4.95	46	9.29	7.96
Cleaned	3.05	14	4.59	3.03
Broached	3.89	15	3.86	3.31
Cold expanded	4.11	13	3.16	2.71
Total	16.0	88	5.50	4.71

*See table 4 for amended data.

Of the seven January 1977 failed bolt holes, three were broached but not cold expanded. Of the remaining failed bolts from the cold-expanded region, two were examined in the laboratory. One of these was not a bolt-hole failure, but a crack that originated from the rail web and grew to within 0.30 inch of the bolt hole. It appeared that the cold expansion retarded the crack growth at that point. The other rail examined in the laboratory had a 5-inch crack originating from the bolt hole with a second crack 1 inch long running parallel to the first. Deep pits at the fracture initiation point, the dark color of the fracture face (Fe_2O_3), deep corrosion pitting of the bolt-hole face, and the bright appearance of the freshly broached and cold-expanded bolt-hole surface strongly suggested to the fractographic experts that both cracks existed prior to cold expansion. They also estimated the major cracks to have been at least 4 inches long at the time of cold expansion. The two remaining rails were not available for laboratory analysis.

The two April 1977 failed cold-expanded bolt holes were cropped and sent to the laboratory for examination. One of the failed bolt holes was broached only; the other showed substantial evidence of a sizable crack that existed prior to the cold-expansion treatment (based upon the type of evidence noted above).

Of the three September 1977 cold-expansion failures, two were examined in the laboratory. Again, one of the failed bolt holes was broached only; the other showed strong evidence of a sizable preexisting crack. The third failure was in one of the three bolt holes with 1/4-inch

cracks cold expanded and left in service. The field-detector test estimated the crack to have grown to 1/2 inch in length. The rail was left in service until the section was relaid in April 1978.

The January 1978 detector-car run reported one bolt-hole failure in the cold-expanded section. Investigation of this failure was not possible as the cropped end of the rail was lost during shipment to the laboratory.

In April 1978, the test section was relaid. The three rails with preexisting 1/4-inch crack were cropped and sent to Boeing for inspection. Fracture-face examination of the rails indicated the cracks to be of considerable age, with no growth in recent months. The rail crack reported in September to have grown from 1/4 to 1/2 inch was still only 1/4 inch in length. The fracture faces of the three rails are shown in figures 2, 3, and 4.

Upon initial examination of table 3, it appeared to us that the NOTHING area had an appreciably higher failure rate than the remaining three treatment groups. This higher failure rate was statistically significant (Chi-Squared test of homogeneity rejected at 0.0001 level). The remaining three treatment groups, on this initial examination, appeared similar with respect to failure rate (Chi-Squared test of homogeneity accepted at 0.10 level). Thus, without modification of the field-test data as suggested by the discussion above, there appeared to be no benefit from the bolt-hole cold-expansion process. The amended rail-failure data, table 4, reflect the change in "true" cold-expanded failures, based upon an examination of the rails.

Table 4.—Bolt-Hole Failures during Field Test (Amended)

Treatment	Miles	Failures	Failures/mile	Failures/mile/year
Nothing	4.95	46	9.29	7.96
Cleaned	3.05	14	4.59	3.93
Broached	3.89	15	3.86	3.31
Cold expanded*	4.11	6	1.46	1.25
Cold expanded**	4.11	3	0.73	0.63

* Includes failures from laboratory examination with sizable cracks undetected at time of initial rail treatment. Excludes non-cold-expanded bolt-hole failures occurring in the cold-expanded region.

**Excludes failures with laboratory-determined preexisting cracks. The three failures were not laboratory examined and thus must be included as potential cold-expansion failures. Also excludes non-cold-expanded bolt-hole failures occurring in the cold-expanded region.

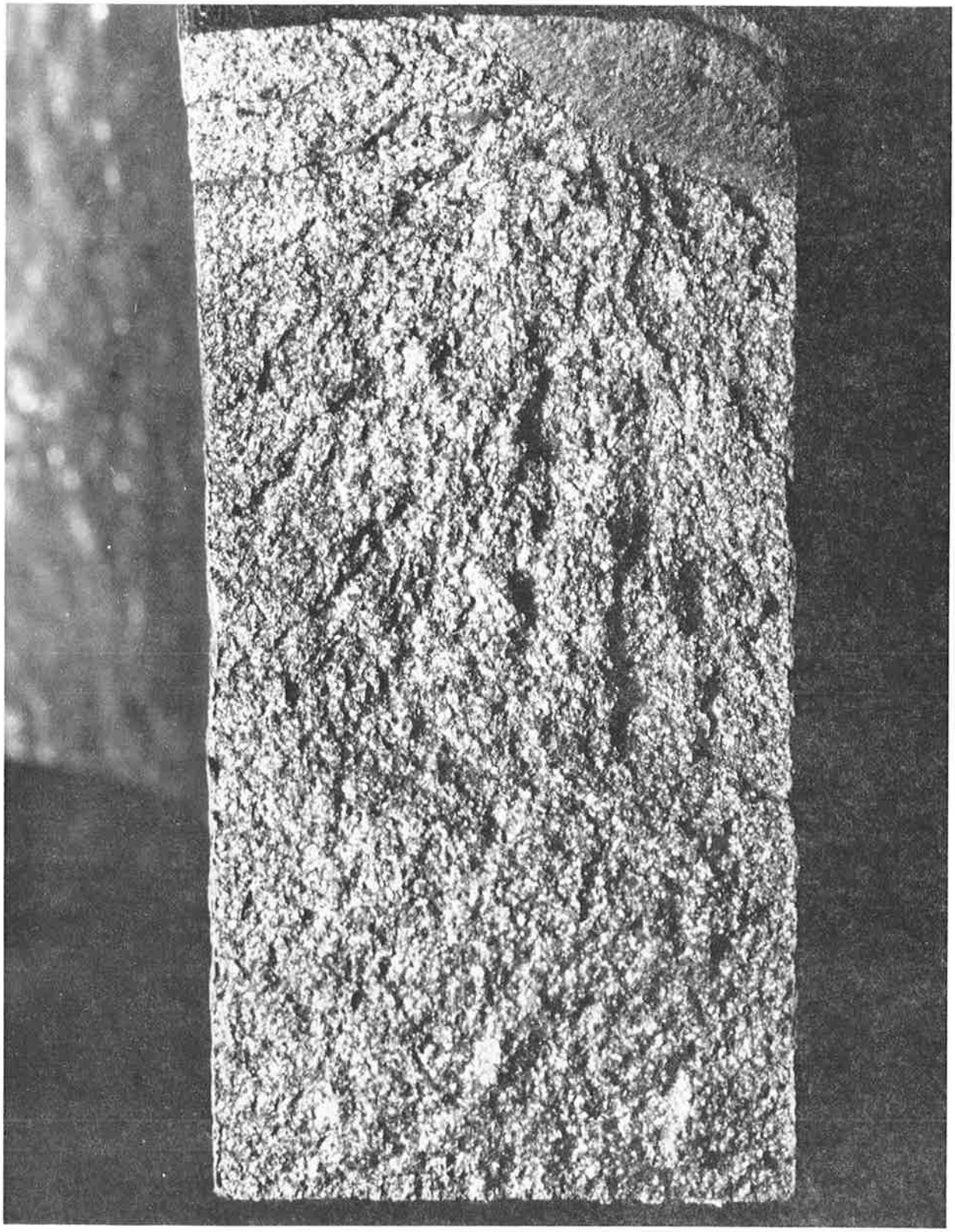

Figure 2.—Preexisting 1/4-inch Crack—Milepost 107.08

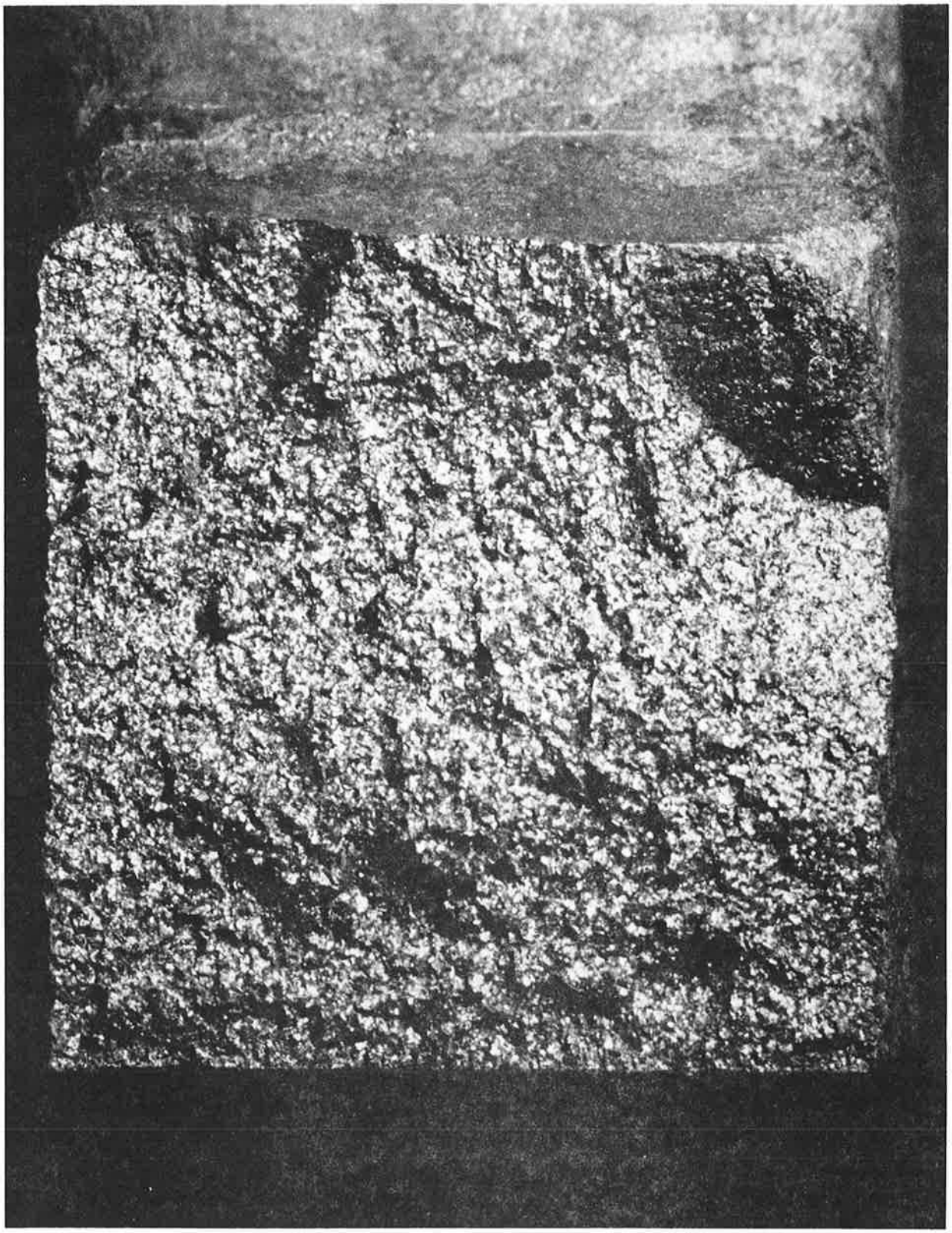

Figure 3.—Preexisting 1/4-inch Crack—Milepost 107.27

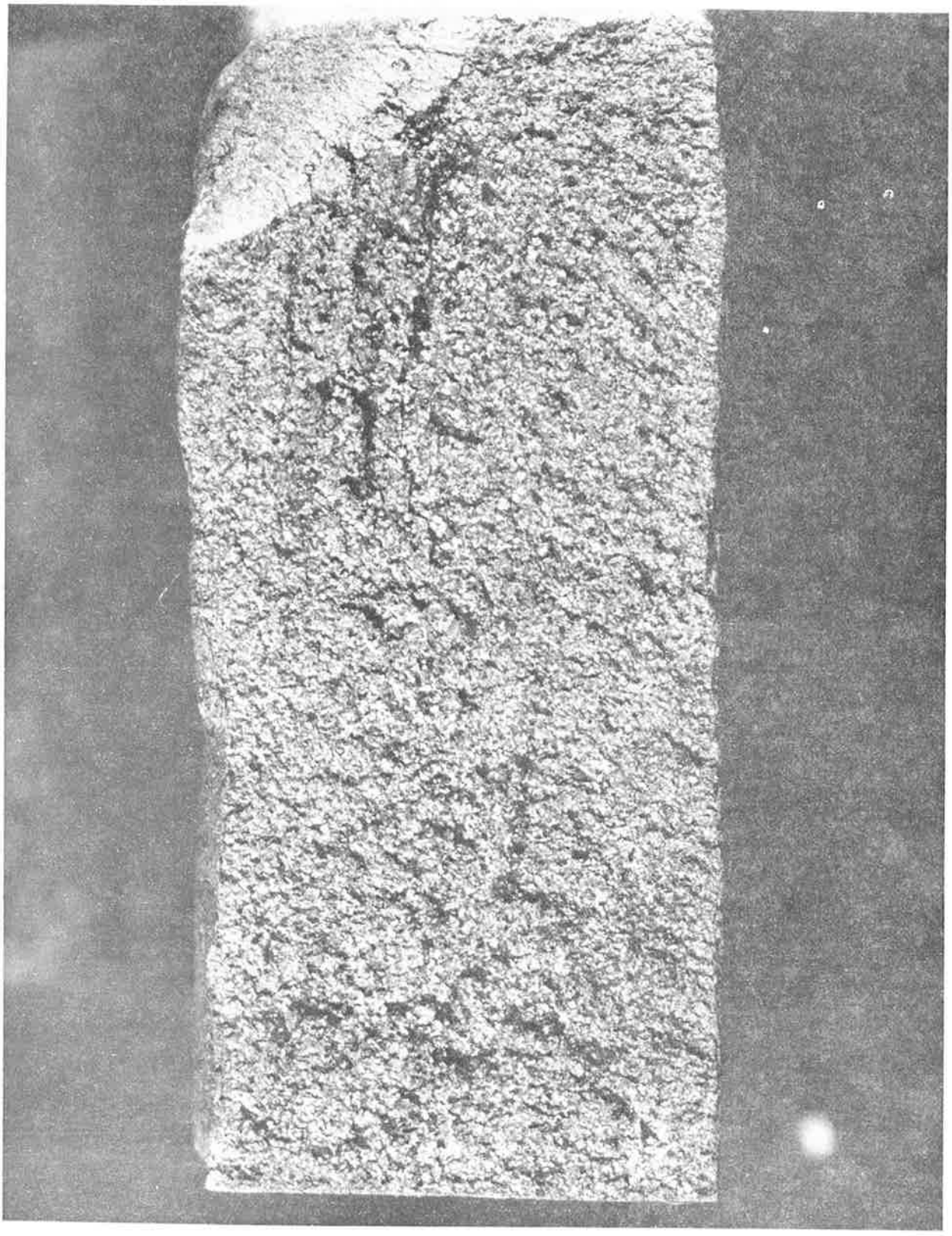

Figure 4.—Preexisting 1/4-inch Crack—Milepost 107.64

2.3 RAIL-FAILURE ANALYSIS

To compare the cold-expanded rail with the other sections of track, information given in table 4 must be considered. Broached-only rail failures from a cold-expanded area are not an adequate measure of the cold-expansion process. Sizable preexisting (no treatment) cracks, however, must be considered when comparing the processes. It is probable that there were some sizable preexisting cracks in the other test sections whose failures were not examined in the laboratory. Omitting the preexisting failures from the cold-expanded area thus would bias test results in favor of the cold-expansion process. For projections of anticipated failure rates in a cold-expanded area swept clean of all appreciable cracks, the preexisting crack failures should not be used.

There was an appreciable difference in failure rate between nontreated areas or "NOTHING" and treated (cleaned, broached, or cold expanded) areas (table 4). This might not be due solely to cold expansion because all joints in the treated areas had their joint-bar bolts tightened, which distributed the load over a substantial region of the end of the rail.

To test for homogeneity in failure rate among the three treated areas, a Chi-Squared test of homogeneity was performed (table 5). There was a significant difference (0.05 level) between the pattern of failures observed and that predicted under the homogeneous-failure-rate hypothesis, even though the field test was cut short and the number of observed failures was low. The largest difference was in the cold-expanded area where 13.02 failures, under homogeneity, were expected and only six were observed, indicating that the failure rate in the cold-expanded area was significantly less than expected.

Table 5.—Test for Homogeneous Failure Rate—Cleaned, Broached, and Cold-Expanded Areas

	Failures		
Treatment	Observed	Expected	(Observed - expected)^2/expected
Cleaned	14	9.66	1.95
Broached	15	12.21	0.58
Cold expanded	6	13.02	3.78
	35	35.00	6.32 = chi-squared statistic

Notes:

P_C = 3.05/11.05 = 0.28 P_B = 3.89/11.05 = 0.35 P_{CE} = 4.11/11.05 = 0.37

where:

P_C = probability bolt-hole failure occurs in the CLEANED area, given it occurs in one of the three treatment areas C, B, CE

P_B = probability bolt-hole failure occurs in the BROACHED area, given it occurs in one of the three treatment areas C, B, CE

P_{CE} = probability bolt-hole failure occurs in the COLD-EXPANDED area, given it occurs in one of the three treatment areas C, B, CE

chi-squared, 2 degrees of freedom, 0.05 critical level = 5.99

The cleaned area also had more failures than expected under homogeneity. The implied relation between failure rates was:

COLD EXPANDED < BROACHED < CLEANED

In comparing the cold-expanded area versus the broached area, the homogeneity hypothesis reduced to a binomial test for $p = 0.514$ versus the one-sided alternative $p < 0.514$ (4.11 miles cold expanded / 8.0 miles broached or cold expanded) = 0.514, where

p = probability that a failure from either the broached or cold-expanded area came from the cold-expanded area

This one-sided test was equivalent to constructing a one-sided upper bound for p and observing whether 0.514 was in the confidence interval. An upper bound with 95% confidence was $p < 0.488$ which stated that the cold-expanded area had a significantly (0.05 level) lower failure rate than the broached area.

Throughout the above analysis, constant failure rate was implied, but certainly was not the case. A monotone increasing failure rate was known to govern in most similar conditions studied. Frequently, a Weibull failure model had given good fit to test data when the aging variable was know. In this situation, the aging variable was cycling under load, which was closely related to accumulated load carried or million gross tons. Although these data were not available, the exponential approximation to a Weibull distribution of data over this small time period (14 months) was reasonable, expecially when considering the variability of environmental and historical conditions of the test section.

In the above analysis, the number of failed cold-expanded bolt holes was six. Three of those bolt holes were examined in the laboratory and found to have cracks existing at the time of bolt-hole treatment. The three remaining bolt holes were not examined in the laboratory, but based upon observations of this study, it is possible that these bolt holes also had preexisting cracks. Although highly improved rail-flaw-detection equipment was used, sizable flaws were not detected in November 1977, but were found by the same car months later, not necessarily in the next pass. This was due partly to difficulties experienced with the detector car in 1977, but indicates that 100% detectability is not certain.

2.4 CONCLUSION OF FIELD STUDY

This field study, conducted with the cooperation of Union Pacific Railroad, demonstrated the potential of the bolt-hole cold-expansion process for improving rail reliability. The study also demonstrated two problems in effectively implementing the process on used track that were not encountered in laboratory testing. First, out-of-round bolt holes did not clean up with the broaching (out of tolerance for hole expansion, discussed in Volume II) and, therefore, were not cold expanded. Thus, they would continue to be a potential for bolt-hole cracks. Secondly, some cracks of significant size (1/2 inch or greater) originating from the bolt hole were not found by the rail-flaw-detection equipment. The first problem can be solved by using a larger starting hole and cold-expansion mandrel for these unusually out-of-round holes. The second problem will require continued development of rail-defect-detection equipment.

The field test demonstrated that rail with cold-expanded holes had a significantly lower bolt-hole failure rate than untreated rail. The estimated reduction in failure rate was by a factor of 1/6. The cold-expanded rail also showed a significantly lower failure rate (by a factor of 1/3) than rails cleaned with bars tightened, and rails with holes broached and bars tightened.

3. STUDIES OF THE EFFECT OF FATIGUE RATIO ON SLEEVE-EXPANDED BOLT HOLES

3.1 INTRODUCTION

The rail-specimen laboratory fatigue tests described in Volume I were conducted at a stress ratio of R = 0.06. The specimens were not subjected to reverse bending, a condition more closely approximating actual rail service loading. Consequently, arrangements were made with the American Association of Railroads (ARR) Research and Test Department to conduct reverse-bending tests (negative fatigue ratios) to verify the life advantage of cold-expanded bolt holes under such conditions.

Four four-hole rail specimens of the configuration shown in figure 14, Volume I, were delivered to the AAR for testing. The test description and results are contained in appendix A.

3.2 DISCUSSION AND CONCLUSIONS

The results of the AAR tests verified the life improvement anticipated from the bolt-hole cold-expansion process in that failure mode of the expanded hole specimens shifted from the bolt hole to other points of the basic rail section. The AAR tests (table 7) show a slightly different failure mode than the tests conducted at Boeing (table 6).

It may be observed from tables 6 and 7 that hole failure of the non-cold-expanded specimens in the negative-R tests occurred at the specimen end holes, while the positive-R loading caused failure at the center holes, indicating a difference in state of stress.

Table 6.—Boeing Four-Hole Specimen Fatigue Tests, R = 0.06

Specimen number	Treatment	Crack length, inch	Cycles to crack	Description of failure
5A-3	Non-cold-expanded	0.32	153,090	Double crack—center hole
5A-4	Non-cold-expanded	0.28	92,050	Hole failure—center hole
6A-2	Non-cold-expanded	—	166,350	Hole failure—center hole
6A-3	Non-cold-expanded	0.28	118,000	Hole failure—center hole
5B-3	Cold expanded	—	1,026,300	No failure
5B-4	Cold expanded	0.28	723,520	Hole failure
6B-3	Cold expanded	—	1,034,430	No failure
6B-4	Cold expanded	—	1,136,660	No failure

Table 7.—AAR Four-Hole Specimen Fatigue Tests, R = -0.2

Specimen number	Treatment	Cycles to crack	Description of failure
5A-7	Non-cold-expanded	333,800	Hole failure—end hole
6A-8	Non-cold-expanded	239,500	Hole failure—end hole
5B-6	Cold expanded	442,700	Total rail failure—symmetrical
6B-6	Cold expanded	996,500	Web failure—near end hole

4. INVESTIGATION OF RAILROAD-RAIL FLAW GROWTH IN VACUUM

4.1 SYNOPSIS

The majority of rail-steel fatigue-crack-growth-rate studies have been conducted in an air environment. To what degree the air environment affects the crack-growth characteristics has not been ascertained. This study was conducted to explore crack-growth characteristics where the crack initiates at a subsurface location, shielded from atmospheric environmental effects.

The study was conducted by C. J. Beevers, Department of Physical Metallurgy, University of Birmingham, England. Specimens taken from 110- and 80-lb/yd used rail were fatigue tested in a vacuum of 1×10^{-5} torr, thus isolated from atmospheric effects. The specific test description and an analysis of results are presented in appendix B.

4.2 CONCLUSIONS

1. In pearlitic rail steels, the R dependence of fatigue-crack-growth rates appears to be reduced in an inert environment compared to a normal air environment. An R or K_{max} dependence, however, still exists in an inert environment. From this, it is expected that internal defects in rails would exhibit a similar behavior and, at high R ratios, crack growth can be expected at ΔK values of 5-6 MN $m^{-3/2}$ or greater.

2. Fractographic evidence indicates that crack growth involves reverse plasticity at the crack tip, but that the mode of crack extension is discontinuous.

3. In pearlitic/ferritic steels, the pearlite/ferrite interface offers an additional path for crack extension.

4. The presence of ferrite films in a pearlitic steel has no deleterious effect upon the ΔK threshold or general fatigue-crack-growth performance.

5.0 COMPARATIVE LIFE OF UNCROPPED WELDED RAIL

5.1 INTRODUCTION

The investigation of cold expansion of rail bolt holes was expanded to include a fatigue evaluation of flash-butt-welded rails containing joint bolt holes to determine the approximate life of welded joints formed from previously used bolted rails. The approach was to provide welded rail joints without cropping the bolt-hole area from the rail to be welded.

5.2 APPROACH

Six flash-butt-welded rail joints containing four bolt holes each were furnished by the Department of Transportation as specimen material. The previously used rails were welded in the as-is condition, including the bolt holes plus crack-detection-circuit electrical "slug" holes in the rail head.

The flash upset of the rail end distorted the bolt holes nearest the weld to form a flat on one side of the hole. The weld flash did not distort or fill the slug holes.

5.2.1 SPECIMEN PREPARATION

The six specimens were cropped to form six 2-foot-long sections, providing four-bolt-hole specimens with the weld at symmetrical $\mathbb{Q}$. The specimens, with the exception of the weld and the slug hole in the rail head, were the same geometry as the four-hole specimens described in figure 14, Volume I.

5.2.2 HOLE PREPARATION

Three specimens were left untreated to provide baseline data. The bolt holes distorted by the flashweld were left in that condition. The bolt holes in the remaining specimens were bored to 1-5/16 inch diameter and sleeve cold expanded with a mandrel interference of 0.040 inch (Vol II). The hole distortion was essentially eliminated by the boring operation prior to sleeve expansion. After completion of the expansion process, the edge of the center bolt holes was approximately 1/2 inch from the edge of the weld upset (fig. 5). Thus, three cold-expanded and three non-cold-expanded specimens were provided for fatigue tests.

5.2.3 FATIGUE TESTS

Fatigue testing of the six specimens was accomplished with an EMR 150-kip fatigue machine under the following load conditions:

- P_{max} = 150,000 lb
- P_{min} = 9,000 lb
- R = 0.06

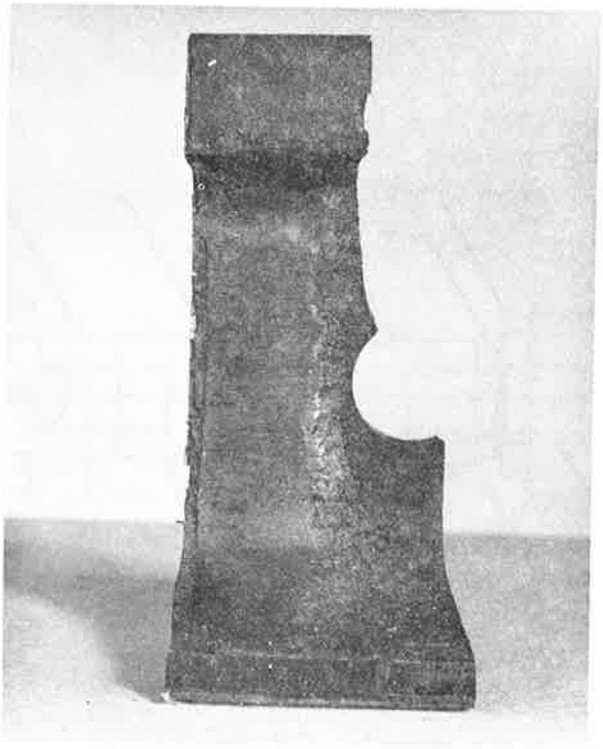

Figure 5.—Sleeve-Expanded Bolt-Hole/Weld Relationship

Load was applied through the rail specimens by the test fixture shown in figure 6. Figure 7 illustrates the load geometry applied to the specimen. The life-cycle results and failure locations are shown in figure 8.

5.2.4 FRACTURE ANALYSIS

All of the specimens shown in figure 8 had classical fatigue modes, as shown in the figures noted below. The failure initiation locations were as follows:

Non-cold-expanded

- Specimen A—end bolt hole, figure 9
- Specimen B—slug hole, figure 10
- Specimen D—end bolt hole, figure 11

Cold expanded

- Specimen C—rail head, figure 12
- Specimen E—slug hole, figure 13
- Specimen F—slug hole, figure 14

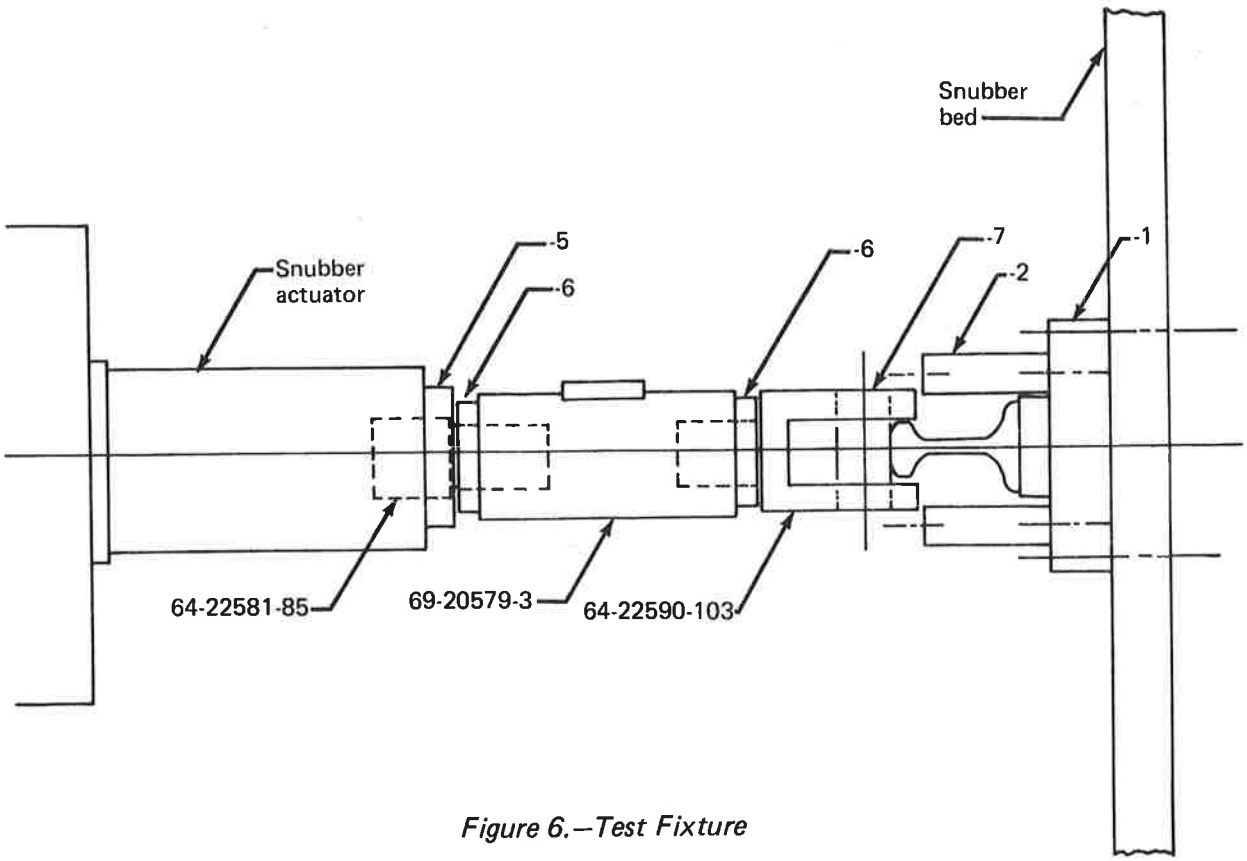

Figure 6.—Test Fixture

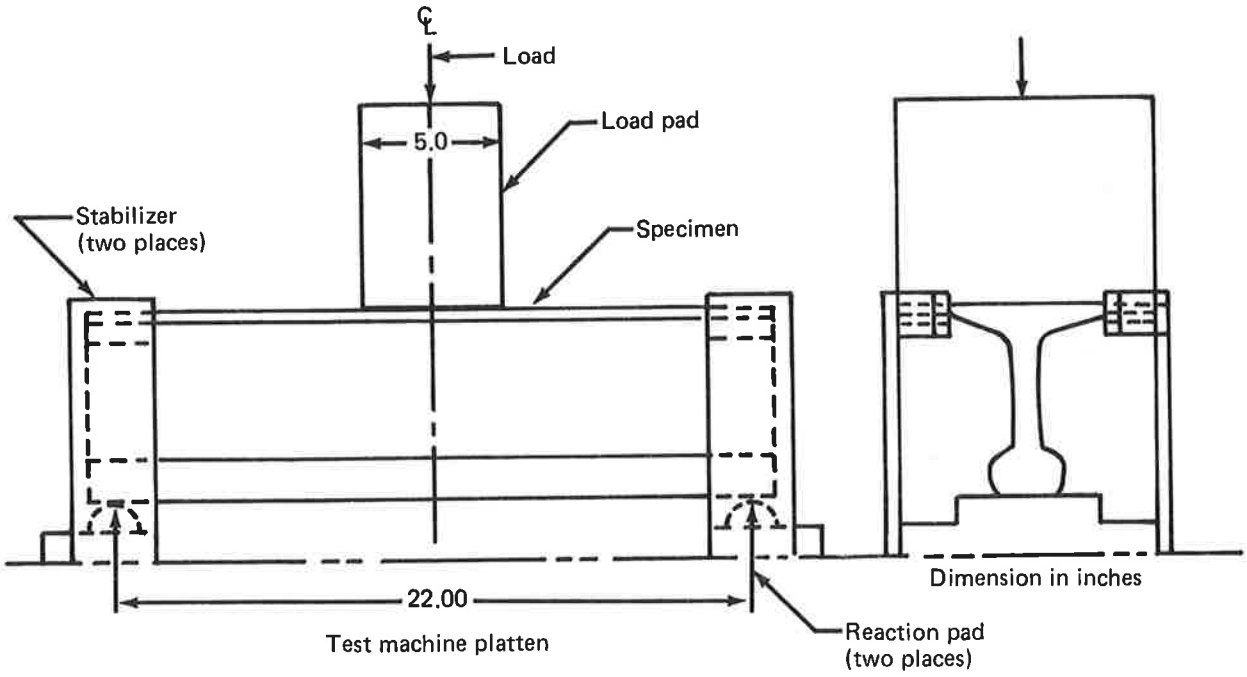

Figure 7.—Load Distribution

P_{max} = 150,000 lb R = .06

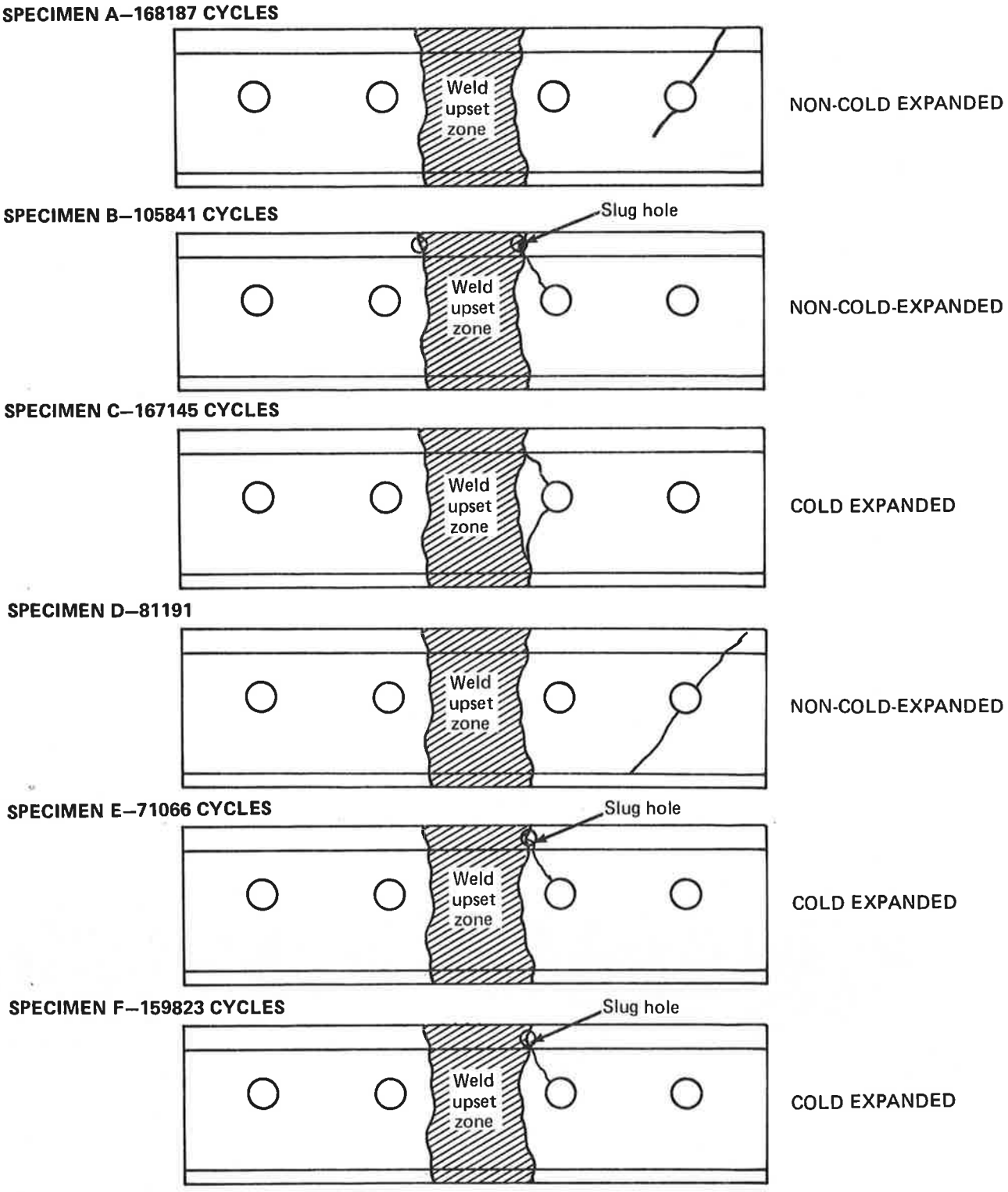

Figure 8.—Failure Locations and Life

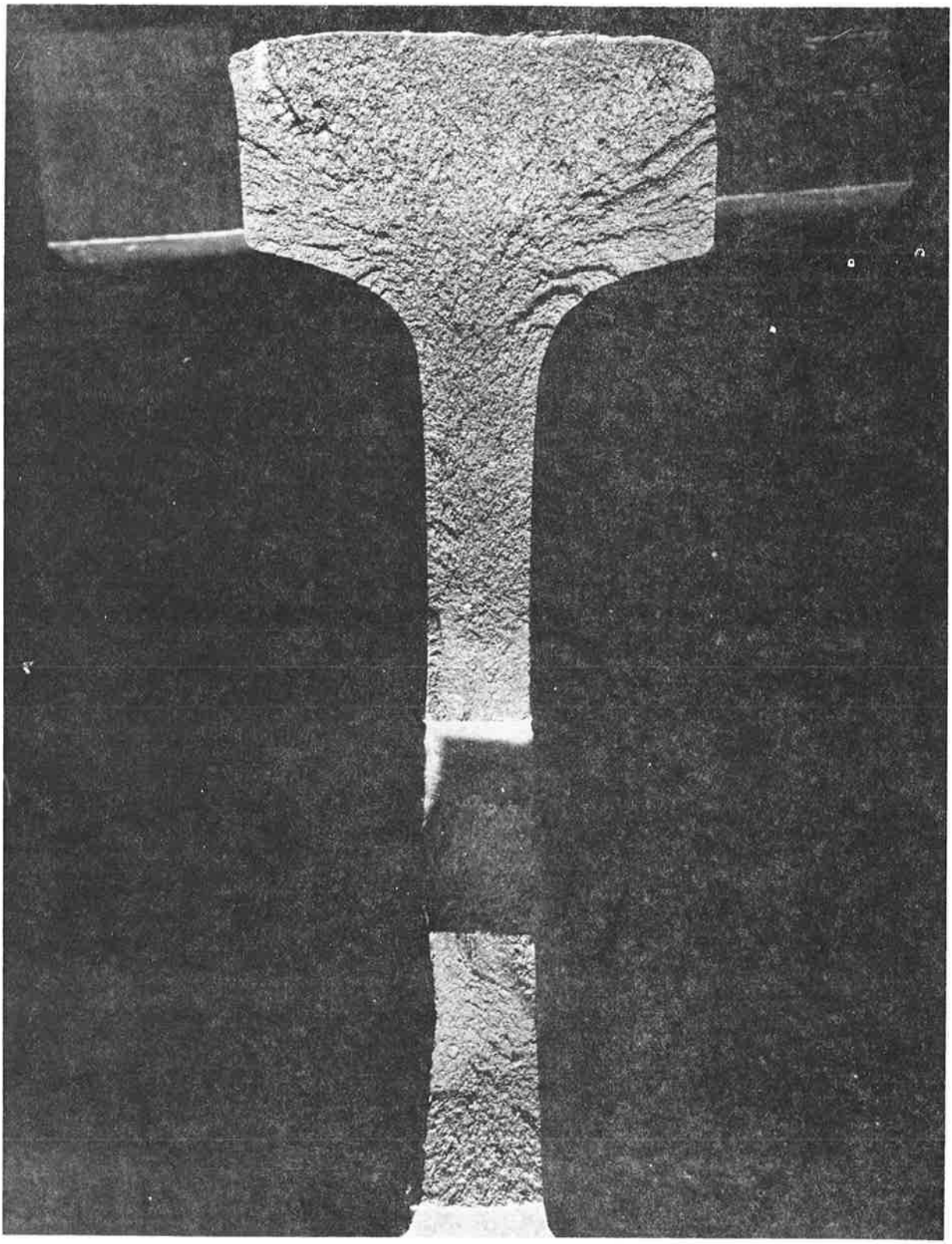

Figure 9.—Failure, Specimen A

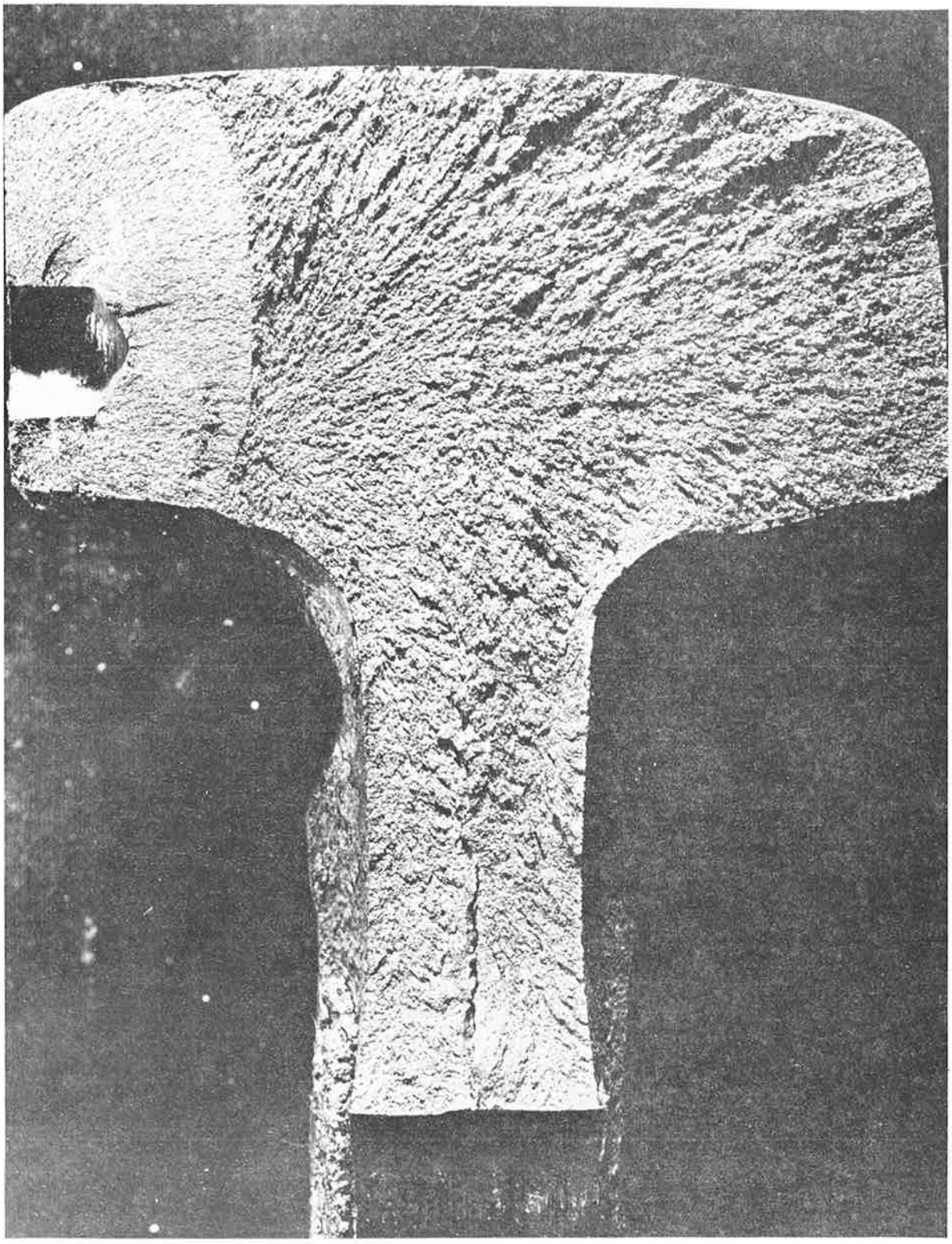

Figure 10.—Failure, Specimen B

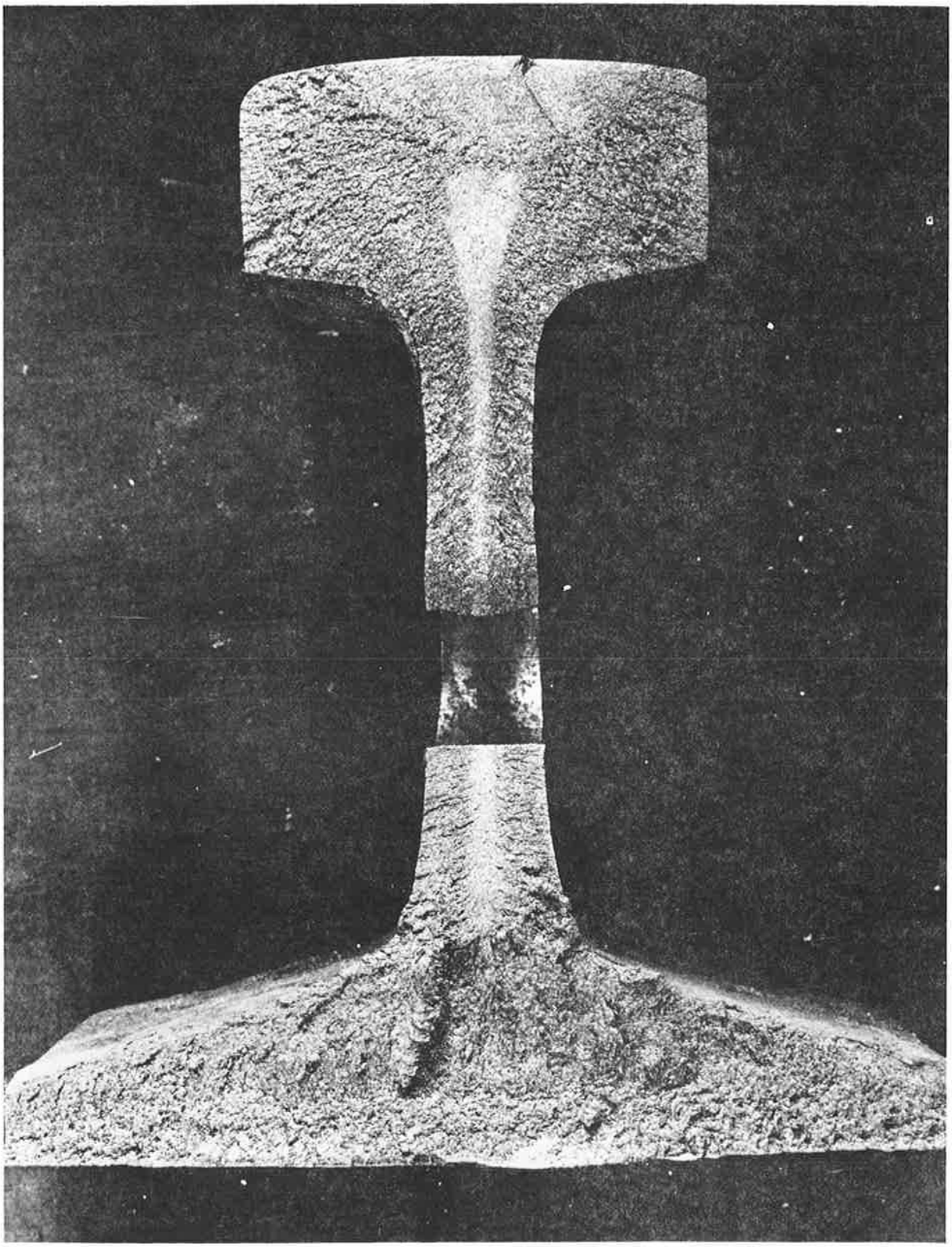

Figure 11.—Failure, Specimen C

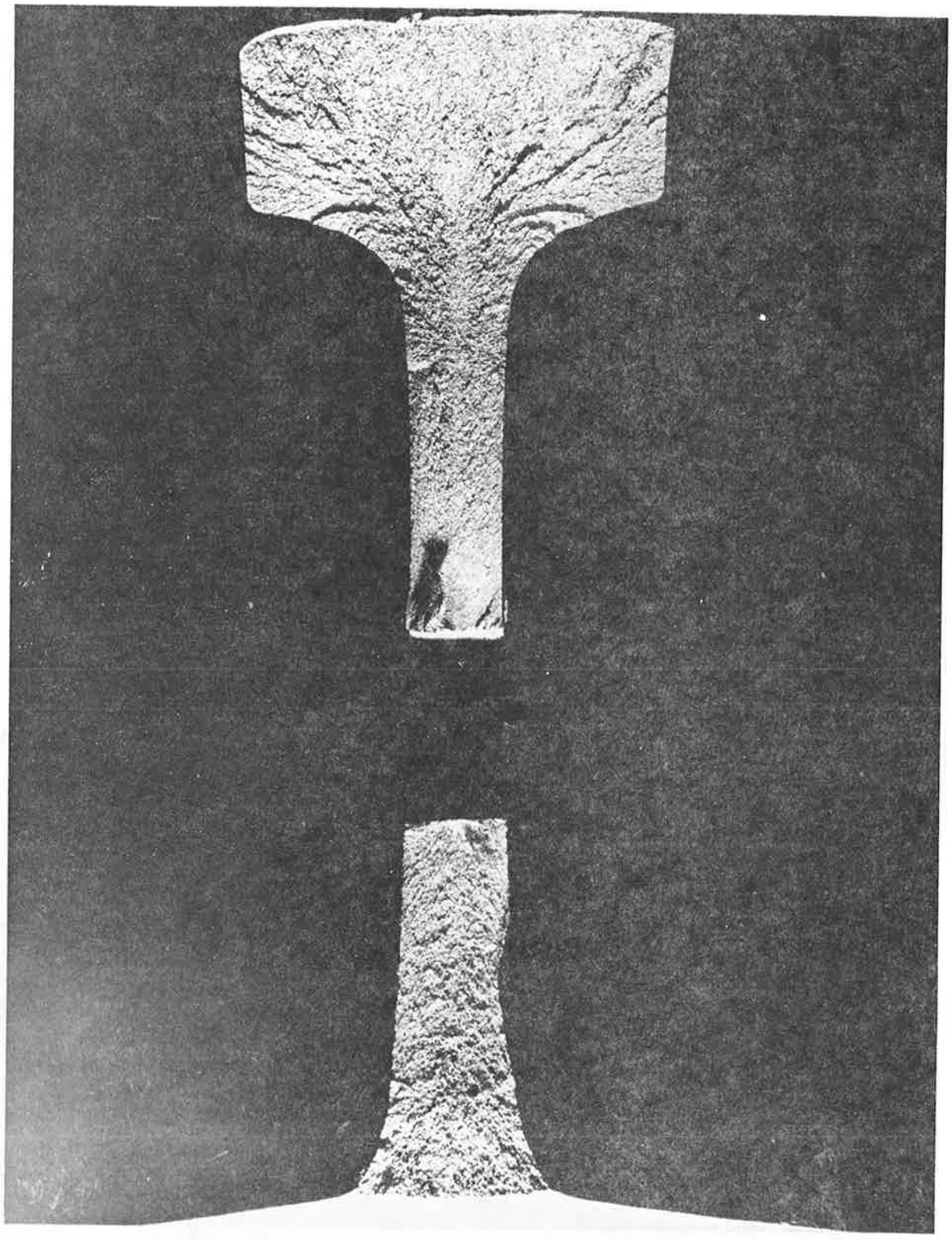

Figure 12.—Failure, Specimen D

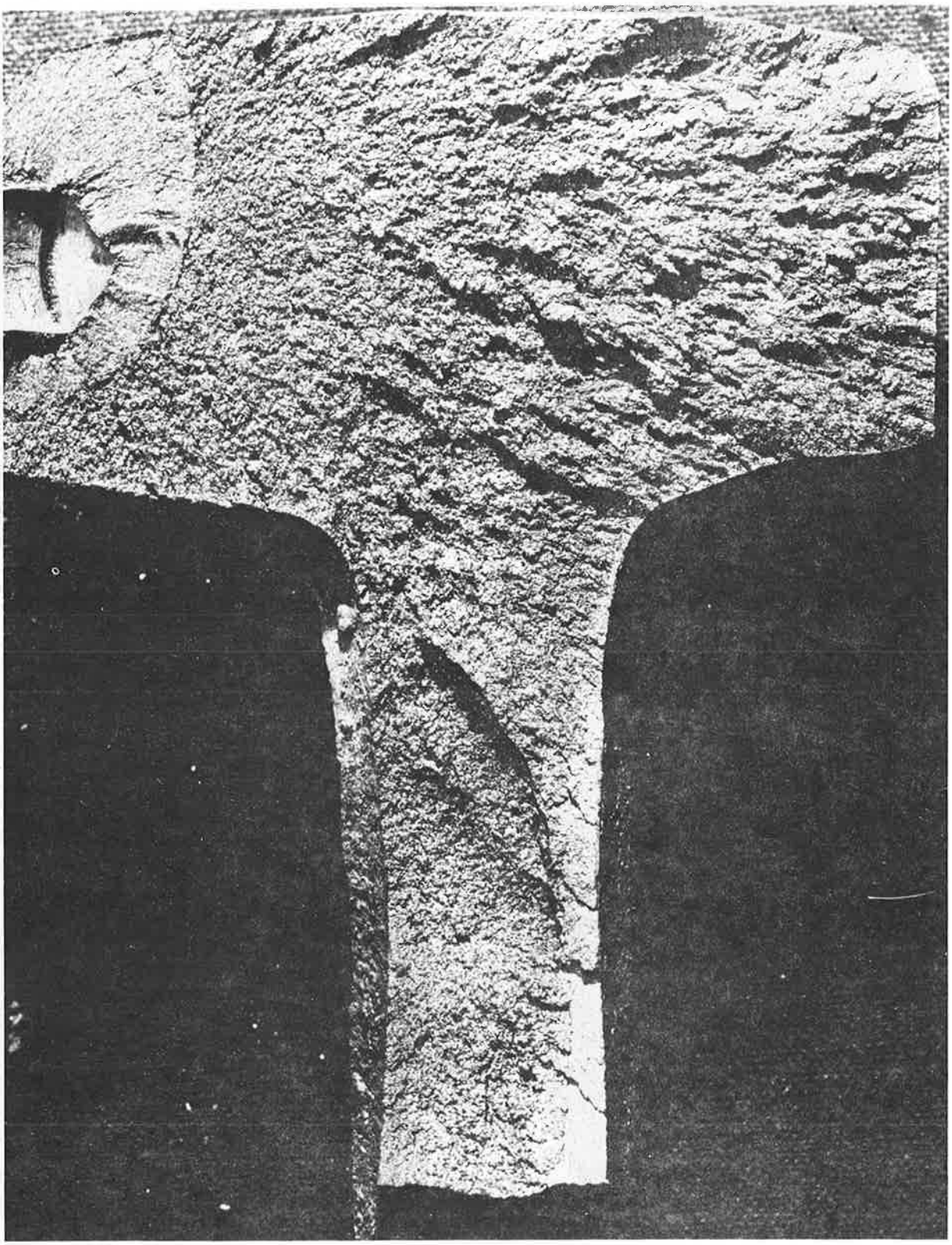

Figure 13.—Failure, Specimen E

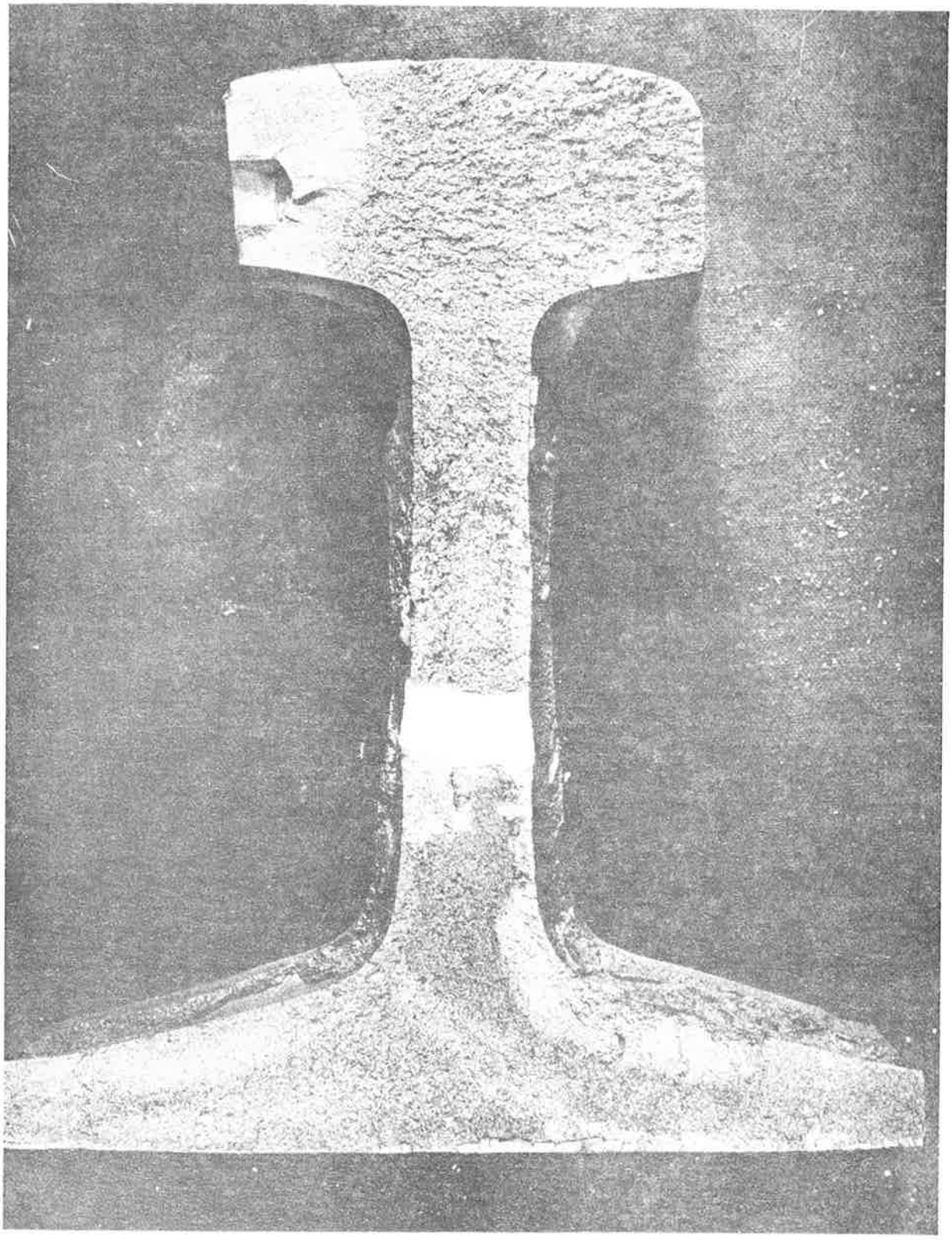

Figure 14.—Failure, Specimen F

5.3 DISCUSSION AND CONCLUSIONS

The narrow fatigue-cycle scatter band (71,066 to 168,187) indicates that each failure initiator has nearly equal impact on welded joint life. If non-cold-expanded specimens are compared, bolt-hole initiation and slug-hole initiation appear to have equal impact on rail life.

As shown in figure 6, the slug hole generally is located in line with the edge of the flashweld upset remaining on the rail web. The natural stress riser created at the edge of the flashweld upset, combined with other surface stress risers such as the slug hole or surface defect (e.g., specimen C), creates a stress concentration as critical to rail life as the untreated bolt hole. When the bolt is cold-expanded, failure initiation is shifted to the weld flash edge, primarily the slug hole.

Where rails containing the slug hole are used with bolted joints, the slug hole is not exposed to the loads experienced in the welded configuration. Also, rail-head batter near the rail end is not as critical to failure mode in the bolted joint as in the welded joint. It is concluded that, if welding is used, some treatment of the rail end in addition to bolt-hole cold expansion is required.

APPENDIX A

ASSOCIATION OF AMERICAN RAILROADS

RESEARCH AND TEST DEPARTMENT

REPORT NO. R-327
(Project No. H-120)

FATIGUE TESTING OF RAIL BOLT HOLES COLD-EXPANDED

BY

BOEING COMPANY

W. J. WISNOWSKI

L. D. FLEMING

AAR TECHNICAL CENTER

Chicago, Illinois

1. REPORT NO.	2. REPORT DATE	3. PERIOD COVERED
R-327	October, 1978	April, 1977-October, 1978

4. TITLE AND SUBTITLE Fatigue Testing of Rail Bolt Holes Cold-Expanded by Boeing Company

5. AUTHOR(S)
M. J. Wisnowski and L. D. Fleming

6. PERFORMING ORGANIZATION NAME AND ADDRESS
Association of American Railroads
Technical Center
3140 South Federal Street
Chicago, IL 60616

7. TYPE OF REPORT
Research

8. CONTRACT OR GRANT NO.
P.O. Y311716-0935 N

9. SPONSORING AGENCY NAME AND ADDRESS
Boeing Commercial Airplane Company
A Division of the Boeing Company
P. O. Box 3707
Seattle, Washington 98124

10. NO. OF PAGES
24

11. NO. OF REFERENCES
1

12. SUPPLEMENTARY NOTES
AAR Metallurgy Division, Project No. H-120

13. ABSTRACT

The Association of American Railroads investigated the improvement in resistance to fatiguing at rail bolt holes by cold expansion of the hole diameter. The specimens were prepared by the Boeing Company using their "Split Sleeve Expansion System" to cold-work the bolt holes.

The loading cycle was selected to simulate the cyclic reversal of flexure of rails in service. However, the loads were much higher than service loads to accelerate fatigue crack nucleation. It was found that the cold-worked specimens failed at other locations before bolt hole failure could occur while un-cold-worked specimens failed at the bolt holes.

14. SUBJECT TERMS	15. AVAILABILITY STATEMENT
Rail Bolt Hole Fatigue	Director, AAR Technical Center 3140 South Federal Street Chicago, Illinois 60616

TABLE OF CONTENTS

LIST OF FIGURES

EXECUTIVE SUMMARY

The Boeing Company performed tests indicating that their "Split Sleeve Expansion System" significantly increased the resistance to fatigue of rail bolt holes under a variety of conditions. The Association of American Railroads conducted tests in which the direction of the applied load was cyclically reversed from downward against the rail head to upward from the base. This loading simulated the flexure of rail under passage of rolling stock more closely than the original loading ranges studied by Boeing. However, the loads were much higher than service loads to accelerate fatigue crack nucleation.

The results of the tests indicated that the improvement of fatigue resistance was maintained in this loading range.

ASSOCIATION OF AMERICAN RAILROADS

RESEARCH AND TEST DEPARTMENT

REPORT NO. R-327
(Project No. H-120)

FATIGUE TESTING OF RAIL BOLT HOLES COLD-EXPANDED BY BOEING PROCESS

INTRODUCTION

Fatigue cracks originating at bolt holes in rails have been a common cause of rail failure. These failures usually occur when joint bars have become loose or in older rails that have been welded in strings where joint bars are not needed.

The Boeing Company has developed a "Split Sleeve Expansion System" which has been proven to reduce bolt hole fatigue as a problem in aircraft parts. This system produces compressive residual stresses around the bolt hole through cold expansion of the hole diameter. The compressive stresses reduce the magnitude of the tensile stress concentration around the bolt hole when the component is subjected to loading. This lower level of stress increases the resistance of the component to fatigue.

Extensive testing was performed by the Boeing Company to adapt their cold expansion system for application to rail bolt holes and to determine the method's effectiveness under a variety of conditions. This work is discussed in Boeing Commercial Airplane Company Report No. D6-44287.

Testing was not conducted by Boeing, however, in a range of loading cycles where the direction of load application would be

reversed. In the test fixture used, the magnitude of the downward load against the rail head, considered a positive load, never was decreased to a negative load, directed upward from the rail base.

The passage of a railroad car produces alternately upward and downward flexure of the rail. Information on the behavior of cold expanded bolt holes under conditions of cyclic load direction reversals is therefore of interest for applications of the system to railroad rails in actual service.

The Association of American Railroads performed tests using such loading conditions on rail specimens prepared by the Boeing Company. However, the loads were much higher than service loads to accelerate fatigue crack nucleation. The work was done under Department of Transportation Contract DOT-TSC-1048.

This report presents the results of the AAR tests.

DESCRIPTION OF SPECIMENS

The four specimens were 112RE sections (55.6 kg/m). Each was 24 in. (0.610 mm) in length with four bolt holes positioned as shown in the schematic of Figure 1. Bolt holes of 1.25 in. (31.8 mm) were drilled into two of the rails and were not cold-expanded. The bolt holes of the other two specimens were drilled with a 1.1875 in. (30.2 mm) diameter and cold-expanded to a diameter of 1.245 in. (31.6 mm) by the sleeve expansion method described in the D.O.T. report. The geometries of the cold-expanded specimens and the non-cold-expanded specimens were therefore nearly identical.

The non-cold-worked specimens were identified as 5A-7 and 6A-8. The cold-worked specimens were identified as 5B-6 and 6B-6.

DESCRIPTION OF TEST

The rail specimen is subjected to a maximum load in the heat-to-base direction of +144,000 lb (641 kN) and a minimum load of -30,000 lb (-133 kN).

In order to produce the negative load, a spring group is situated under the rail base directly below the position at which the downward load is applied to the rail head. The applied load is provided by two Amsler jacks kept in sequence with each other by connection for pressure dumping.

The height of the spring group is adjusted to produce a constant force of -46,000 lb (205 kN) so that the desired maximum and minimum loads on the rail are achieved by cycling the load applied by the jacks between +190,000 lb (845 kN) and +16,000 lb (71 kN).

The test setup is shown in the photograph of Figure 2.

The rail specimen is cyclically loaded between the set maximum and minimum at a frequency of 200 cycles per minute until failure.

RESULTS OF TEST

Specimen 5A-7 (Un-cold-expanded)

A crack was observed through one of the two outer bolt holes after 333,800 loading cycles. The position and extent of the crack was revealed by a dye check as shown in the photograph of

Figure 3. A view of the fracture surface is shown in Figure 4. The crack initiated in fatigue mode on the side of the bolt hole closer to the rail head as indicated by the arrows in Figure 4. The fatigue crack propagated only a small distance before sudden failure occurred.

Specimen 6A-8 (Un-cold-expanded)

A crack was observed after 239,500 cycles. As can be seen in Figure 5, the crack is similar in appearance to the one in specimen 5A-7. However, the crack propagated in fatigue to a considerably greater distance toward the rail head before sudden failure occurred. The fatigue crack is the smoother region of the fracture surface adjacent to the bolt hole in Figure 6. The point of initiation is shown by arrows in that photograph.

Specimen 5B-6 (Cold-expanded)

The rail broke after 442,700 cycles between the two inner bolt holes. The break was complete, as shown in Figure 7. The fatigue crack initiated at the bottom tip of one rail flange and propagated as a sudden failure across the rail. The fatigue crack is the smooth region in the view of the fracture surface in Figure 8.

Specimen 6B-6 (Cold-expanded)

The rail broke after 996,500 cycles. The crack ran through one of the outer bolt holes, as shown in Figure 9. The fracture, however, originated at two stamped characters on the rail web. One initiation site was the letter "O" at the point where it intersects the bolt hole and the other was the numeral "2". These

characters can be seen more clearly in the close-up view of the rail in Figure 10.

The fatigue pattern can be seen converging at the "O" in Figure 11. At this point of initiation, the identation of the stamping serves as a stress raiser in addition to the edge of the bolt hole. Therefore, had the bolt hole not been cold-expanded, this rail might have failed at a far lower number of cycles than did the un-cold-expanded specimens tested. The cold expansion greatly increased its endurance over that of the un-cold-expanded specimens even with the presence of the double stress raiser. It should also be pointed out that the first initiation site of the fatigue crack was probably at the stamped numeral "2" away from any bolt hole. This is shown in Figure 12.

CONCLUSIONS

The cold expansion of the bolt holes produced the expected improvement in fatigue endurance. Failure of the cold expanded specimens was due to factors other than the presence of the holes while failure of the un-cold-expanded specimens was a direct result of the bolt holes.

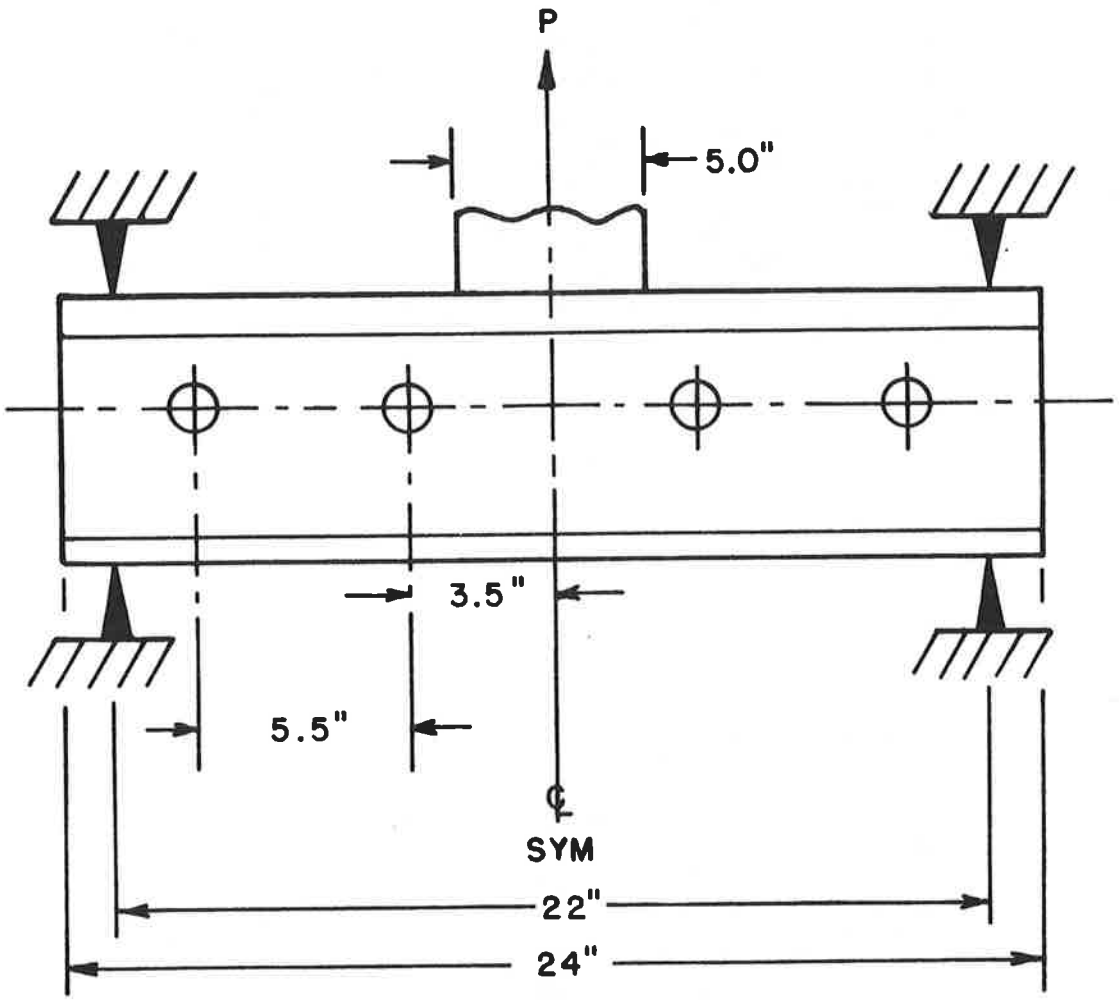

Figure 1.—4-Hole Rail Specimen Load Arrangement

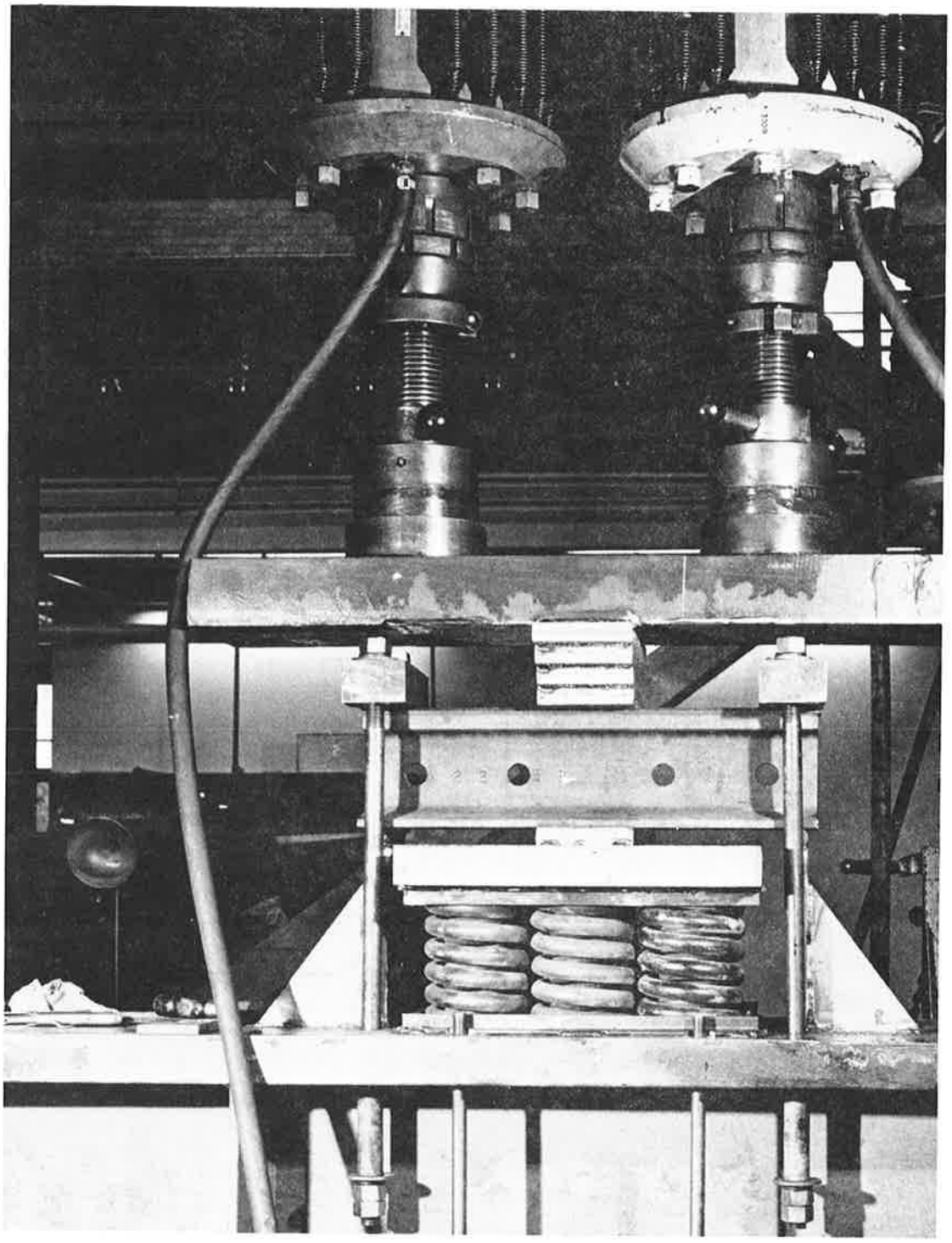

Figure 2.—Photograph of Test Setup

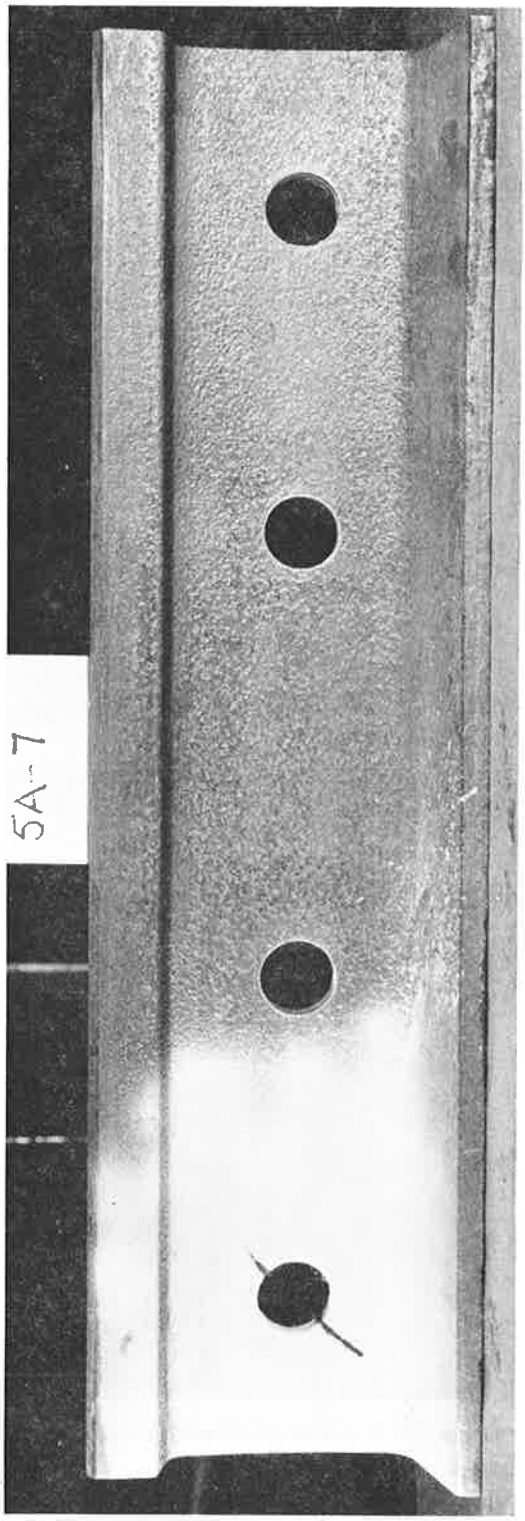

Figure 3.–Specimen 5A-7: Side View after Failure

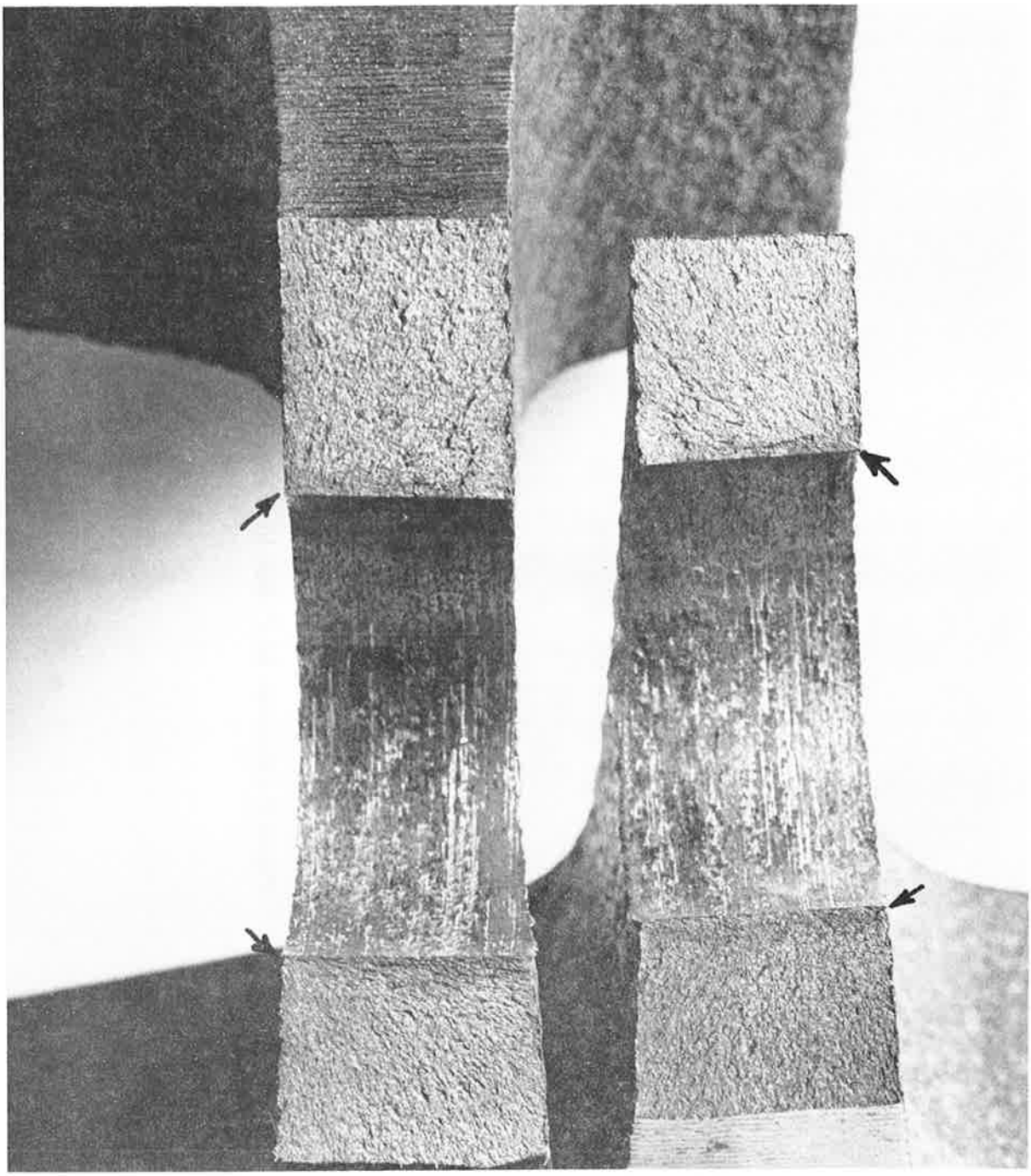

Figure 4.—Specimen 5A-7: View of Fracture Surface. Point of Fracture Initiation Indicated by Arrows

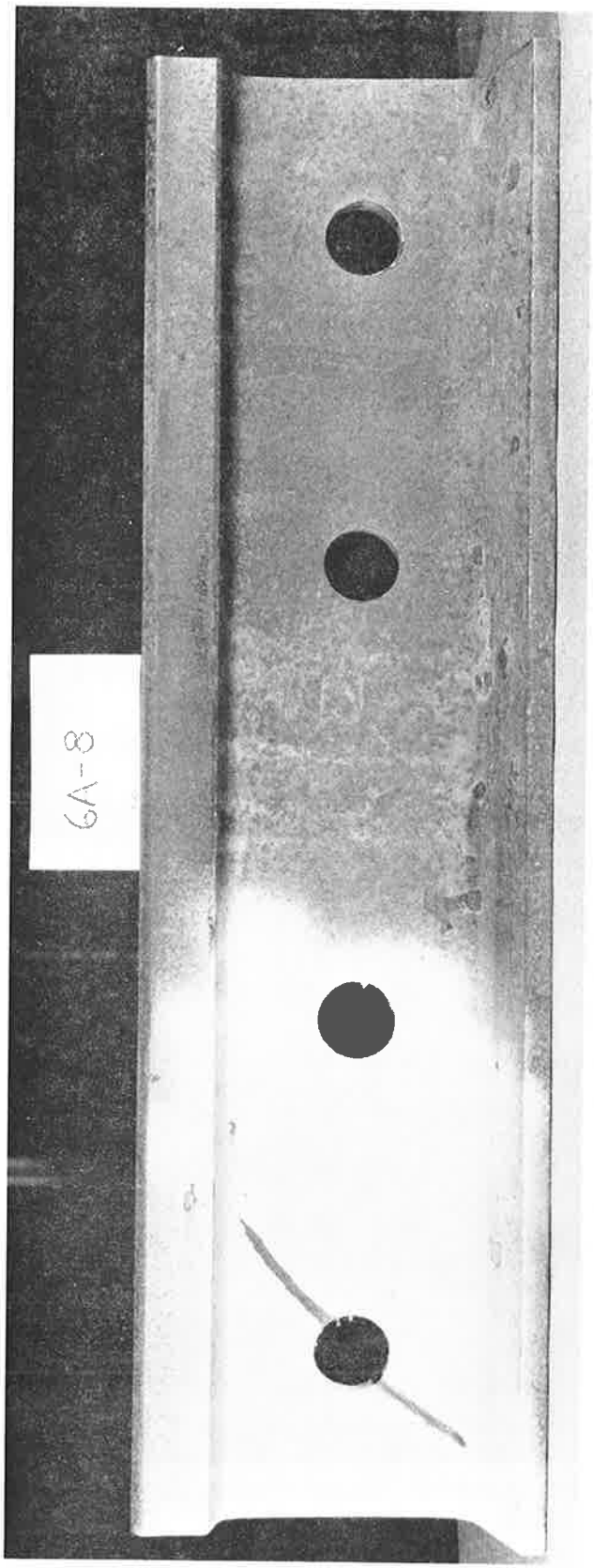

Figure 5.–Specimen 6A-8: Side View after Failure

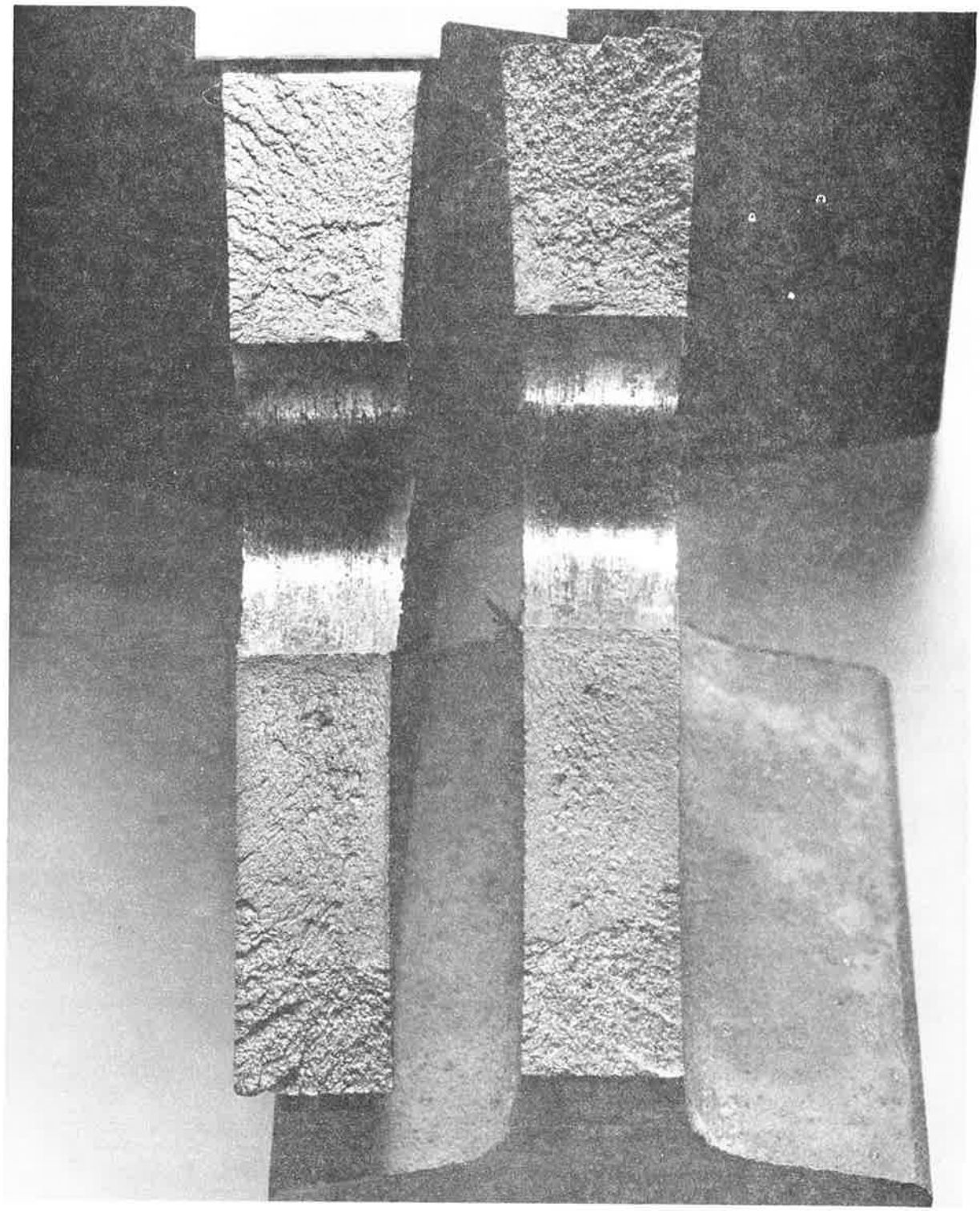

Figure 6.—Specimen 6A-8: View of Fracture Surface. Point of Fatigue Initiation Indicated by Arrows

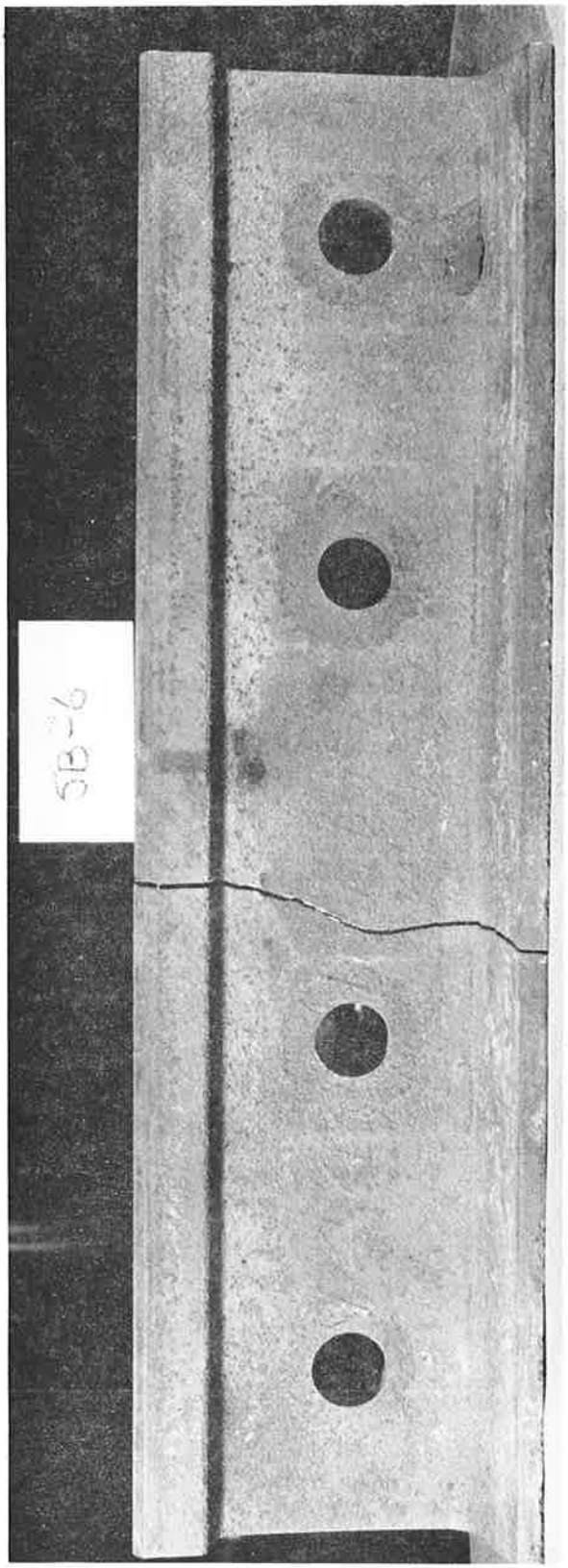

Figure 7.–Specimen 5B-6: Side View after Failure

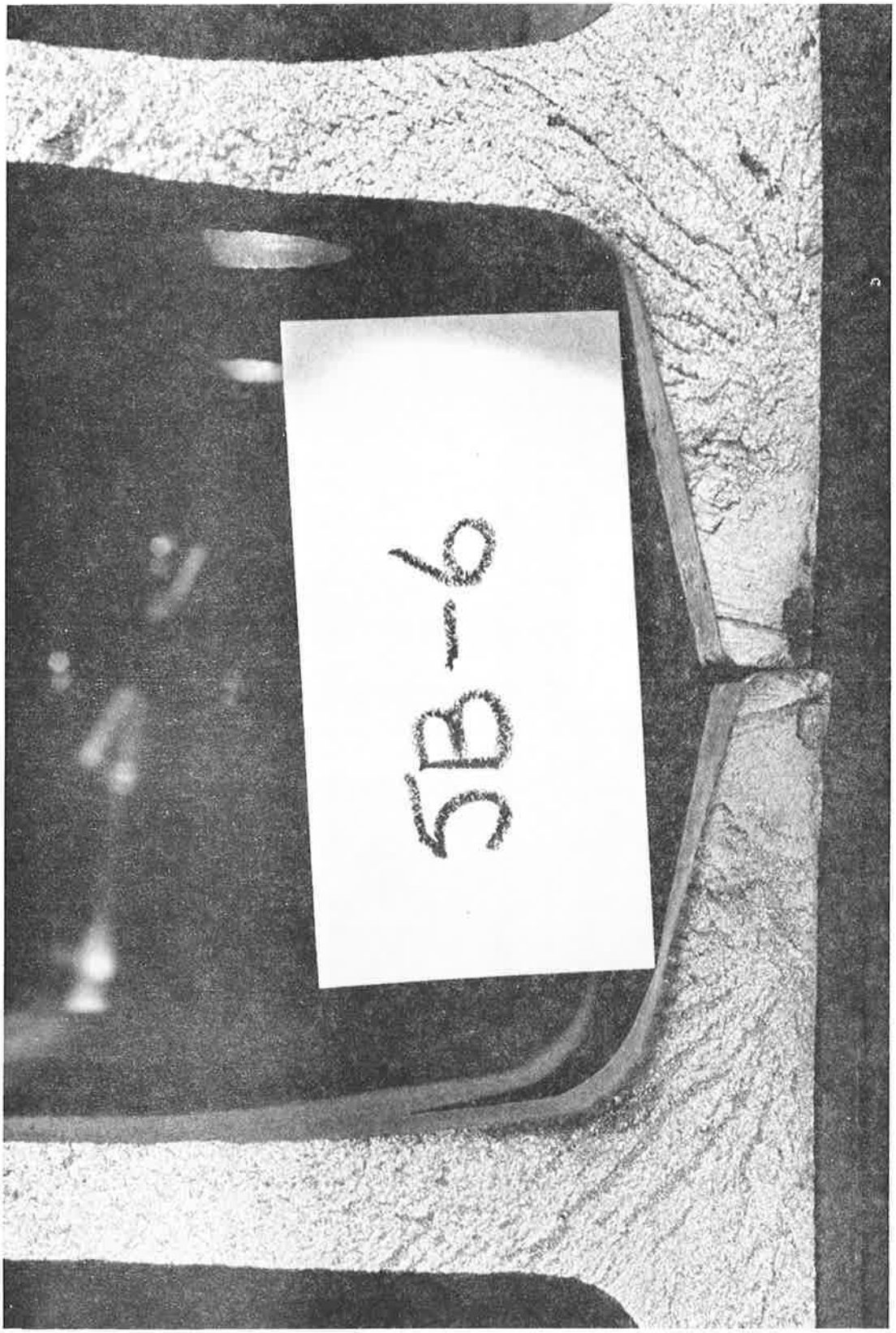

Figure 8. —Specimen 5B-6: View of Fracture Surface

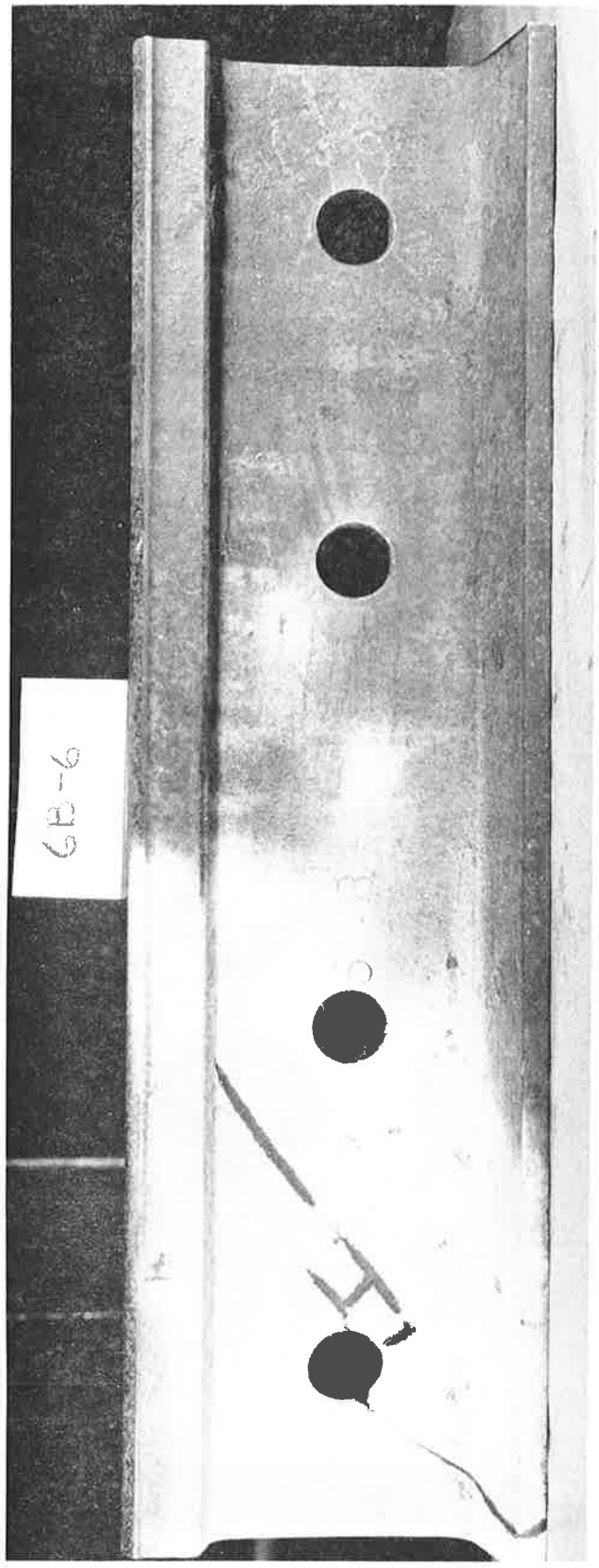

Figure 9.—Specimen 6B-6: Side View after Failure

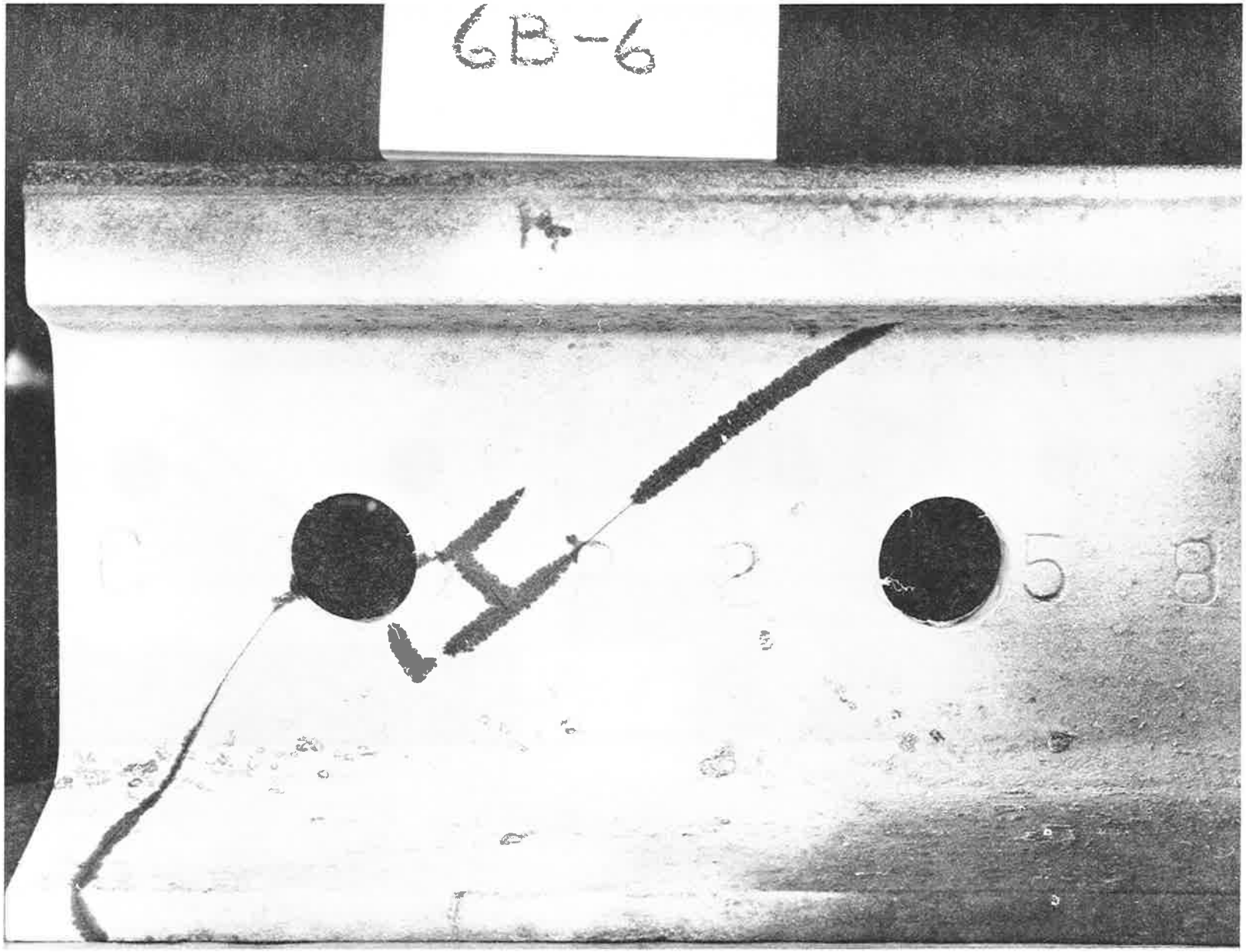

Figure 10.—Specimen 6B-6: Close-Up of Crack. The Two Points of Failure Origin Indicated by Arrows.

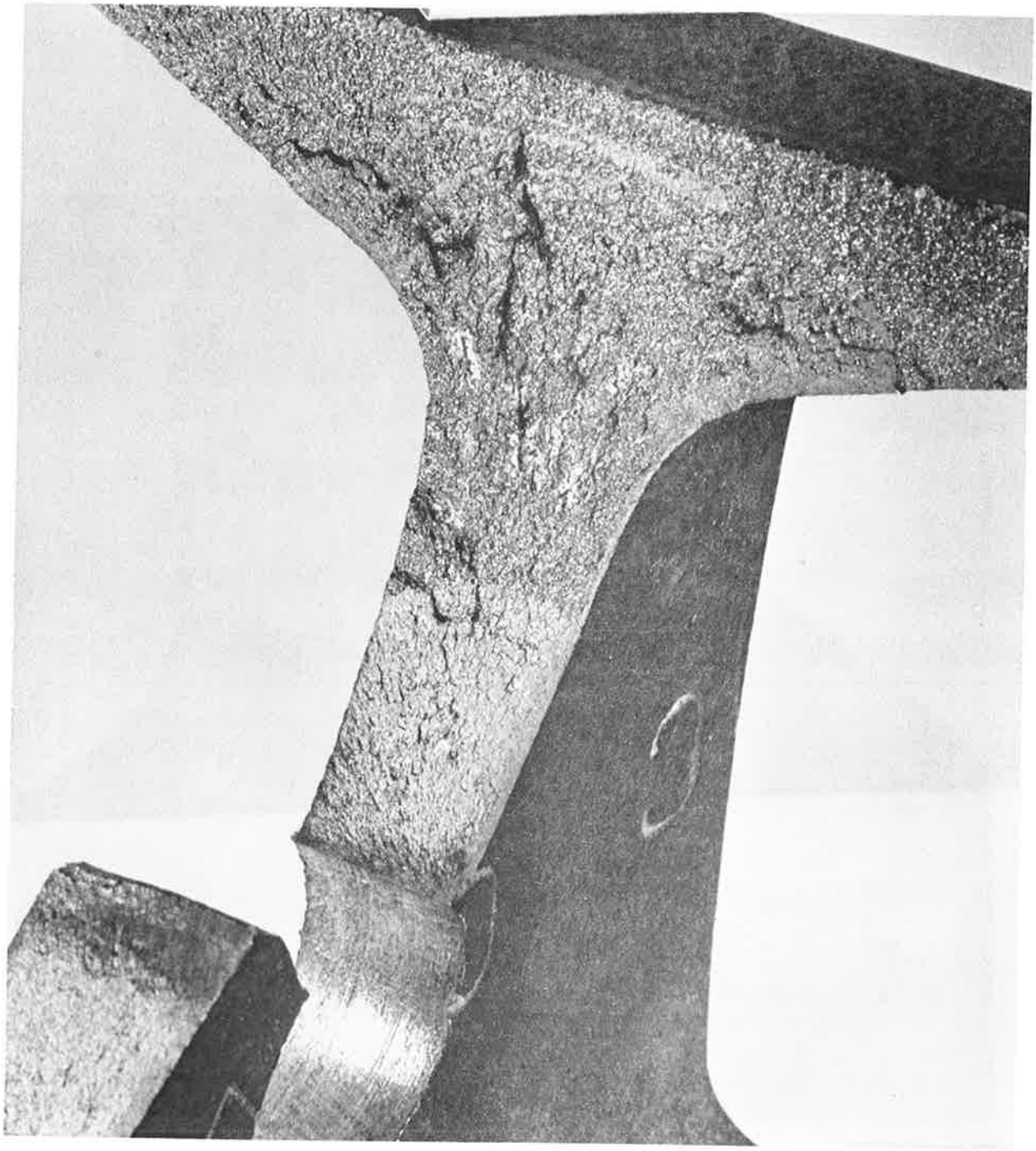

Figure 11.– Specimen 6B-6: View of Fracture at Bolt Hole

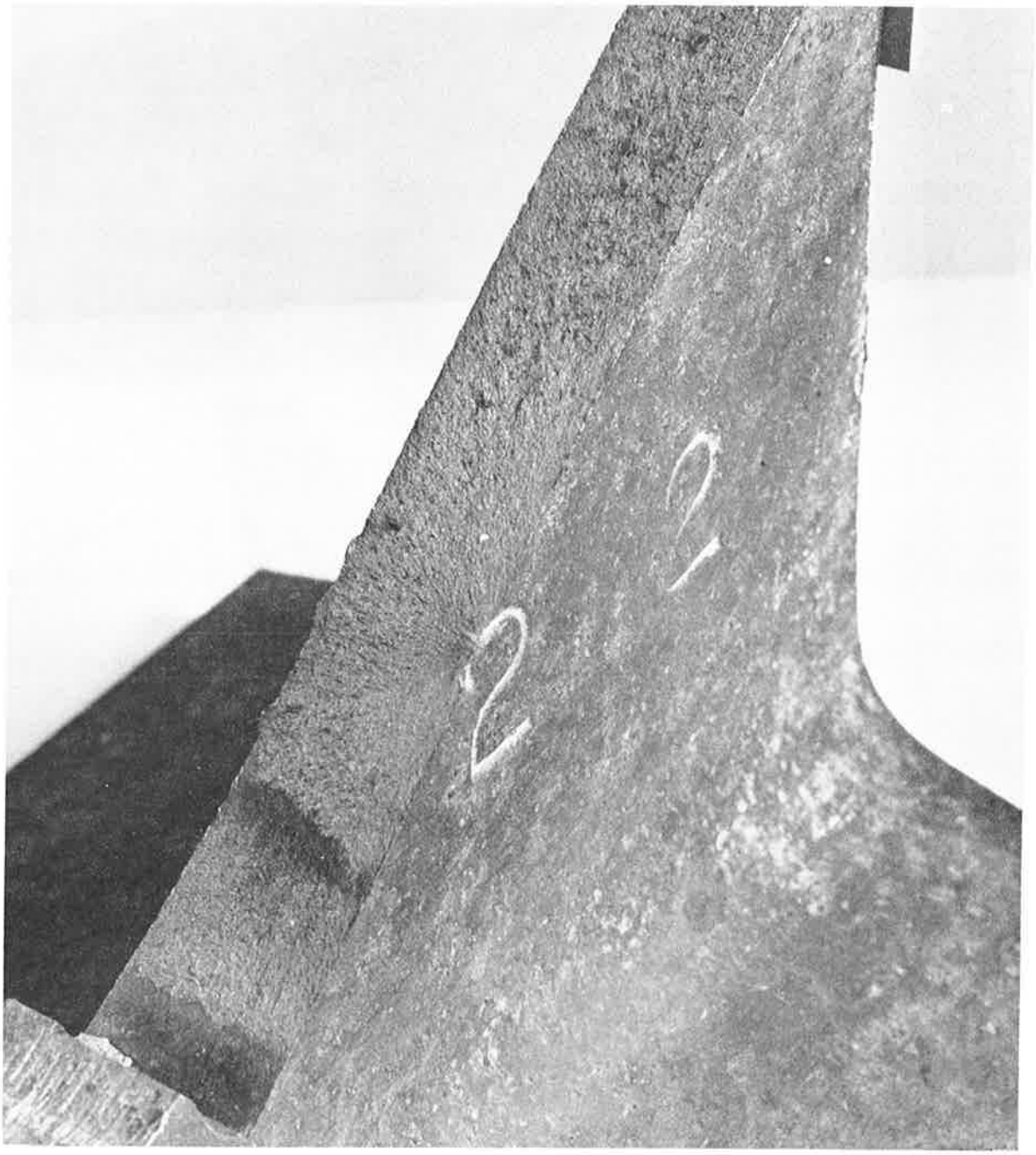

Figure 12.—Specimen 6B-6: View of Fracture Surface Near Primary Origin

SI CONVERSION FACTORS
(Taken from ASTM E380)

To Convert From	To	Multiply By
Inch (in.)	Metre (m)	2.540000 E-02
Pound-Force (lbf)	Newton (N)	4.448222 E+00

APPENDIX B

AN ASSESSMENT OF THE FATIGUE CRACK GROWTH PROPERTIES OF RAIL STEELS IN VACUUM

A report prepared for The Boeing Commercial Airplane Company under Contract Y 311 683-0935N by C.J. Beevers.*

* Department of Physical Metallurgy and Science of Materials, The University, Edgbaston, Birmingham, B15 2TT, U.K.

CONTENTS

FIGURES

1. INTRODUCTION

There have been several studies of the fatigue crack growth behavior of medium carbon pearlitic steels (1-6). These investigations have shown that the growth rates of fatigue cracks can be influenced by microstructure, yield stress, and R ratio. An example of the influence of R ratio on the log ΔK v. log da/dn plots for an 0.55C 1.5% Mn steel is shown in Fig. 1. It should be noted that this data refers to tests carried out over an extensive but low ΔK range and that the growth extends to values as low as 10^{-8}mm/cycle. The R effect is much reduced at intermediate ΔK values. The presence of high manganese >2% can lead to the formation of martensite on air cooling from 900 or 950^{o}C. The martensite was shown (6) to lead to a limited ΔK growth range and to rapid crack growth at reduced values of K_{max} (Fig.2). Examination of fracture surfaces at a macroscopic level of all pearlitic steels showed that for specimens tested in laboratory air, there were extensive deposits of corrosion products on the surface. Metallographic sectioning and SEM studies showed that fatigue crack growth in air in these pearlitic steels occurred by a mixed mode involving cracking of cementite/ferrite interfaces, carbide lamellae and pearlite colony boundaries.

More recently Federson et al. (7) have tested a range of rail steels over the ΔK range 20 to 50 ksi $\sqrt{in}$. Fowler (8) has also examined the fatigue crack growth behaviour of rail steels over a wide ΔK range and has shown that the presence of free ferrite in the microstructure tends to reduce the fatigue crack growth rate. The specific role of the air environment in influencing the mode of crack growth and the crack growth rates was not ascertained.

This report is concerned with the response of rail steels to cyclic loading under the relatively inert conditions of a

vacuum of 10^{-5}torr. Two rail steels have been tested over a range of R ratios and the crack growth characteristics established. Detailed examination of the fractured samples has been carried out in an attempt to identify the modes and mechanisms of fatigue crack propagation in an inert environment.

2. RAIL STEELS

Two rail steels designated A and B were provided. A was 110 lbs/yd and B 80 lbs/yd. Two separate samples were taken from the head of each rail for chemical analysis, the results of these tests are presented in Table 1.

2.1. Test Specimens

Compact Tension test specimens were machined from the rails in the mode illustrated in Figure 3. This permitted the study of crack growth within material from the head of the rail. The dimensions of the specimens for steel A and B are presented in Figure 4.

2.2 Microstructure of Rail Steels

Metallographic sections from the head of rail steel A were prepared and are illustrated in Figure 5 (a) (b) and (c). The micrographs show elongated inclusions in the xx-yy and yy-zz planes, generally in the yy direction. Thin films of ferrite are also present in the microstructure, presumably formed at the prior austenite grain boundaries. The pearlite colonies are well resolved with a fine pearlite content. No packets or islands of coarse pearlite of other microstructures such as martensite were observed.

Metallographic sections of Steel B were also prepared and

presented in Figure 6 (a) (b) and (c). Continuous ferrite films were observed in the microstructure with large inclusion and elongated in the yy direction. The pearlite was much coarser than in steel A and can be resolved within the individual colonies even at a magnification of x 250. If we assume that the ferrite formed by precipitation at the prior austenite grain boundaries then the prior austenite grain size was in the region of 0.15mm.

2.3. Mechanical Properties of Rail Steels

Tensile test specimens were machined from Rail A and Rail B. Dimensions of the specimens are presented in Figure 7. The tensile axis of the test piece was parallel to the direction yy. The specimens were tested on an Instron Universal Testing Machine at a cross head speed of ~0.5 cm/min and at a temperature of 20°C. The results from these tests indicating the strength and ductility of the rail steels are presented in Table 2.

3. PROCEDURES FOR THE TESTING OF THE COMPACT TENSION SPECIMENS

The specimens were prepared for testing using the following procedure. The surfaces of the specimens ahead of the notch were polished to a 1 um diamond finish and lines 1 mm apart were scribed on the surface using a sharp cutting point. The current leads and potential probes were attached on the front face of the specimen. The current leads are 12 mm apart and the potential probes 4 mm apart.

3.1. Crack Length Measurement

The crack lengths are measured on the surface of the specimen optically and by the potential drop method.

Figure 8 shows a schematic illustration of the equipment and circuits used in the measurement of potential changes in the specimen. In the tests carried out in this program the specimen temperature was that of the laboratory air temperature i.e. $20^{o}C \pm 2^{o}C$. The specimen was electrically insulated from the testing machine obviating the possibility of ground loops or alternative current paths by the use of Tufnol annuli in the loading columns. Soft iron wires coated in PTFE were spot welded onto the test piece 1 mm either side of the crack. The spot welds were supported by the application of an expoxy resin. The iron wires were spot welded to screened copper cable and the junctions held in an aluminium block to minimise thermal effects. A constant current of 30 amps was supplied to the specimen from a Farnell Instrument current source. The potential difference between the probes on either side of the crack was measured using a Keighley Instrument Model 155 Null Detector Microvoltmeter with fullscale range from 1 uV to 1,000 V. A Keighley Instrument Model 260 Nanovolt source is used to back off sufficient of the output from the probes to enable the microvoltmeter to be used on a sufficiently sensitive range. The output from the microvoltmeter passed through a C-R damping circuit to reduce excessive noise and was then fed into either an X-Y or strip chart recorder. For the present work the change in potential between the probes for a millimeter of crack growth was in the range 35 to 55 uV. The system had a long term stability of ±1.5 uV. Crack lengths from the changes in potential were obtained from a potential versus a/W calibration.

3.2. Testing Facility

The specimens were tested in an Ansler Vibrophone at a frequency of ~90Hz. The wave form of the loading profile was approximately sinusoidal. Cracks were initiated from the notch

at K_{max} levels of ~25 $MNm^{-3/2}$ and a systematic load reduction procedure was employed to obtain sharp fatigue cracks. This procedure involved load reductions intervals such that the crack grew approximately four times the size of the maximum plastic zone associated with the crack at the previously higher load level. This procedure minimised possible stress history influences as established in earlier work [4,5]. The threshold stress intensity level ΔK_{th} was associated with a growth rate of $\sim 10^{-8}$ mm/cycle. To establish a ΔK_{th} value involved a minimum of 2×10^{7} load cycles. The threshold was obtained in the a/W range 0.36 to 0.45. Subsequent crack growth extended the crack from the threshold region and this was normally achieved under constant load ratio conditions.

The vacuum tests were carried out in a vacuum chamber, the outline of which is illustrated in Figure 9. The chamber is pumped by a rotary and oil diffusion pump with a liquid nitrogen trap. This arrangement permitted long term tests to be carried out with a vacuum of better than 10^{-5} torr. The exclusion of water vapor and other vapors by the use of a liquid nitrogen trap has been found to be extremely benefical as a means of maintaining an inert environment.

4. FATIGUE CRACK GROWTH DATA

The data to be presented in the section was obtained from specimens tested over a range from threshold to accelerated growth with associated pop-ins.

4.1 Steel A tested in Laboratory Air

The results obtained from the fatigue crack growth in laboratory air of steel A at R = 0.75 and R = 0.08 are presented in the form of $\log \frac{da}{dN}$ versus $\log \Delta K$ and $\log K_{max}$ respectively in

Figures 10 and 11.

4.2 Steel A tested in Vacuum

Specimens A 05 to A 09 were tested in vacuum ($.<10^{-5}$ torr) at R ratios of 0.76, 0.11, 0.27, 0.67 and 0.45. The log $\frac{da}{dN}$ versus log ΔK and K_{max} plots are presented in Figures 12 and 13 respectively.

4.3 Steel B tested in Vacuum

Specimens B 02, B 03 and B 04 were tested in vacuum at R ratios of 0.78, 0.12 and 0.45 respectively. The log $\frac{da}{dN}$ versus log ΔK and log K_{max} curves are presented in Figures 14 and 15 respectively.

5. MACROPHOTOGRAPHS OF FRACTURED SPECIMENS

5.1 Steel A tested in Air

Macrophotographs of specimens A 03 and A 04 tested in air at R = 0.75 and 0.08 respectively are presented in Figure 16.

5.2 Steel A tested in Vacuum

Macrophotographs of specimens A 05 and A 08 are presented in Figure 17 (a-d). A macrophotograph of specimen A 09 is presented in Figure 18.

5.3 Steel B tested in Vacuum

Macrophotographs of specimens B 02, B 03 and B 04 are presented in Figure 18 b c and d.

6. METALLOGRAPHIC SECTIONS OF FRACTURED SPECIMENS

Specimens after fatigue and monotonic fracture were sectioned so that the plan xx-yy (Figure 3) at the midsection thickness and containing the fracture edge could be examined. Good edge retention of the fracture faces was considered an important feature of this part of the investigation. Figures 19a and 19b illustrate the path taken by the fatigue cracks as demonstrated by the behaviour of the branch cracks. Crack growth parrallel to the pearlite lamellae, cutting across pearlite colonies and around pearlite colonies can be identified. At the low R ratios the extent of fatigue crack branching was much reduced compared with the behavior observed in specimen A 05. An example of the fatigue fracture surface and a branch crack is illustrated in Figure 20.

In steel B the ferrite films - pearlite interface offered an alternative crack propagation route. The various routes of crack propagation in steel B specimen B 02 are illustrated in Figures 21 and 22. Note the discontinuous nature of the branch crack in Figure 21. In Figure 23 the branch crack has grown through the ferrite and pearlite. The crack path was insensitive to the presence of inclusions and this is also illustrated in Figure 23. This behaviour was also observed in steel A.

The metallographic section of A 05 examined in the light microscope was also investigated by scanning electron microscopy. Figures 24 and 25 illustrate the growth of fatigue cracks parallel to and across pearlite lamellae. In Figure 25 fracture in the ferrite ahead of the crack tip whilst maintaining the cementite lamellae intact can be detected.

7. SCANNING ELECTRON MICROSCOPE (SEM)

OBSERVATIONS OF THE FATIGUE FRACTURE SURFACES

7.1. Steel A tested in Air

Specimen A 03 and A 04 after fatigue and final separation were sectioned to provide the fracture face for examination in the SEM. Figure 26 illustrates the fatigue fracture morphology in the initiation region. The furrow or ribbed appearance in this micrograph is a most common feature on most specimens examined and is attributed to the mode of fracture associated with the Lameller nature of the pearlite microstructure. Figures 27 to 31 illustrate the various features at initiation, threshold, low growth rates and intermediate growth rates. The underlying microstructure in the form of the pearlite colonies and the lamellae microstructure is never far away from the impression given by the fracture surface.

7.2. Steel A tested in Vacuum

Specimens A 05, A 06, A 07, A 08 and A 09 were closely examined over the whole fatigue crack growth range and examples of characteristic areas will be presented in this section. Figures 32 to 41 show characteristic fracture surface morphologies, there was no discernible change of morphology with R ratio. A feature observed on the vacuum tested specimens was that of the fissure striation (Figure 32, 36, and 39). The fatigue fracture surfaces also revealed detailed structural features at the threshold (Figures 33, 34 and 37). This was quite different from the air tests where corrosion products prevented detailed study. Figure 38 shows the presence of a branch crack and one interpretation of this micrograph is that the crack propagated around and across the pearlite colonies.

7.3. Steel B tested in Vacuum

The fatigue fracture surfaces of specimens B 02, B 03 and B 04 were examined in detail in the SEM. The presence of the ferrite films in microstructure of steel B are clearly evident in the micrographs (Figure 42, 45, 46). The furrow or ribbed structure was not as apparent in Steel B as in Steel A. The fissure striations were observed (Figure 44) and in Figure 47 the microstructural sensitive crack growth morphology as reported previously for steels (4, 5, and 6) can be recognised.

8. DISCUSSION

The major feature of the log da/dN versus log ΔK curves is the effect of environment on the R dependence. The results in Figs. 10-15 and the information in Table 3 illustrate the degree of this R dependence. Comparison of the macrophotographs of steel A tested in air and vacuum (Figs 16-18) show that the extent of surface corrosion products was markedly diminished by the inert environment of the vacuum chamber. It is reasonable to assume therefore that environmental activity at the crack tip was not a primary factor in the R dependence of the growth curves for tests in vacuum. In steel A tested in air the R dependence was similar to that observed previously (4,5). The effect of the inert environment was to raise the threshold ΔK values for the high R tests, that is, from 3.8 MN $m^{-3/2}$ to 5.2 MN $m^{-3/2}$. The influence of environment at the lower R range appears to be less marked than at the high R range in steel A. In general however, the effect of an inert environment on steel A was to reduce the R dependence of the ΔK threshold values and also the crack growth rates.

In steel B (Figs 14 and 15) the growth rate curves exhibit a much less marked R dependence than steel A. Fowler (8) found that a steel containing free ferrite had a reduced growth

rate when compared to a fully pearlitic steel. Comparison of steels A and B show that this feature did not reveal itself in the results for inert environments. The threshold ΔK for the low R in steel B was somewhat less than that for steel A. In general steel B might seem to be behaving in a way that previous results would predict (9) whilst steel A is somewhat anomalous. The rationale for this statement comes from the observations on low carbon ferrite (10), aluminium alloys (11), titanium alloys (12) which have shown clearly that the R dependence of fatigue crack growth in vacuum is such that the value of γ in the relationship

$$K_{th} = K_{tho} (1-R)^{\gamma}$$

approached zero. One view (9) of the difference between air and vacuum tests was that the air environment introduced additional crack growth modes and allowed growth to continue to lower stress intensity levels. This point cannot be fully resolved for the steels because of the corrosion products formed during the air tests. However, as indicated earlier macroscopic examination revealed a marked difference between the air and vacuum tests with the implication that environmental attack was limited in the vacuum tests.

An alternative explanation of the relatively strong R dependence of steel A (Figs. 12 and 13) is the role of fatigue crack closure. There was direct evidence for closure during the low R tests but no quantitive measure of its magnitude in terms of length of crack closed or closure load. The evidence for closure came from the behaviour of the p.d. system. When the test was stopped and the load reduced the crack length apparently diminished, this is a common feature and the p.d. returns to its original value on reapplication of the load. However, in this case substantial numbers of cycles (up to 500,000) were required to achieve the crack length at the point

of load reduction. This behaviour would indicate that welding of the crack faces near the tip occurred and that the crack had to be regrown through this region. The reason for this behaviour was the presence of crack closure forces and the presence of crack closure forces would lead to a K_{max} or R dependence in the fatigue crack growth characteristics. Why this should be particularly so for a pearlitic steel is not clear at the present time. However, in some coarse grained titanium alloys (13) the R dependence in vacuum is sustained and this is attributed to the role of fatigue crack closure.

The metallographic sections and fractographic observations revealed several features which have not been reported previously in pearlitic and pearlitic/ferritic steels. The presence of fissure - striations was a general feature for steel A and B and occurred over a wide K range (Figs. 32, 36, 39 and 44). There was no conclusive evidence that the striations were associated with individual load cycles. In general terms they support a view of growth which involves reverse plasticity at the crack tip. Whether this mode of growth can be generalised to all conditions of crack orientation with respect to the pearlitic-ferrite microstructure is open to question. Nevertheless, the identification of a reverse plasticity mode which must always be in competition with brittle striations and cleavage fatigue is of interest in a microstructure where ferrite/cementite and ferrite/pearlite interface separation could play an important role. The details of this mode of crack extension are not entirely clear. In Fig. 25 and Fig. 49 a micrograph and a schematic illustration of a crack growing across pearlite lamellae are presented. The ferrite is clearly fracturing ahead of the crack tip leaving intact the cementite lamellae. This clearly involves a discontinuous mode of crack extension which could not be modelled on a simple reverse plasticity concept. As well as crack growth through pearlite

lamellae it was observed to occur parallel to the lamellae (Fig 24) and also at the pearlite colony boundaries (Figs 19 and 20).

In steel B an additional mode of crack growth namely separation at ferrite/pearlite interfaces was observed (Fig 22). Crack growth also occurred through the ferrite films as seen in the SEM micrographs (Fig 42). The crack path did not appear to have particular preferences and crack propagation occurred in the pearlite, ferrite and at the ferrite interfaces.

Inclusions were present in both steel A and B. There was no indication that they offered preferential paths for crack propagation (Fig 23). It should be noted however that the main crack path was nominally perpendicular to the major axes of most of the inclusions.

9. CONCLUSIONS

1. In pearlitic rail steels the R dependence of fatigue crack growth rates appears to be reduced in an inert environment compared to a normal air environment. An R or K_{max} dependence however still exists in an inert environment. From this it is expected that internal defects in rails would exhibit a similar behaviour and at high R ratios crack growth can be expected at ΔK values of 5-6 MN $m^{-3/2}$ or greater.

2. Fractographic evidence indicates that crack growth involves reverse plasticity at the crack tip but that the mode of crack extension is discontinuous.

3. In pearlitic/ferritic steels the pearlite/ferrite interface offers an additional path for crack extension.

4. The presence of ferrite films in a pearlitic steel has no deleterious effects upon the ΔK threshold or general fatigue crack growth performance.

10. REFERENCES

1. C.E. Richards and T.C. Lindley. Engn. Frac Mech. 1972 4 951.

2. P.R.V. Evans, N.B. Owen, and B.E. Hopkins. JISI. 1970 208 560.

3. A.R. Rosenfield, G.T. Hahn, and J.D. Embury. Metallurgical Transactions 1972 3 2797.

4. R.J. Cooke and C.J. Beevers. Engn. Frac. Mech. 1973 5 1061.

5. R.J. Cooke and C.J. Beevers. Mat. Sci. and Eng. 1974 13 201.

6. C.J. Beevers, R.J. Cooke, J.F. Knott, and R.O. Ritchie. Met. Sci. J. 1975 19 119.

7. C.E. Federson, R.D. Buchtheit, D. Broek. Battelle Report, July 1976. Fatigue Crack Propagation in Rail Steels.

8. Fowler, G.J. Ph.D. Thesis, Fatigue Crack Initiation and Propagation in Pearlitic Rail Steels. University of California, Los Angeles.

9. C.J. Beevers. Fracture, 1977 ICF 4 p. 239.

10. S. Druce and C.J. Beevers to be published.*

11. B. Kirby and C.J. Beevers to be published.*

12. M. Halliday and C.J. Beevers to be published.*

13. M. Hicks and C.J. Beevers to be published.*

ACKNOWLEDGMENTS

The author is indebted to B. Kirby and M. Hicks for making available recent observations which are included in this report.

* Department of Physical Metallurgy and Science of Materials, The University, Edgbaston, Birmingham, B15, 2TT, U.K.

Table 1.—Chemical composition of Rail Steels A (∿ 110 lbs/yd) and B (∿ 80 lbs/yd)

	Carbon	Manganese	Silicon	Phosphous	Sulphur
A	0.70	0.76	0.17	0.014	0.021
B	0.64	0.65	0.27	0.020	0.043

Table 2.—Mechanical Properties of Rail Steels

Steel	lbs/yd.	Yield Strength ksi	Ultimate Tensile Strength ksi	Elongation %
A	110	66	122	15
A	110	67	126	13
B	80	57	114	14
B	80	62	121	16

Table 3.- Δk_{th} Values for Steels A and B.

Specimen No.	Environment	R ratio	a/W	ΔK_{th} MN $m^{-3/2}$
A03	Air	0.76	0.45	3.8
A04	Air	0.08	0.43	10.0-11.0
A05	Vacuum	0.76	0.37	5.2
A06	Vacuum	0.11	0.43	8.9
A07	Vacuum	0.27	0.38	8.7
A08	Vacuum	0.67	0.39	5.9
A09	Vacuum	0.45	0.40	6.3
B02	Vacuum	0.78	0.40	5.4
B03	Vacuum	0.12	0.40	7.4
B04	Vacuum	0.45	0.41	6.5

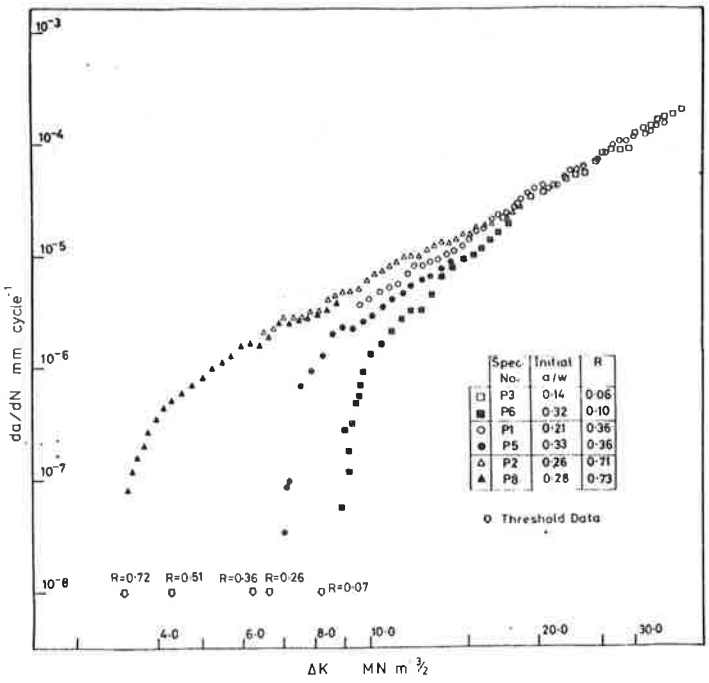

Figure 1.—The Influence of R Ratio on the Log ΔK v Log da/dN Curves for a 0.5% C 1.5% MN Pearlitic Steel Tested in Air at Room Temperature.

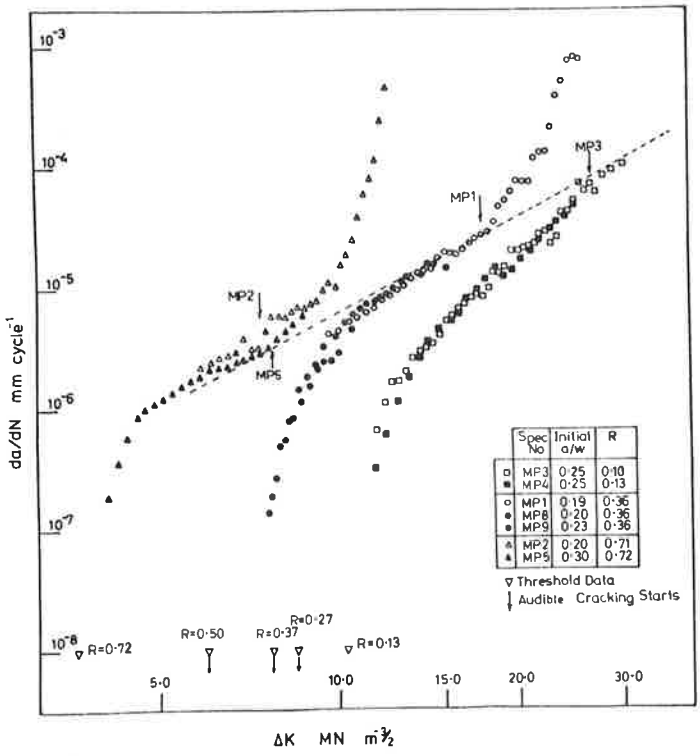

Figure 2.—The Influence of R Ratio and the Presence of Martensite on the Log ΔK v Log da/dN curves for a 0.5% C 2.2% MN Pearlitic Steel Tested in Air at Room Temperature.

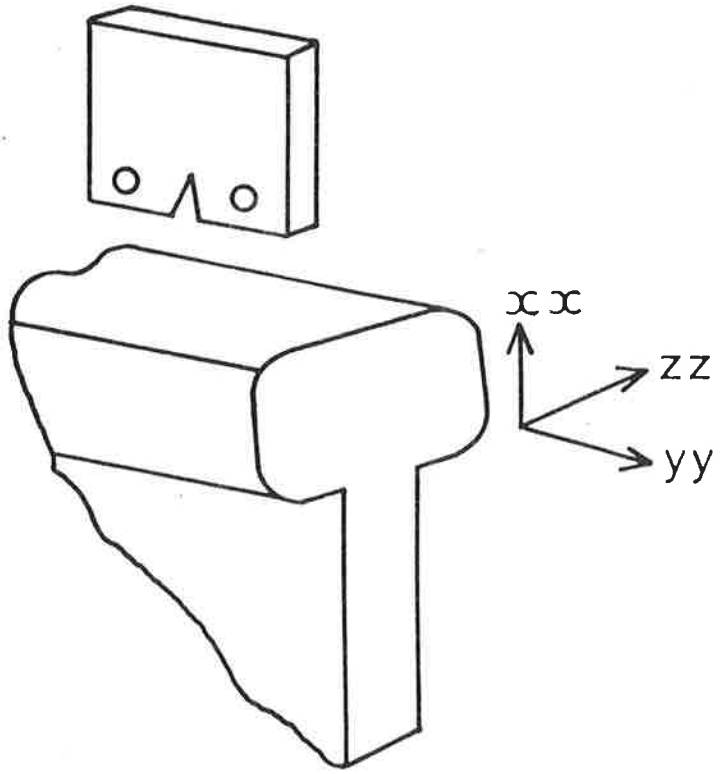

Figure 3.—Schematic Representation of Specimen Orientation in Relation to Rail

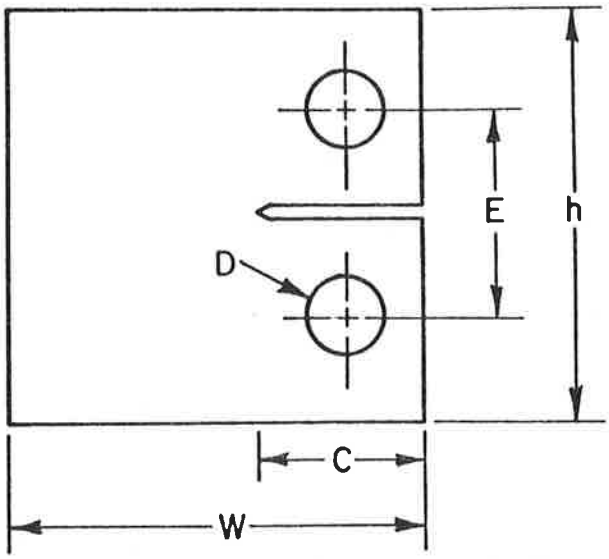

	W	D	C	L	E	Thickness
Steel A	50	10	22	48	22	15
Steel B	50	10	22	48	22	13

Tolerance 0.05mm.

Figure 4.—Details of Specimen Dimensions (mms)

Magnification x 400.
a) Plane xx – yy (Figure 3).

Figure 5.—Micrographs from rail steel A. Etch - Super Picral.

Magnification x 400.
b) Plane yy – zz (Figure 3).

Figure 5.—Metallographic Section of Rail Steel A. Etch Super – Picral.

Magnification x 400.
c) Plane xx — zz (Figure 3).

Figure 5.—Micrographs from Rail Steel A. Etch — Super Picral.

Magnification x 250.

(a) Plane xx - yy (Figure 3).

Figure 6.—Metallographic Section of Rail B. Etch — Super Picral.
a) Plane xx — yy (Figure 3).

Magnification x 250.
b) Plane yy – zz (Figure 3).

Figure 6.—Melallographic Section of Steel B. Etch – Super Picral.

Magnification x 250.
c) Plane xx – zz (Figure 3).

Figure 6.–Metallographic Section of Steel B. Etch – Super Picral.
b) Plane yy – zz (Figure 3).

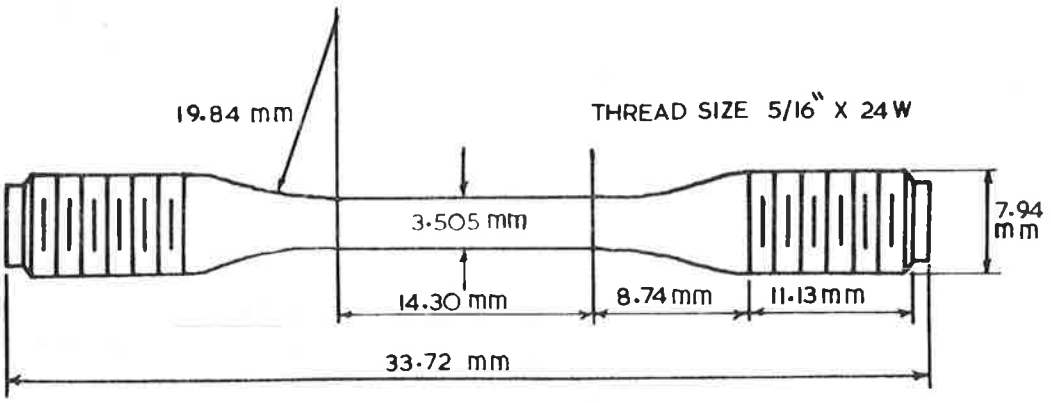

Figure 7.—Dimensions of Specimen used to Obtain Mechanical Properties of Steel A and B

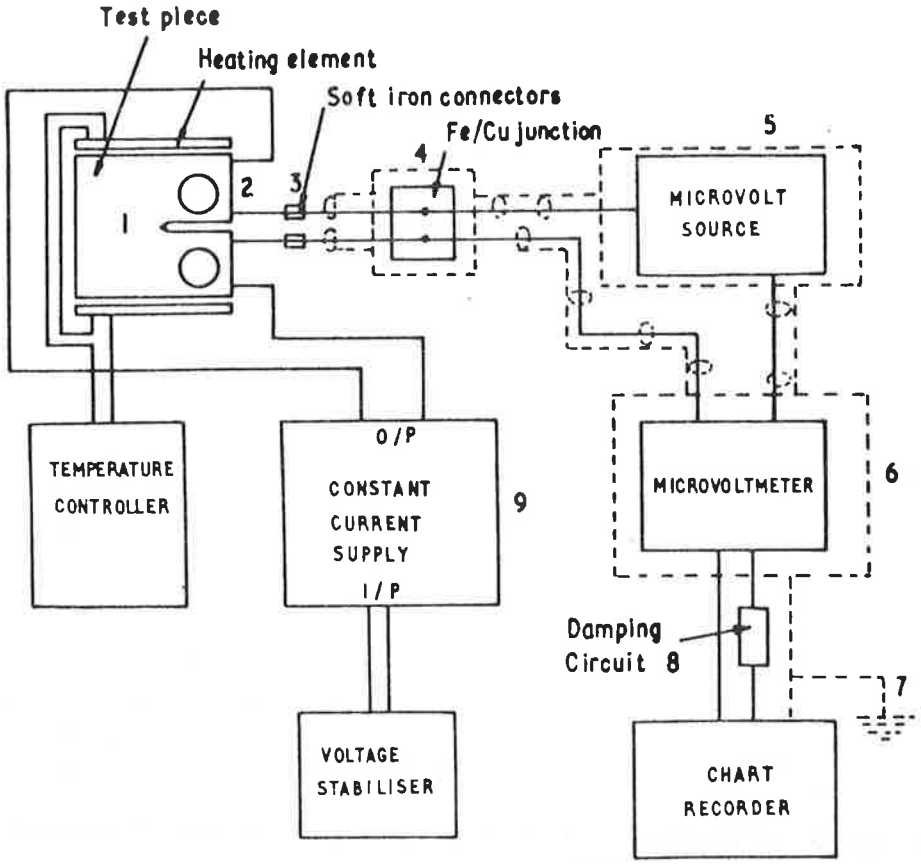

Figure 8.—A Schematic Illustration of the Equipment and Circuits Used to Measure Potential Changes in the Specimen

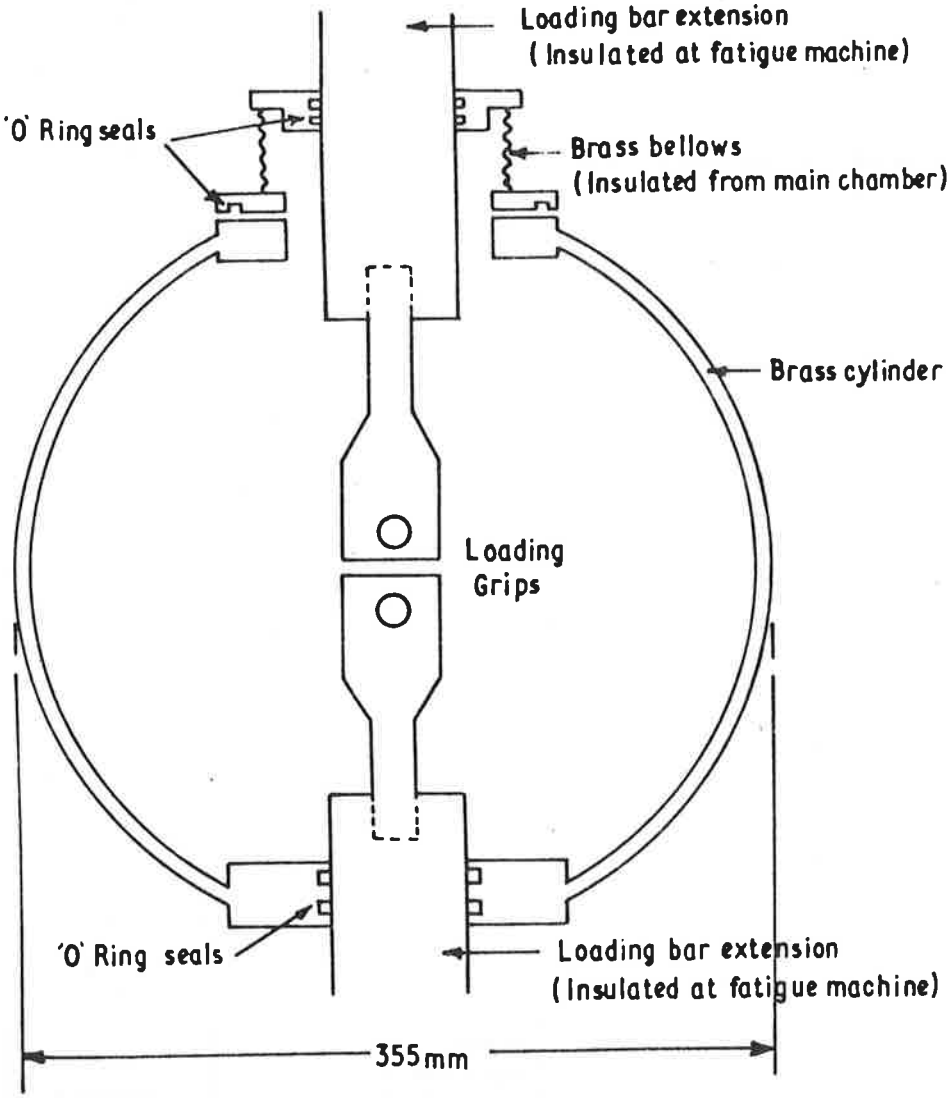

Figure 9.—A Schematic Illustration of the Vacuum Chamber Attached to the Amsler Vibrophore

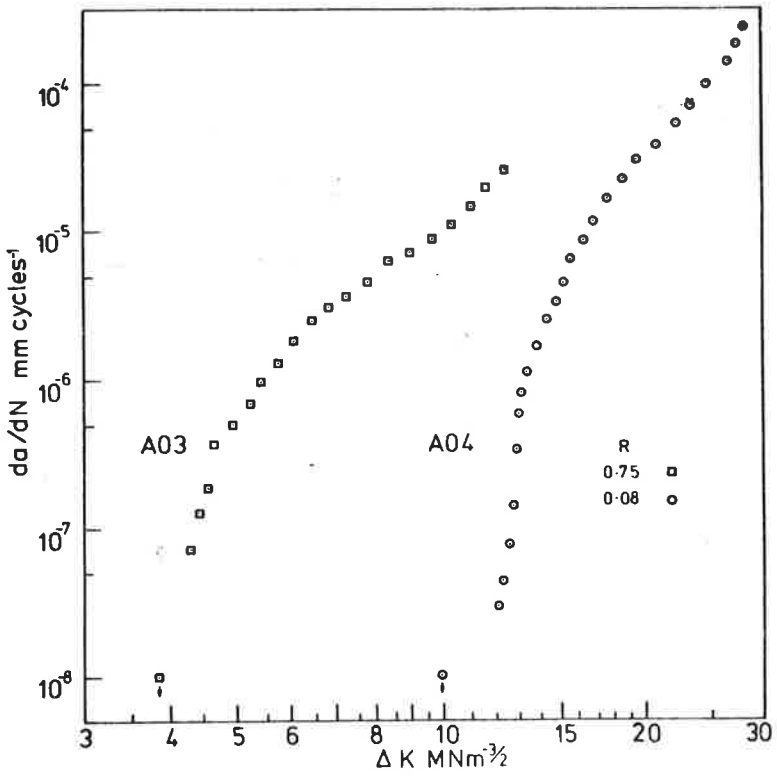

Figure 10.—The Log ΔK versus Log da/dN Curves for Steel A Specimens A03 and A04 Tested in Air at R = 0.75 and 0.08 Respectively

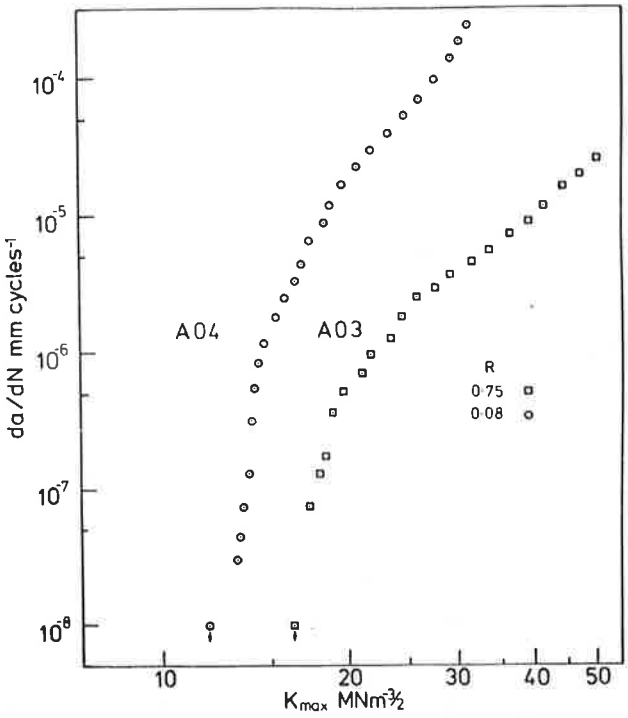

Figure 11.—The Log K_{max} versus Log da/dN Curves for Steel A Specimens A03 and A04 Tested in Air at R = 0.75 and 0.08 Respectively

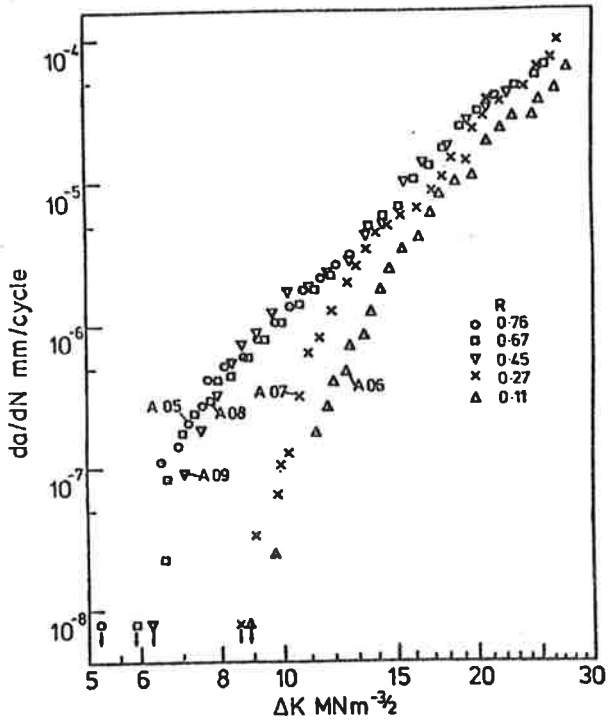

Figure 12.—The Log ΔK versus Log da/dN Curves for Steel A Tested in Vacuum at R Ratios of 0.76, 0.11, 0.27, 0.67 and 0.45

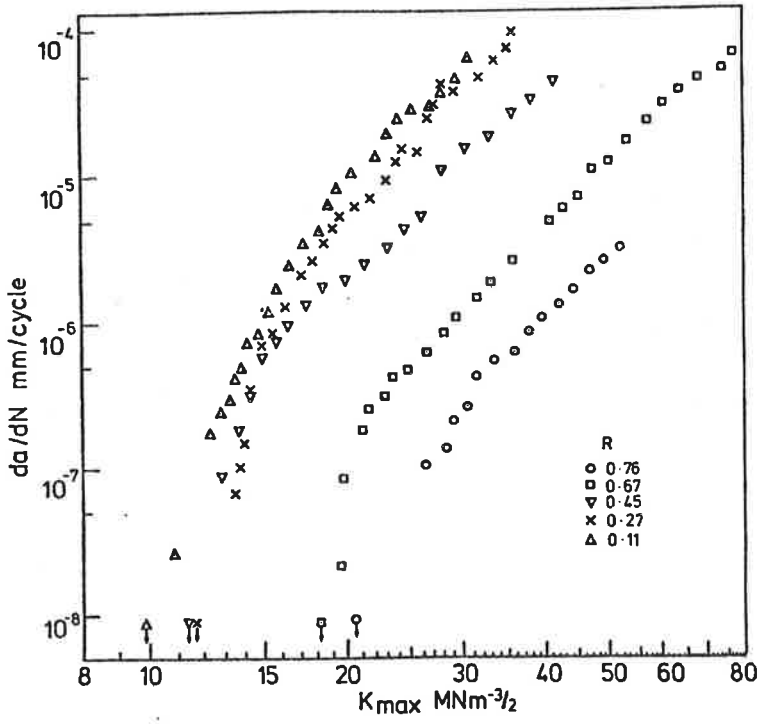

Figure 13.—The Log K_{max} versus Log da/dN Curves for Steel A Tested in Vacuum at R Ratios of 0.76, 0.11, 0.27, 0.67 and 0.45

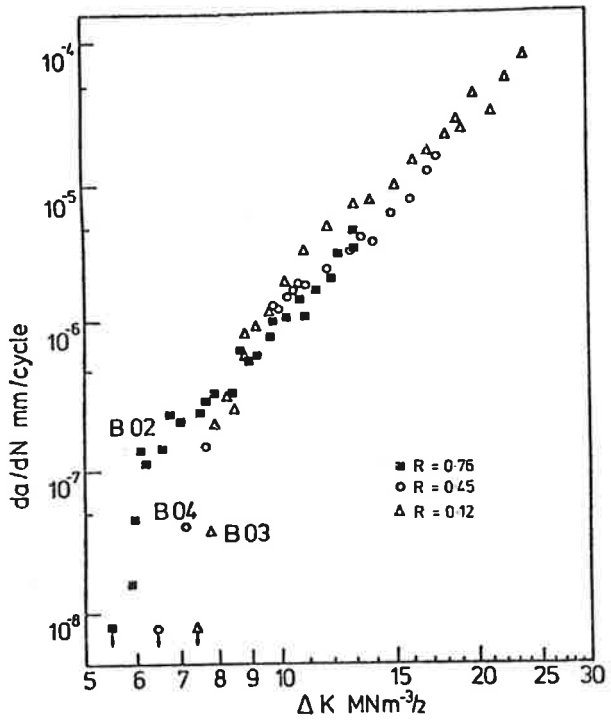

Figure 14.—The Log ΔK versus Log da/dN Curves for Steel B Tested in Vacuum at R Ratios of 0.78, 0.12 and 0.45

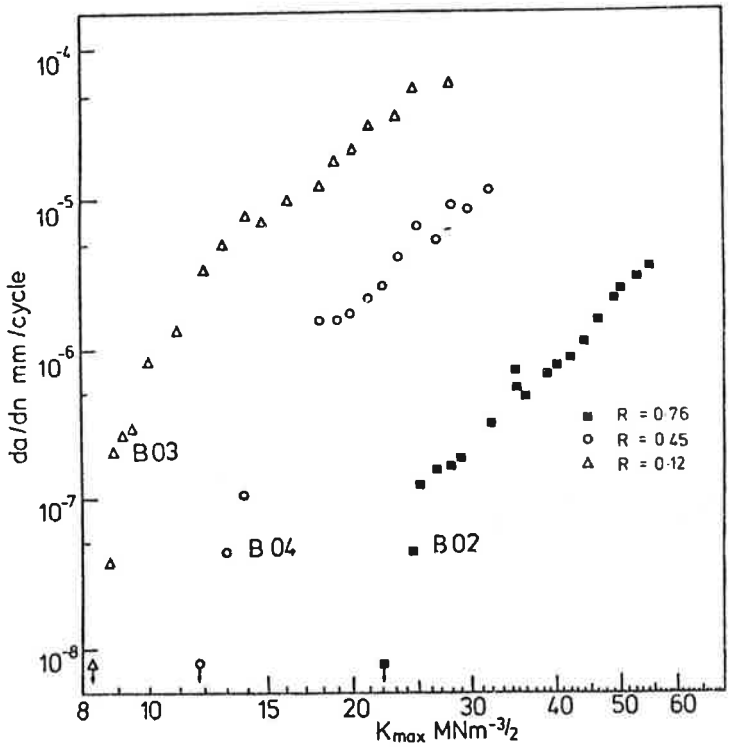

Figure 15.—The Log K_{max} versus Log da/dN Curves for Steel B Tested in Vacuum at R Ratios of 0.78, 0.12 and 0.45

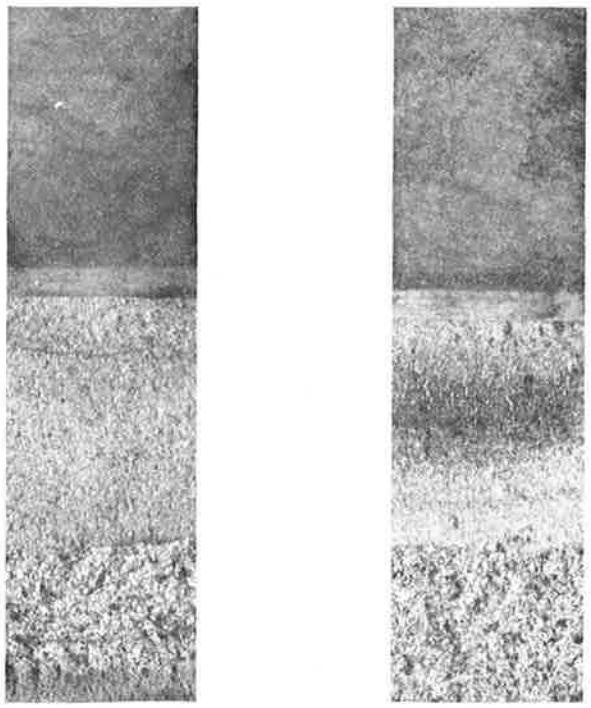

Figure 16.—Macro Photographs of Specimens (a) A03 and (b) A04 Tested in Air at R = 0.75 and 0.08 Respectively

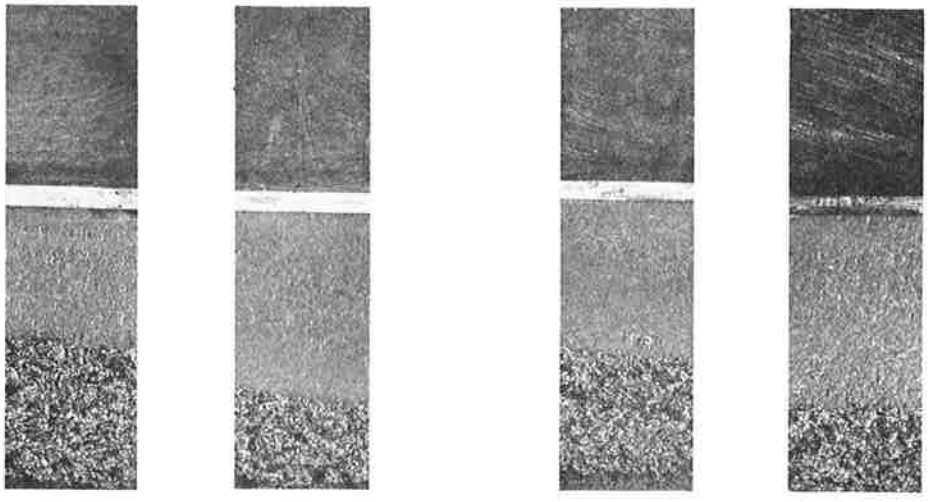

Figure 17.—Macrofractographs of Specimens, (a) A05, (b) A06, (c) A07, (d) A08 of Steel A Tested in Vacuum

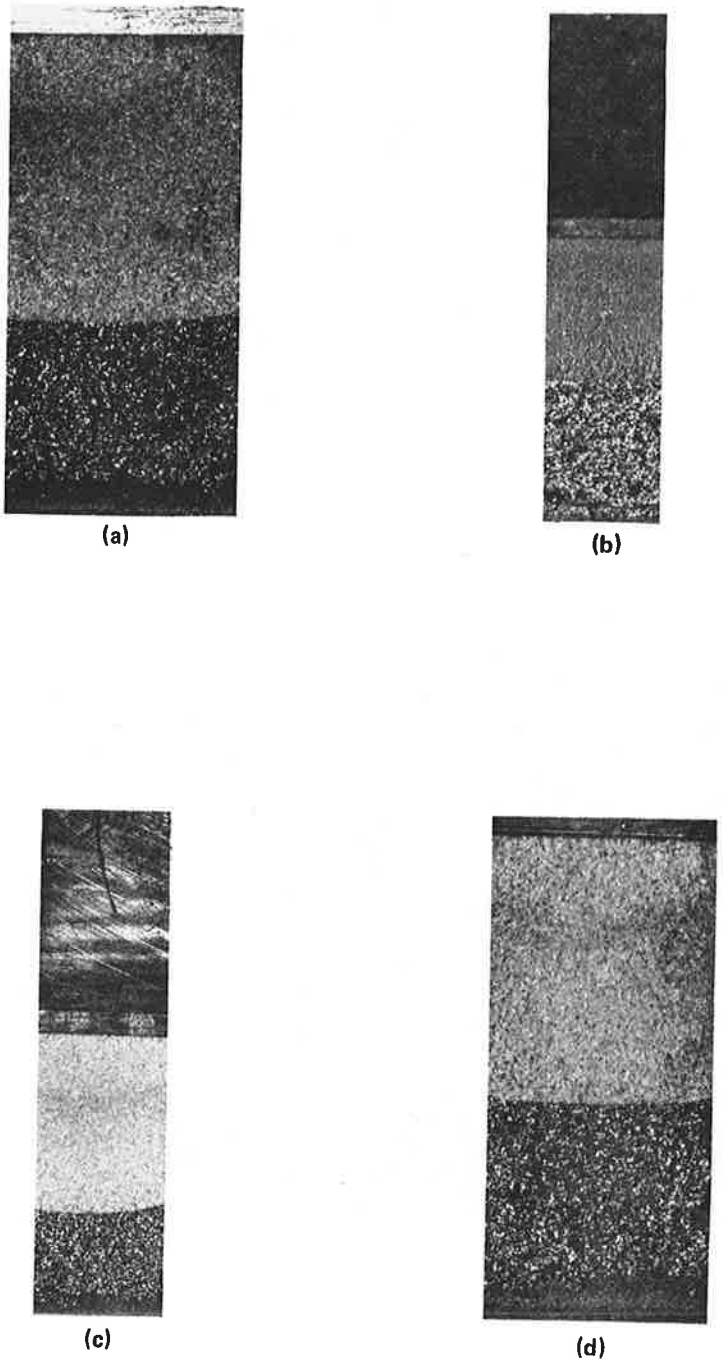

Figure 18.—Macrophotographs of (a) Steel A Specimen A09 Tested in Vacuum. Steel B Tested in Vacuum, (b) B02, (c) B03 and (d) B04

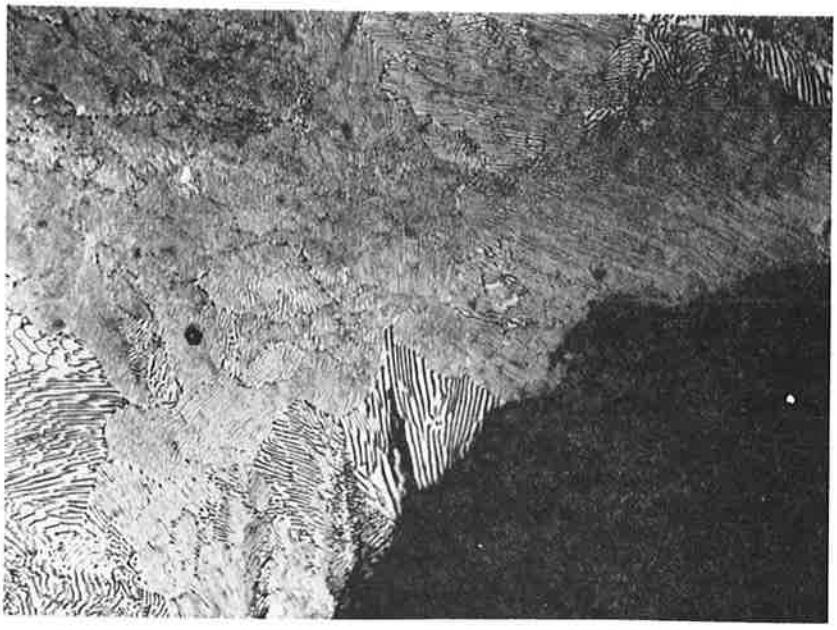

(a)

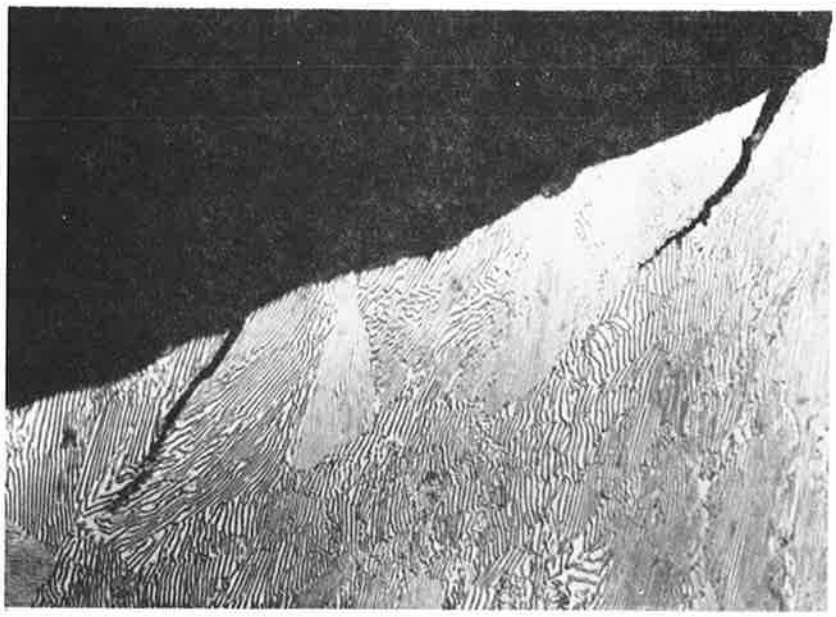

(b)

Magnification x 1,000

Figure 19.—Metallographic Sections Through the Fatigue Fracture Face of Specimen A05.

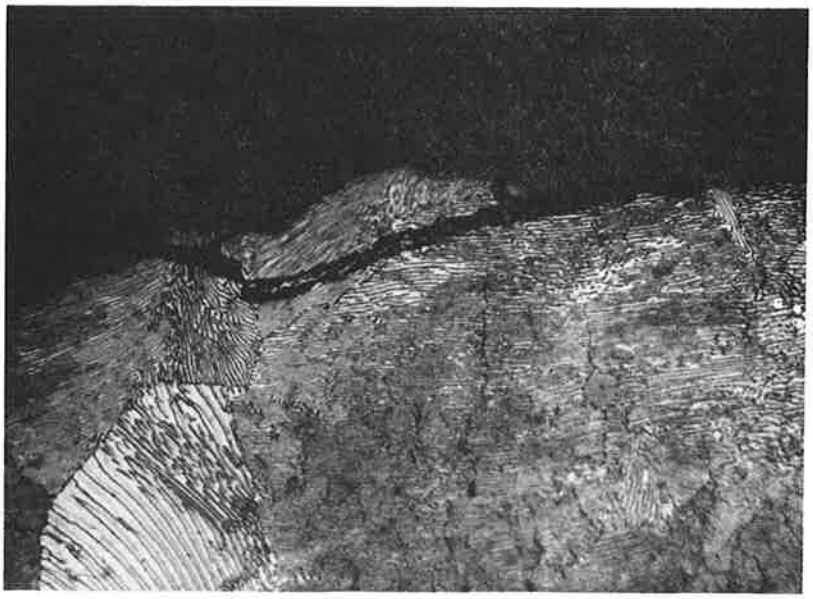

Magnification x 1,000

Figure 20.—Metallographic Section Through the Fatigue Fracture Face of Specimen A06

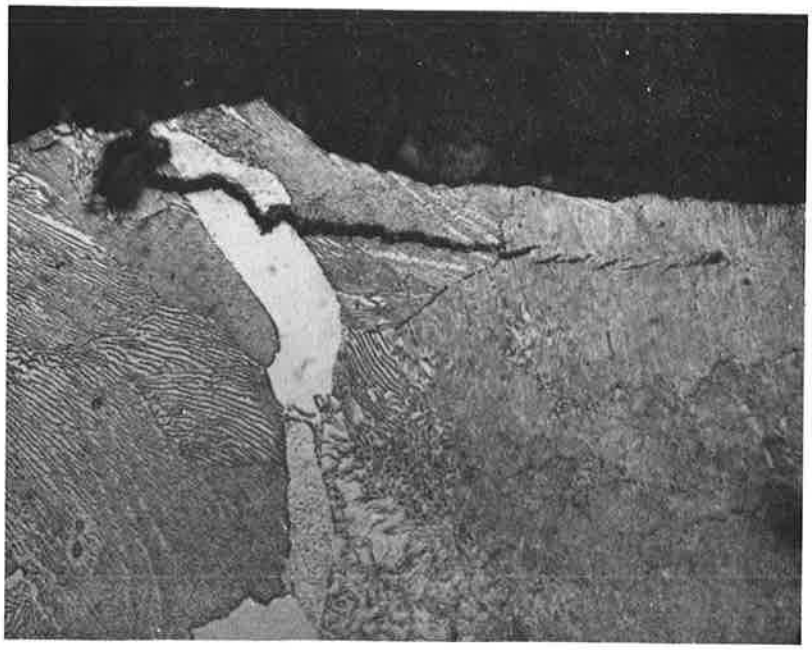

Magnification x 1,000

Figure 21.—Metallographic Section Through the Fatigue Fracture Face of Specimen B05

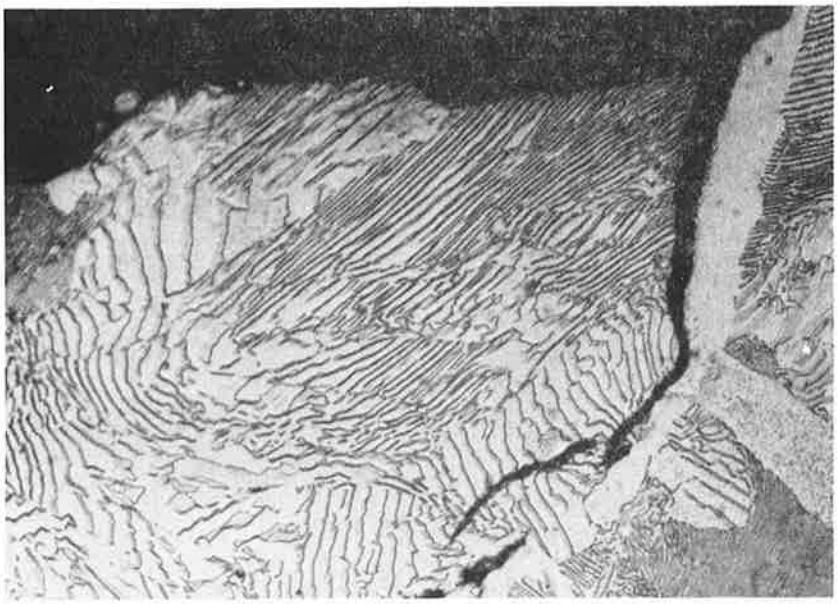

Magnification x 1,000

Figure 22.—Metallographic Section Through the Fatigue Fracture Face of Specimen B05

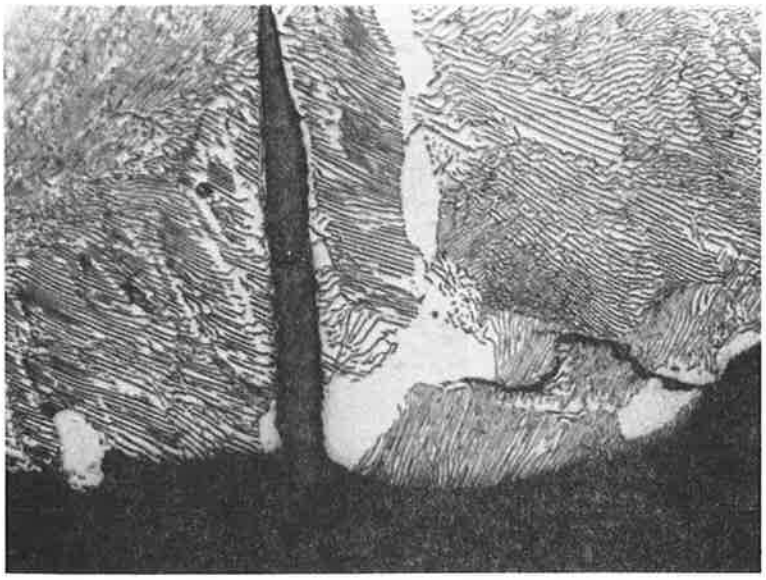

Magnification x 1,000

Figure 23.—Metallographic Sections Through the Fatigue Fracture Surface of Specimen B05

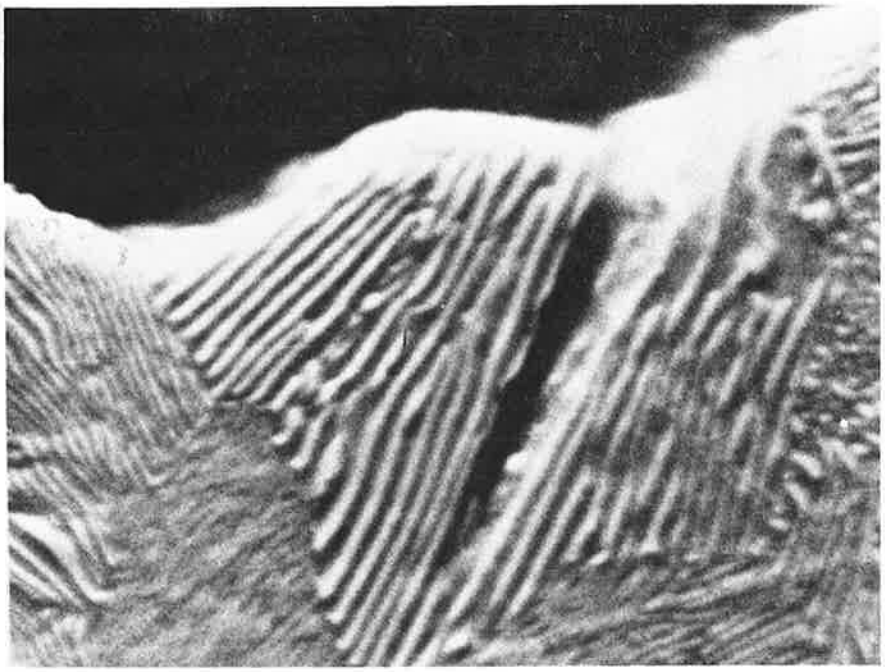

Magnification x 10,000

Figure 24.—An SEM Picture of an Metallographic Section through the Fatigue Fracture Surface of Specimen A05

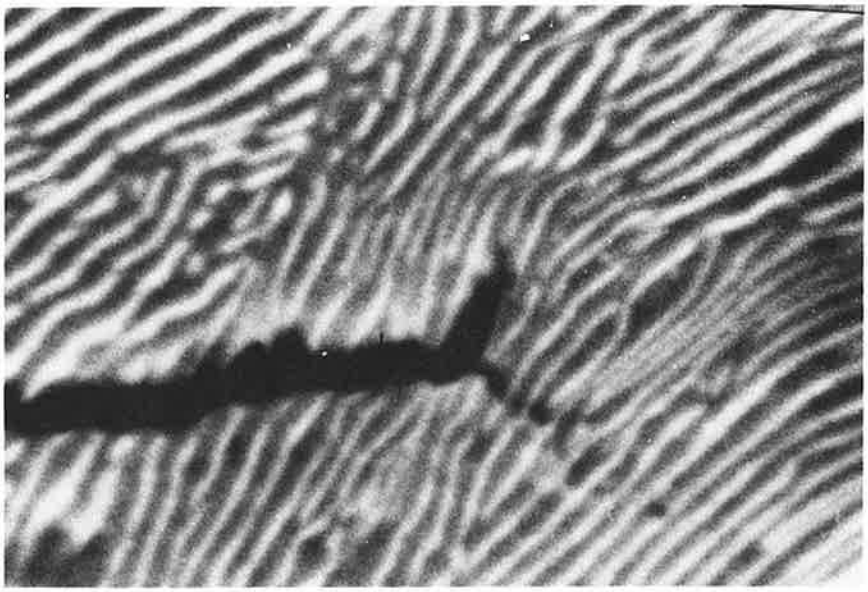

Magnification x 10,000

Figure 25.—An SEM Picture of a Metallographic Section Through the Fatigue Fracture Surface of Specimen A05

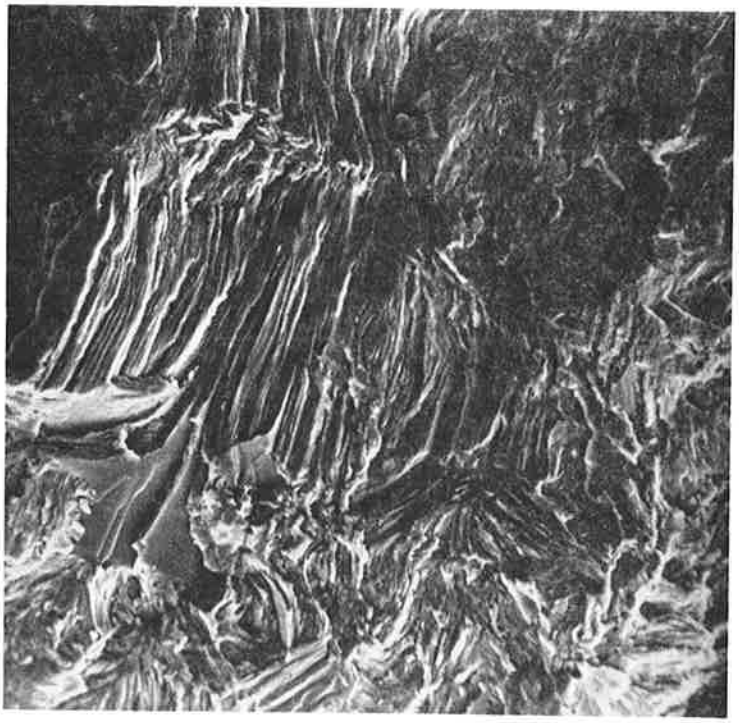

Magnification x 560 A03

Figure 26.—An SEM Micrograph of Steel A Tested in Air. Initiation $\Delta K \sim 25\ MN\ m^{-3/2}$

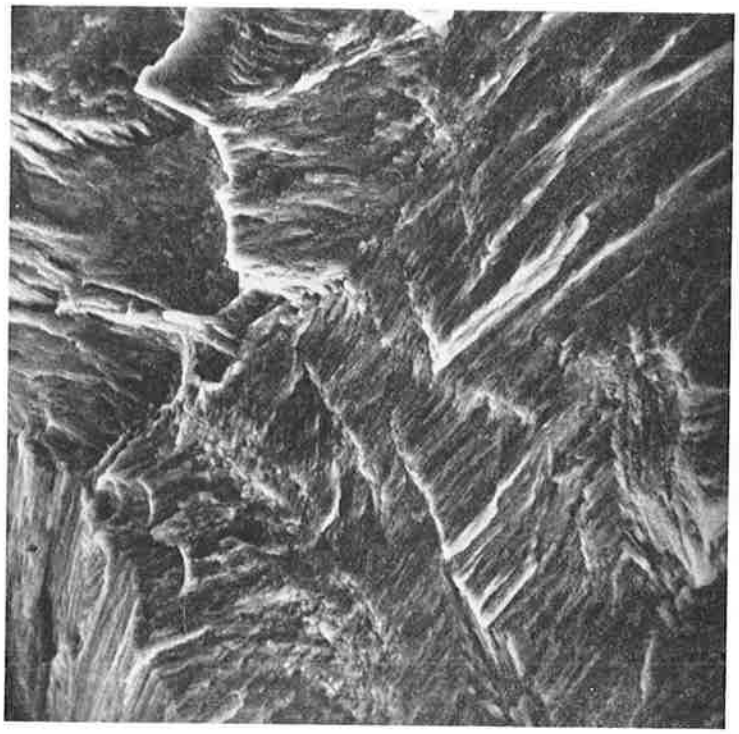

Magnification x 1,200 A03

Figure 27.—An SEM Micrograph of Steel A Tested in Air. Slow Growth Region $\Delta K \sim 4.7\ MN\ m^{-3/2}$

Magnification x 2,200 A03

Figure 28.—An SEM Micrograph of Steel A Tested in Air. Intermediate Growth Rate Region $\Delta K \sim 10$ MN $m^{-3/2}$

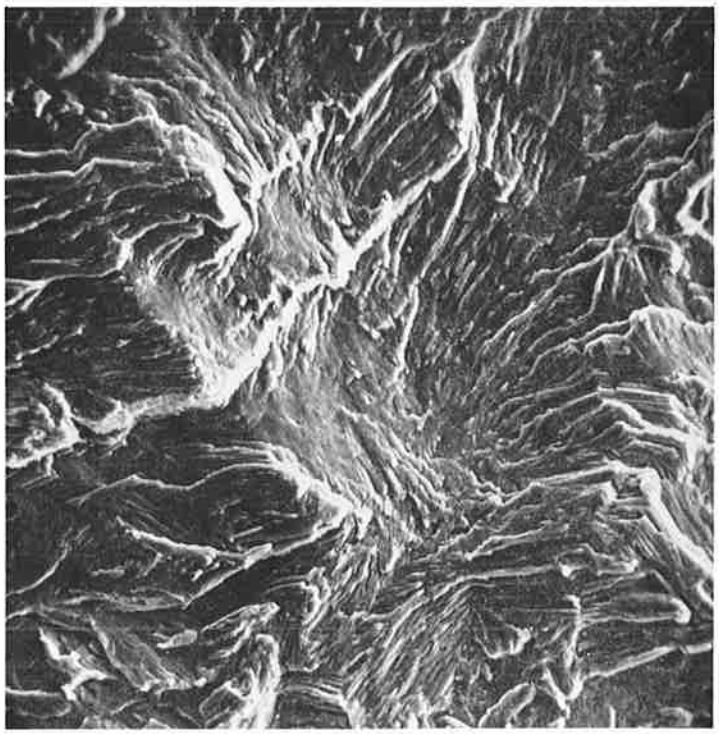

Magnification x 2,400 A04

Figure 29.—An SEM Micrograph of Steel A Tested in Air. Initiation $\Delta K \sim 25$ MN $m^{-3/2}$

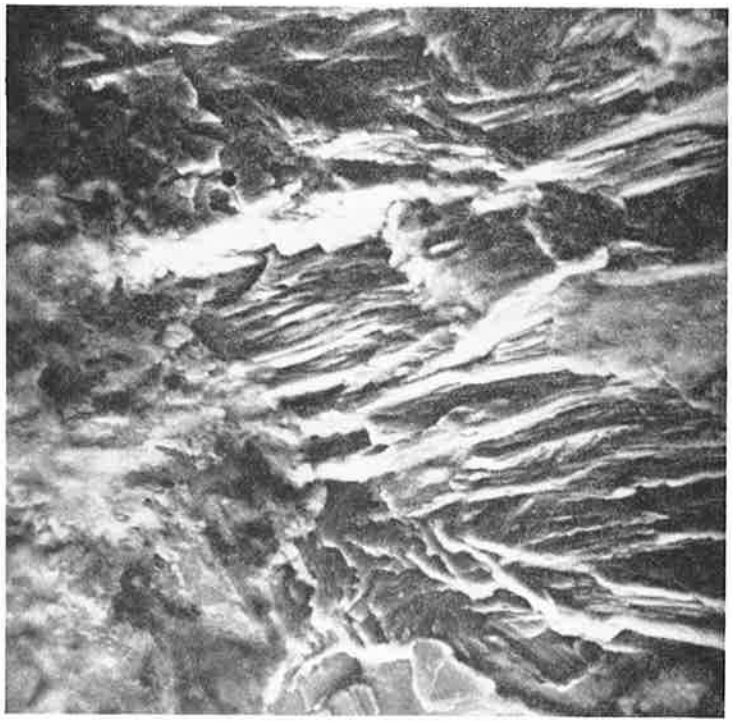

Magnification x 1,500. A04.

Figure 30.— SEM Micrograph of Steel A Tested in air. Threshold region $\Delta K \sim 10.5$ MN $m^{-3/2}$

Magnification x 1,150. A04.

Figure 31.—SEM Micrograph of Steel A Tested in air. Slow growth rate region $\Delta K \sim 12.5$ MN $m^{-3/2}$

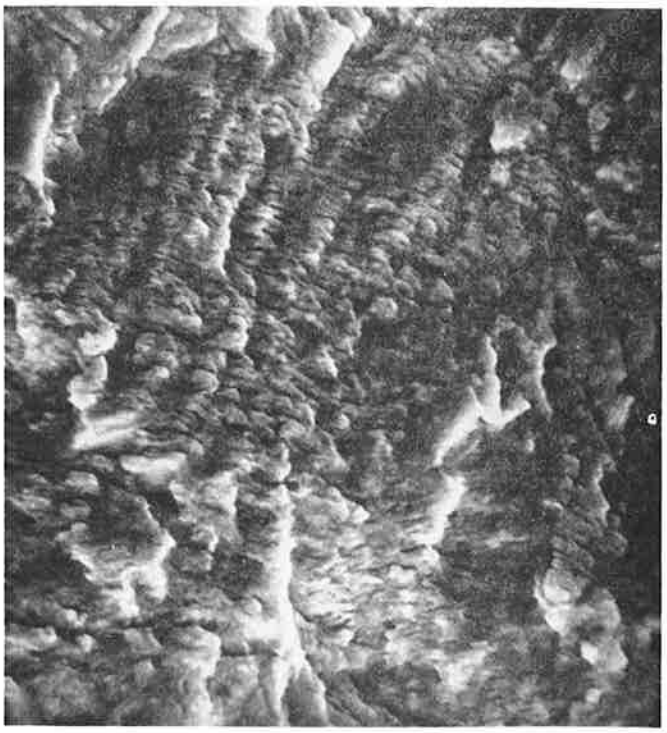

Magnification x 2,200. A05.

Figure 32.—SEM Micrograph of Steel A Tested in Vacuum. Initiation $\Delta K \sim 25$ MN $m^{-3/2}$

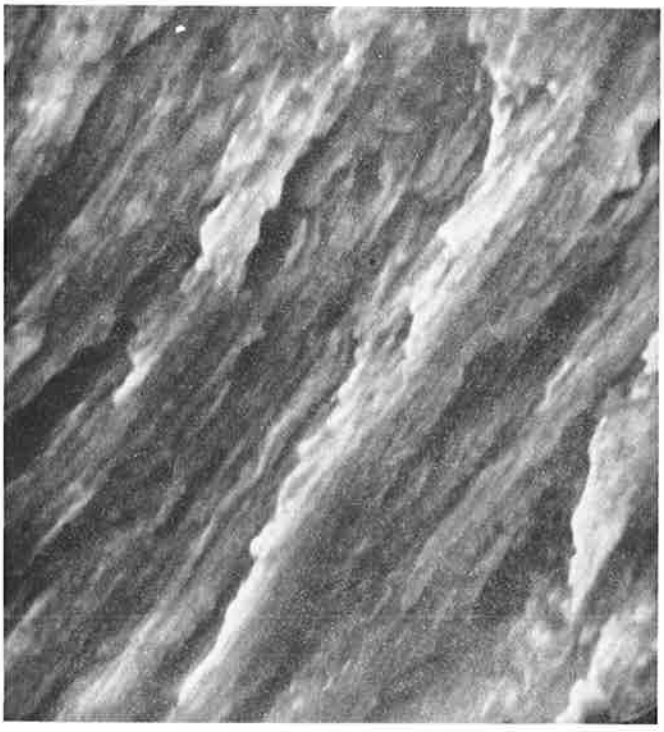

Magnification x 5,300. A05.

Figure 33.—SEM Micrograph of Steel A Tested in Vacuum. Threshold Region $\Delta K \sim 6$ MN $m^{-3/2}$

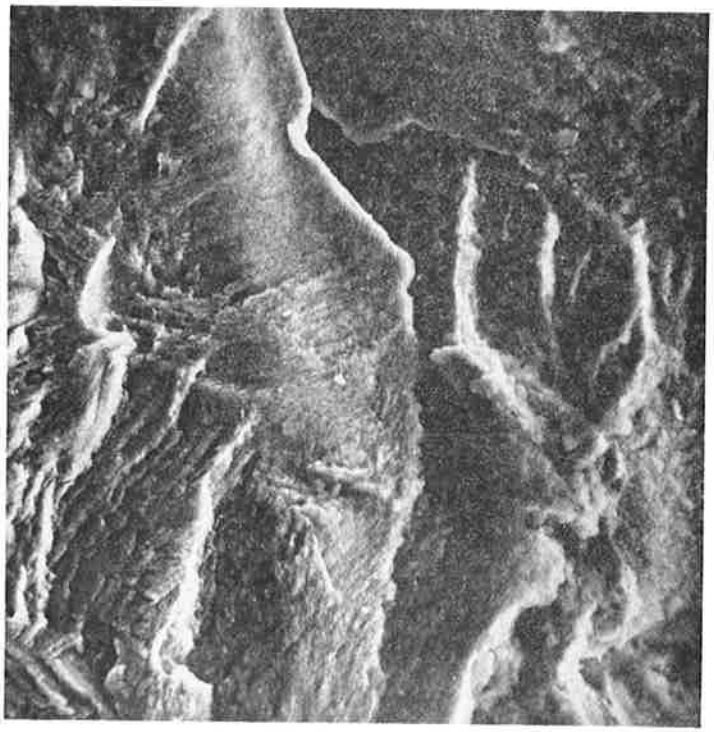

Magnification x 1,200. A07.

Figure 34.—SEM Micrograph of Steel A Tested in Vacuum. Threshold Region $\Delta K \sim 9.5\ MN\ m^{-3/2}$

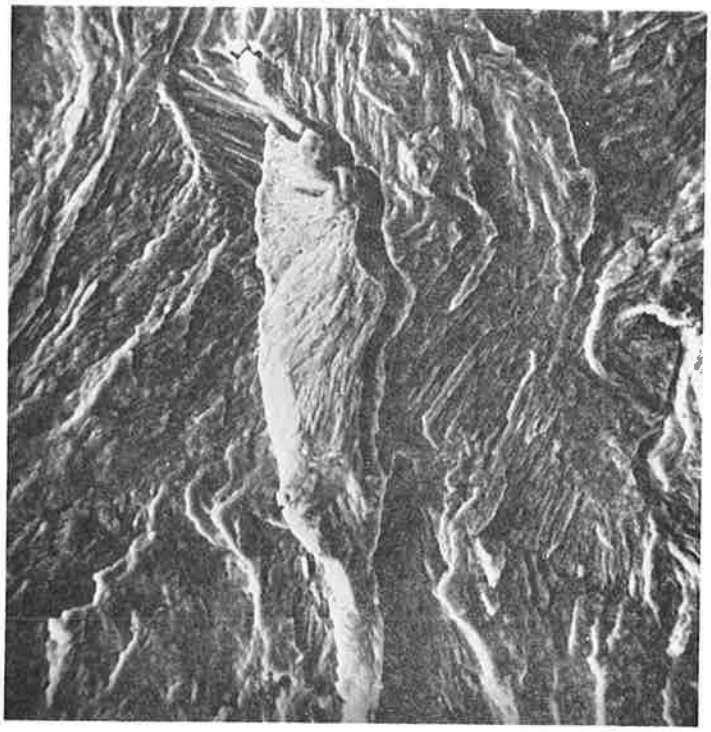

Magnification x 600. A07.

Figure 35.—SEM Micrograph of Steel A Tested in Vacuum. Intermediate Growth Rate $\Delta K \sim 18.5\ MN\ m^{-3/2}$

Magnification x 2,400. A07.

Figure 36.—SEM Micrograph of Steel A Tested in Vacuum. Intermediate - High Growth Rate $\Delta K \sim 25$ MN $m^{-3/2}$

Magnification x 2,400. A06.

Figure 37.—SEM Micrograph of Steel A Tested in Vacuum. Threshold Region $\Delta K \sim 10$ MN $m^{-3/2}$

Magnification x 6,000. A06.

Figure 38.—SEM Micrograph of Steel A Tested in Vacuum. Intermediate Growth rate $\Delta K \sim 13$ MN m $^{-3/2}$

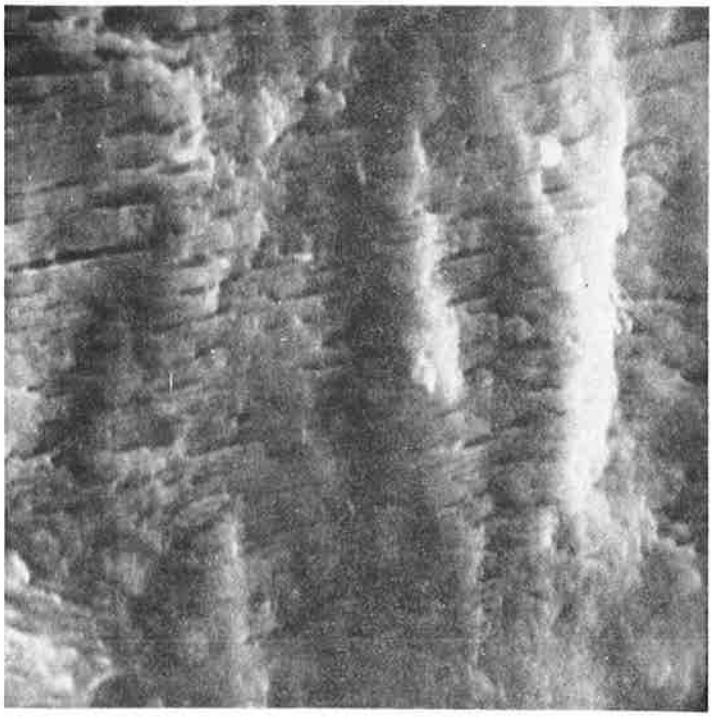

Magnification x 5,700. A08.

Figure 39.—SEM Micrograph of Steel A Tested in Vacuum. Initiation Region $\Delta K \sim 25$ MN $m^{-3/2}$

Magnification x 2,400. A09.

Figure 40.—SEM Micrograph of Steel A Tested in Vacuum. Threshold Region $\Delta K \sim 7$ MN $m^{-3/2}$

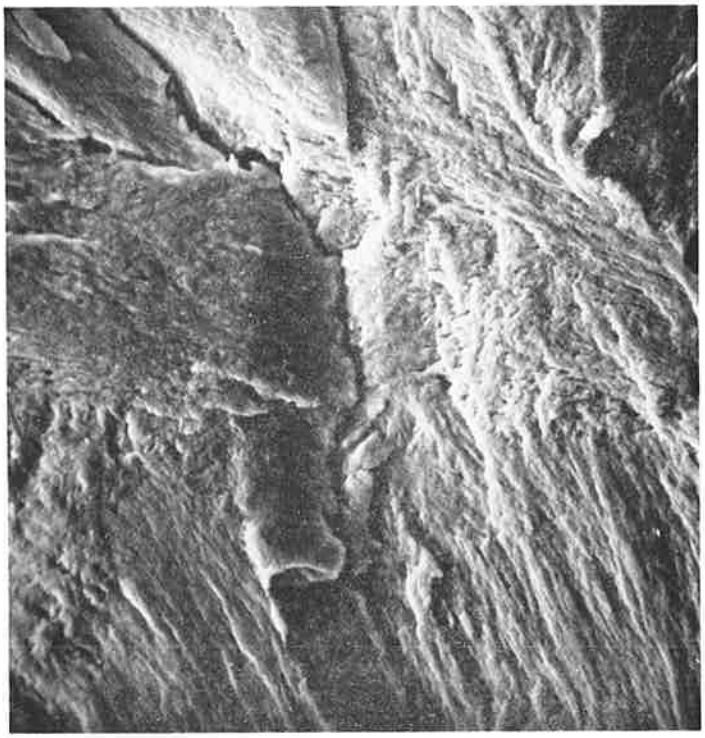

Magnification x 1,100. A09.

Figure 41.—SEM Micrograph of Steel A Tested in Vacuum. Intermediate Growth Rate $\Delta K \sim 22$ MN $m^{-3/2}$

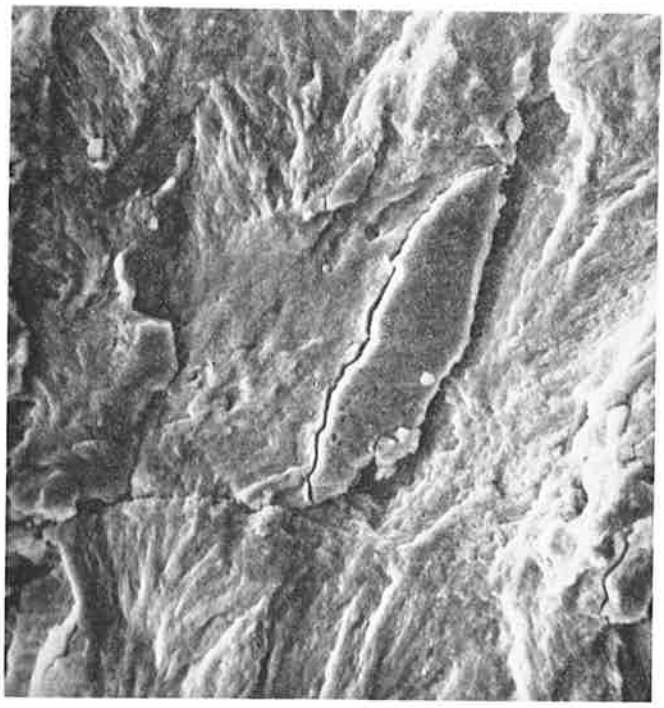

Magnification x 1,100. B03.

Figure 42.—SEM Micrograph of Steel B Tested in Vacuum. Initiation Region $\Delta K \sim 25$ MN $m^{-3/2}$

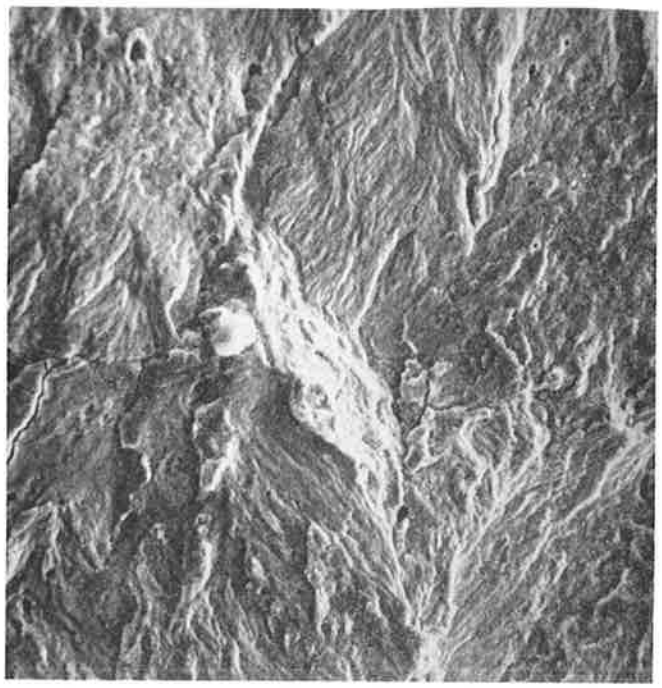

Magnification x 550. B03.

Figure 43.—SEM Micrograph of Steel B Tested in Vacuum. Threshold Region $\Delta K \sim 7.6$ MN $m^{-3/2}$

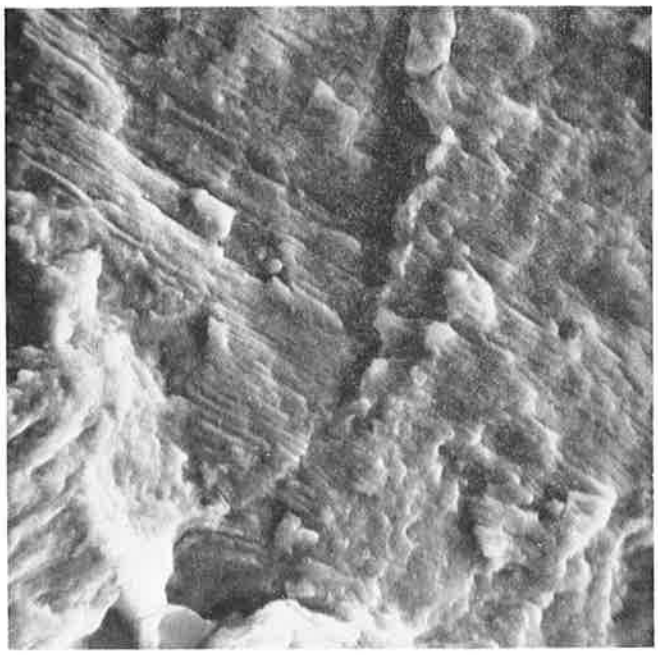

Magnification x 2,200. B03.

Figure 44.—SEM Micrograph of Steel B Tested in Vacuum. Intermediate Growth Rate $\Delta K \sim 16$ MN $m^{-3/2}$

Magnification x 1,100. B02.

Figure 45.—SEM Micrograph of Steel B Tested in Vacuum. Initiation Region $\Delta K \sim 25$ MN $m^{-3/2}$

Magnification x 2,200. B02.

Figure 46.—SEM Micrograph of Steel B Tested in Vacuum. Threshold Region $\Delta K \sim 6.5$ MN $m^{-3/2}$

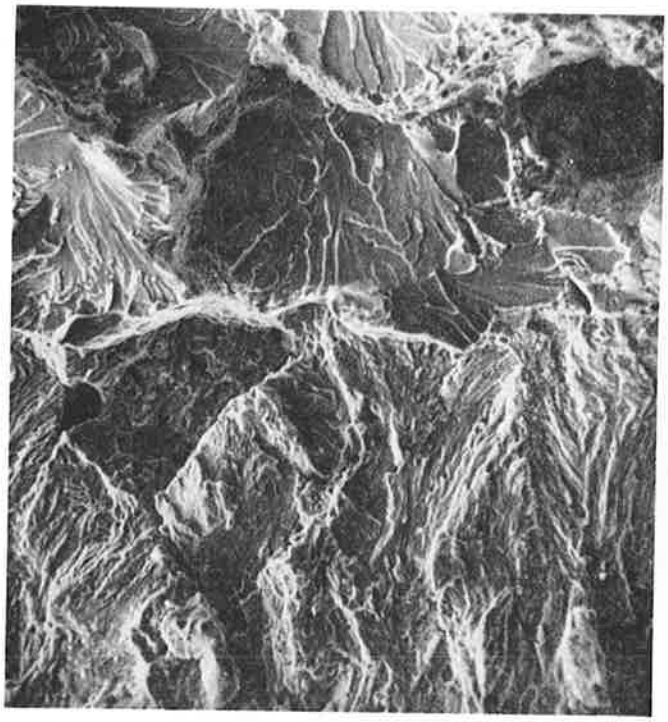

Magnification x 240. B02.

Figure 47.— SEM Micrograph of Steel B Tested in Vacuum. Intermediate Growth Rate $\Delta K \sim 13$ MN $m^{-3/2}$

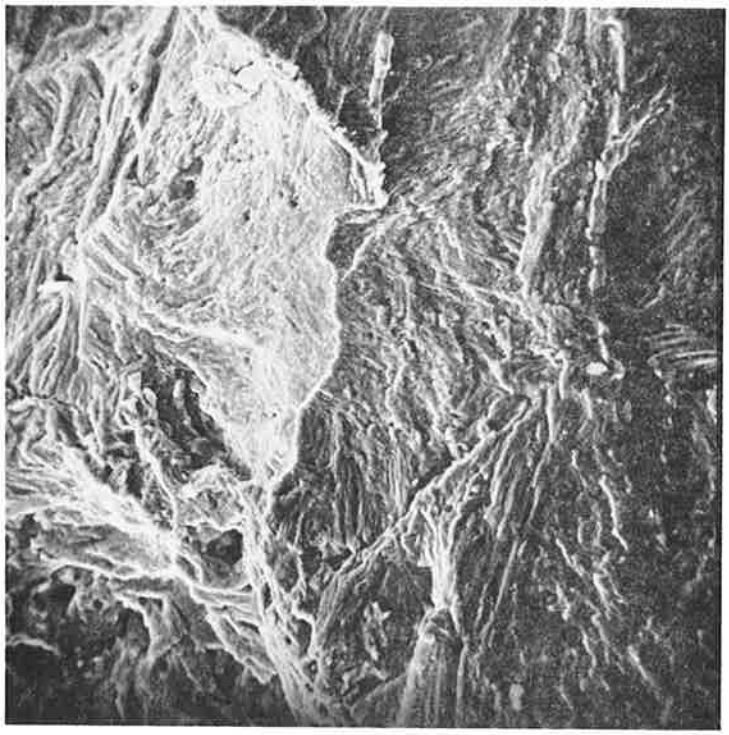

Magnification x 600 B04

Figure 48.—SEM Micrograph of Steel B Tested in Vacuum. Intermediate Growth Rate Region $\Delta K \sim 15\ MN\ m^{-3/2}$

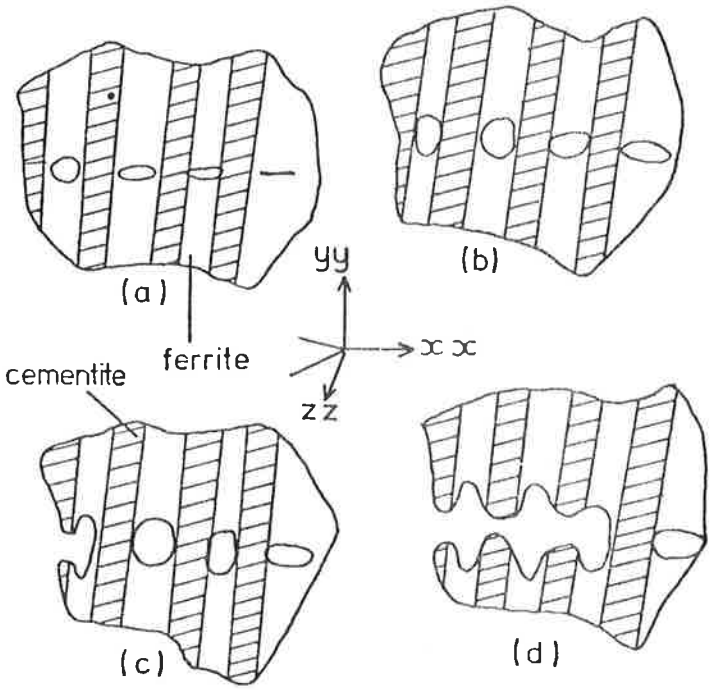

Figure 49.—A Schematic Illustration of the Mode of Fatigue Crack Growth in Pearlite

110 Copies